QUANTITATIVE ANALYSIS OF POSITIVE-DISPLACEMENT COMPRESSOR MODELS TESTED IN EXTRAPOLATION SCENARIOS

By

KALEN S. GABEL

Bachelor of Science in Mathematics
Northwestern Oklahoma State University
Alva, OK
2017

Bachelor of Science in Mechanical Engineering
Oklahoma State University
Stillwater, OK
2019

Submitted to the Faculty of the
Graduate College of the
Oklahoma State University
in partial fulfillment of
the requirements for
the Degree of
MASTER OF SCIENCE
December, 2022

QUANTITATIVE ANALYSIS OF POSITIVE-DISPLACEMENT COMPRESSOR MODELS TESTED IN EXTRAPOLATION SCENARIOS

Thesis Approved:

Dr. Craig Bradshaw

Thesis Advisor

Dr. Dan Fisher

Dr. Rushikesh Kamalapurkar

ACKNOWLEDGMENTS

I would first like to thank my parents for their continuous love and unwavering support throughout my masters studies and my life. Mom and Dad, you both have provided the foundation on which I fall back on in the hard times and grow on in the good times. Thank you.

I want to thank my sister for her caring love and ever useful advise. Thank you for always being an open ear and a great sister to me.

In addition to my family support, my professional support has helped carry me to new heights I had previously not thought possible. Dr. Craig Bradshaw, I want to thank you for your patience with me as a graduate student and for your guidance throughout my time at Oklahoma State. You have undoubtedly shaped my future for the better.

Going through graduate school has put me in front of quite a few people. Some of these have been lab mates, technicians, other faculty members and staff. While I cannot adequately express my appreciation for all of these people here, the best I can do is recall some who have made lasting impacts. I want to thank Seth for his support and all the fun times we had in the lab. Saad and Andrew, it was always a good time hanging out in the office and on the town. I want to thank Matin and Amir for coming into the office and being great office mates. Lastly, I want to thank all of my lab mates Mazharul, Mohsin, Abraham, Amjid, and Shahzad. It was a pleasure to share time in graduate school with all of you.

Acknowledgments reflect the views of the author and are not endorsed by committee members or Oklahoma State University.

Name: KALEN S. GABEL

Date of Degree: DECEMBER, 2022

Title of Study: QUANTITATIVE ANALYSIS OF POSITIVE-DISPLACEMENT COMPRESSOR MODELS TESTED IN EXTRAPOLATION SCENARIOS

Major Field: MECHANICAL AND AEROSPACE ENGINEERING

Abstract: Testing and evaluation of select semi-empirical compressor models is carried out to quantify performance in modulation (variable speed), extrapolation, and additionally, variable superheat scenarios. Three representative literature models and an artificial neural network (ANN) model are benchmarked against the industry standard AHRI model. A methodology quantifying model performance, compared against experimental data, in said scenarios is presented. Data used is of high-fidelity taken from either a hot-gas bypass load stand or compressor calorimeter. Scroll, screw, reciprocating, and spool compressor technologies were collected with R410A, R1234ze(E), R134a, and R32 refrigerants totaling 434 experimental points. Data is divided into training, extrapolation, variable speed, and variable superheat data splits to examine model performance. Mean Absolute Percentage Error (MAPE) is computed for mass flow rate and power after training models with training data and evaluating them against the other data splits. Two literature models are true semi-empirical formulations while the other, the ANN, and AHRI model are more empirical in nature. Neither semi-empirical model predicted all compressors. When the compressor type is predicted, the semi-empirical models yield MAPE's less than 8%, 5%, and 4% for mass flow rate and power prediction in extrapolation, modulation, and variable superheat scenarios, respectively. The exception is the Popovic and Shapiro model performing at 21% MAPE in variable superheat power prediction for the spool compressor with R1234ze(E). The ANN showed highest errors of 9.3%, 12%, and 17% in extrapolation, modulation, and variable superheat scenarios, respectively. All models outperformed the AHRI model by several orders of magnitude in these scenarios.

TABLE OF CONTENTS

LIST OF TABLES

Table Page

LIST OF FIGURES

NOMENCLATURE

VARIABLES	UNITS	DESCRIPTION
AU	W/K	Heat Transfer Coefficient
C	-	Clearance Factor
f	Hz	Frequency
N	RPM	Compressor Rotational Speed
n	-	Polytropic Exponent
ν	kg/m^3	Specific Volume
RPD	m^3/rev	Piston Displacement Rate
RPM	rev/min	Rotational Speed
ΔT_{sup}	K	Superheat Temperature
$\dot{Q}$	kW	Heat Transfer
Δs	J/kg-K	Change in Entropy
V_s	m^3	Fictitious Swept Volume
$\dot{W}$	kW	Power

GREEK SYMBOLS	UNITS	DESCRIPTION
α	-	Power Loss Coefficient

SUBSCRIPTS	DESCRIPTION
amb	Ambient
cyl	Cylinder

c	Condensing
cal	Calculated
d	Discharge Dewpoint
dis	Discharge
ex	Exit
in	Inlet
out	Outlet
s	Suction Dewpoint
suc	Suction

LIST OF SYMBOLS

ANN	Artificial Neural Network
EFF.	Efficiency
MAE	Mean Absolute Error
MAPE	Mean Absolute Percentage Error

CHAPTER I

INTRODUCTION

Today compressor manufactures are challenged by a rapidly changing regulatory environment shifting focus toward mitigating climate change and global warming. Modeling compressor performance plays a vital part in predicting overall system behavior, ensuring system efficiency requirements are met, and minimizing the energy footprint of these machines.

When manufactures test their systems through simulation it is desired that a variety of operating conditions be predicted accurately. Additionally, part-load conditions sometimes require the compressor to be operated at a different operational speed than full-load conditions. These two situations present unique needs that a model must fulfil, that is, extrapolation and modulation capability. Semi-empirical models may have the potential of meeting these two needs.

1.1 Literature Review

All compressor models exist on a spectrum, ranging from black-box (statistical correlations) to white-box (distributed models). Black-box models require little information about the machine itself, while white-box models need detailed input information sometimes only known by the manufacturer. The most well known black-box model is the industry standard 10-coefficient map standardized by AHRI 540 AHRI (2020). Grey-box or semi-empirical models aim to hit the middle ground between the two extremes. These models are more computationally efficient than white-box models

enabling them to be implemented into system simulations while retaining additional fidelity that black-box models typically do not.

This work aims to identify select semi-empirical compressor models from literature, quantify performance at extrapolation and modulation scenarios, and give insights into a future model capable of predicting multiple compressor technologies in said scenarios. Shao et al. (2004) presents a map based modeling approach for predicting mass flow rate, power, and COP at different supply frequencies for a rolling piston compressor. The equations of the model are fitted as second order functions of evaporating and condensing temperatures with one cross term. A mass flow rate and power ratio are defined which relate variable speed operation to that at a constant speed. This approach is adopted by Aprea and Renno (2008) to predict variable speed reciprocating compressor data. A separate black-box style approach by Qiao et al. (2014) used pressure ratio and normalized speed to predict scroll compressor performance in a transient multi-evaporator system simulation. The model utilized curve fit coefficients in expressions for volumetric efficiency, power, and discharge enthalpy.

The above models differ from semi-empirical methods because they rely on equations which are functions of high-level variables, such as pressure ratio. On the other hand semi-empirical approaches are reliant on tuned parameters within equations that closer resemble the physics of various phenomena occurring within the compressor, such as suction pressure loss and suction heat transfer. Navarro et al. (2007) presents a phenomenological model based on an isentropic compression process for analyzing reciprocating compressors using propane. Compressor efficiency and volumetric efficiency is presented as a set of implicit equations which need 10 parameters, each claimed to have physical interpretation, to be curve fitted. It reproduced compressor and volumetric efficiency with an error lower than 3% under a range of operating conditions. Corber et al. (2007) then uses the model to predict reciprocating compressor performance with R407C. The work used all parameters fitted with propane

to estimate performance with R407C except one phase change factor which is altered slightly. Results showed deviations of less than 5% for compressor efficiency in all tests except one. Tello-Oquendo et al. (2019) presents a semi-empirical model based on Navarro et al. (2007)'s work to predict scroll compressor performance and the method is extended to capture vapor injection scroll compressors using R407C. Results obtained were $\pm$ 5% for compressor and volumetric efficiency.

Other work on semi-empirical models utilize different reference processes or capture different phenomena. Popovic and Shapiro (1995) present a method derived for reciprocating compressors based on a volumetric efficiency, polytropic compression process, and three defined control volumes. Two compressors, 8 different working fluids, and 122 total data points are used for validation. It predicts mass flow rate, power, and discharge temperature using 8 model inputs. Jahnig et al. (2000) presented a similar model for small hermetic reciprocating compressors used in household refrigerators. The model is based on volumetric efficiency, assumes a polytropic compression process, and utilizes five parameters determined by fitting to experimental data. Mackensen et al. (2002) derived a model for reciprocating, screw, and scroll compressors. The model is here again based on a polytropic process and volumetric efficiency. An efficiency factor was found to be necessary and is a function of the operating conditions.

A formulation found throughout the semi-empirical compressor modeling literature is presented in Winandy et al. (2002*b*). The model captures bulk phenomena occurring throughout the refrigerant evolution from suction to discharge stub of a scroll compressor. It incorporates heat transfer acting on the suction and discharge gas flows, and heat transfer coefficients are fit to data. The model represents the compression process in two steps; isentropic to the built in volume ratio then adiabatic and isochoric to the discharge pressure. This model has been adapted to capture reciprocating compressors Winandy et al. (2002*a*), rolling piston compressors Moli-

naroli et al. (2017), screw compressors Giuffrida (2016), liquid and vapor injected scroll compressors Winandy and Lebrun (2002), and oil flooded scroll compressors James et al. (2016).

In addition to semi-empirical modeling, recently, machine learning based approaches have been used for compressor performance prediction in HVAC&R systems. Ziviani et al. (2018) studied ANN performance applied to positive displacement compressor and expanders. Ledesma et al. (2015) predicted reciprocating compressor performance using an ANN and proposed an iterative algorithm to change the number of neurons in the hidden layer until a leveling of the mean squared error (MSE) occurs, which sets the minimum number of neurons needed. Ma et al. (2020) proposed a compressor mapping methodology to inform training data selection used during the ANN development. Points were added to the training data based on which points exhibited the highest absolute percentage error (APE) between ANN prediction and experimental data. Wan et al. (2021) applied multiple machine learning techniques including convolution neural networks, deep neural networks, random forest, and support vector regression to predict mass flow rate and power for transient and steady state compressor performance. Other studies found in literature applying machine learning to HVAC&R compressor modeling include Sanaye et al. (2010) who predicted rotary vane compressor performance, Yang et al. (2009) predicted scroll, screw, and reciprocating performance, Barroso-Maldonado et al. (2017) predicted reciprocating compressor performance, and Zendehboudi et al. (2017) modeled variable speed scroll compressors with vapor injection.

After developing a model that sufficiently predicts a compressors performance, some researchers have evaluated model accuracy at conditions extending beyond their training data (extrapolation). Li (2012) presented semi empirical model for hermetic scroll and reciprocating compressors with a focus on extrapolation. Conditions where the saturated suction temperature is 10°C or the saturated discharge temperature

is 15°C away from data points used for parameter fitting showed an accuracy of 5%. Jahnig et al. (2000) finds that their model extrapolates within 5% error with condensing and evaporating temperatures that extend training data by 10°C. Aute et al. (2015) examined five compressor models, Jahnig et al. (2000), Qiao et al. (2014), Navarro et al. (2007), the AHRI formulation AHRI (2020), and a variation of the AHRI method. The models were tested at different superheat values than that of the training data used to fit model parameters. It was found AHRI method performed best at power prediction, while other models were unusable for power prediction. The corrected AHRI model using Dabiri and Rice (1981) performed best at mass flow prediction. The main limitation of the study was it used data from compressor data sheets, which are often generated from the AHRI map and likely to bias the results.Cheung et al. (2018) estimated compressor map (AHRI (2020)) uncertainty to explain inaccuracies in mass flow rate and power prediction in extrapolation scenarios. Further, Cheung and Wang (2018) uses the same method to test five semi-empirical compressor mass flow rate formulations. The authors find that redundant coefficients whether empirical or physical reduce model accuracy in extrapolation scenarios.

The present work aims to fill a gap in literature by evaluating select semi-empirical compressor models at extrapolation and modulation scenarios with multiple different compressor technologies using high-fidelity, experimental, compressor performance data to train the models and quantify performance. The present study differs from the studies in the above paragraph in that Li (2012) and Jahnig et al. (2000) use only reciprocating compressors and Cheung and Wang (2018) uses only scroll compressors. Aute et al. (2015) uses some data generated by the AHRI model, where this study aims to use only experimental data.

1.2 Feasibility Study

In an attempt to find compressor models that span the entire range of compressor types operating in vapor compression cycles, a small survey of centrifugal compressor modeling literature was done. The systems that models applied centrifugal compressor modeling to focused on automotive, oil and gas, chiller applications Brondum et al. (1998), air compressors for PEM fuel cells Zhao et al. (2017), and some experimental research of an Organic Rankine Cycle driven centrifugal compressors operating in a refrigeration cycle Demierre et al. (2015). The majority of models in this survey did not apply directly to refrigeration and heat pump applications; which a review paper by Fang et al. (2014) helps establish. The study looks into empirical models in the literature for HVAC&R simulation, but found that most models exclusively apply to the automotive sector. The accuracy of these automotive models applied to HVAC&R centrifugal compressor modeling is limited and accurate modeling remains a problem unsolved, as stated by the authors and described further below. The following descriptions are from the most relevant papers covered in the dynamic compressor model search.

Kurz (2004) presented a paper on the physics of centrifugal compressor operation with topics including: the thermodynamics of gas compression, the aerodynamics of centrifugal compressors, and important subsystems such as seals and surge control. The author presents the first and second laws of thermodynamics together with basic laws of fluid dynamics to describe the fundamental working principles of centrifugal compressors. Bernouli's law and Euler's law are used to model the fluid flow through the compressor and a general description of the surge, stall, and choke phenomena is given. The paper does not present one overall model to describe centrifugal compressor performance, but instead presents major laws of physics to help understand the working principles. As mentioned above Fang et al. (2014) produced a review study

on the empirical models for efficiency and mass flow rate of centrifugal compressors. They found that most empirical models only exist for automotive turbochargers and no such empirical models exist for refrigeration compressors. Eleven mass flow models and eight efficiency models are evaluated with each one needing coefficients fitted from experimental data. A test rig for an air cycle refrigeration system is set up for model validation. The study ranks the top three models for accuracy based on a mean average deviation for mass flow rate and efficiency. It is found that accurate models remain a problem unsolved for refrigeration centrifugal compressors. Zhao et al. (2017) studied semi physical modeling and control of a high speed centrifugal compressor for the air feeding of a polymer electrolyte membrane fuel cell. In this model the dynamics of mass flow, pressure, and efficiency are presented. Parameter estimation via interior point estimation is used to estimate the seven empirical coefficients for the model. The model is validated against measured data and yielded efficiency root mean squared errors of 5.1%, 6.2%, 7.2%, 7.6% at speeds of 200, 230, 260, and 280 krpm. The mass flow rate error was not quantified. The compressor model is implemented into an overall fuel cell model exhibiting good performance according to the authors. Popovic and Shapiro (1998) performed a modeling study on a centrifugal compressor in a navy ship chiller application. The authors develop a model that predicts mass flow, exit temperature, and power consumption. It uses blade angles, Euler's equation, a slip factor, and two empirical relations in its formulation. The model was not accurate yielding $\pm$ 20% and $\pm$ 15% accuracy for mass flow rate and power consumption. The outlet compressor temperature was found to be $\pm$ 3 F of measured data. The model seems to be refrigerant dependent which is a shortcoming, but the authors state that a variable slip factor, more detailed diffuser model, and more complete operational data would improve the model. Mass flow rate was not measured making the validation data less valuable. Braun et al. (1987) describes a mechanistic compressor model for a variable speed capacity controlled

centrifugal chiller. The model uses conservation of mass, momentum, and energy along with some empirical relations to describe power consumption. The approach utilizes velocity triangles, a dimensionless flow coefficient, a theoretical work coefficient, a polytropic process, and isentropic efficiency and polytropic work coefficient as a function of dimensionless flow coefficient. The last two coefficients are empirically fit to performance data of vaneless centrifugal compressors from studies by Weisner and Caswell (1959), Weisner (1960). The RMS difference between measured and modelled performance is 85 kW for power. The model was implemented into an overall chiller model for system simulation and performance evaluation with different refrigerants.

This section is presented to discuss combining the models that describe the two technologies, centrifugal and positive displacement, into one. To do that requires performance variables within the models to overlap with the physical parameters describing both dynamic and positive displacement compressors. It is worth noting that a valuable metric, volumetric efficiency, does not apply to describing dynamic compressor performance because, unlike a positive displacement machine, a dynamic machine uses the increase in momentum of a fluid control volume to generate pressure rise. A positive displacement machine isolates a control volume and reduces the volume of said control volume. Therefore, an important performance metric for positive displacement machines is not used in the analysis of a centrifugal machine at all.

A major difference in the fluid flow through a dynamic compressors verses positive displacement is the aerodynamic phenomena known as surge, stall, and choke that can occur in a centrifugal machine. These instabilities are not generally found or accounted for in positive displacement compressor modeling. Models that estimate this are of value for dynamic compressors, which are typically selected to operate in a region that is most efficient for that compressor and far from the stall or surge lines. Variable operating conditions can affect the efficiency greatly and push the compressor toward surge or choke.

A general thermodynamic description of the processes occurring in a compressor seemed initially promising to describe both dynamic and positive displacement machines. This is because isentropic efficiency, polytropic efficiency, and adiabatic efficiency can be found with the same parameter inputs that are found in positive displacement and dynamic compressors. Temperature, pressure, specific heat, entropy, enthalpy, polytropic exponent, and other variables are used as inputs. These all can be used to estimate the power requirement of a compressor based on the energy required to achieve desired outlet state, i.e., discharge pressure and temperature. However, a main difference in the characterization of a centrifugal compressor verses a positive displacement compressor is in the formulation of non-dimensional flow coefficients to describe the fluid flow. The mass flow rate for dynamic compressors usually involves blade tip speeds, impeller radius, rotational speed, and slip factors. In Popovic and Shapiro (1998) the isentropic efficiency is empirically related to the guide vane angle and the dimensionless enthalpy is plotted as a function of the flow coefficient for the compressor. These parameters, guide vane angle and dimensionless enthalpy do not exist for positive displacement performance description. The closest metric to the flow coefficient is volumetric efficiency, which as mentioned above cannot be extended to represent dynamic compressors.

Developing a model that combines both dynamic and positive displacement technologies requires a single set of model parameters to be similar in nature. That is, the physics, or more precisely, the inputs to the models need to be similar. Overall modeling of the two compressor types together necessitates the inputs and outputs to be the same or very close. To illustrate some of the major differences between performance characterizing variables, Table 1.1 and 1.1 show model parameters taken from Zhao et al. (2017) to represent dynamic compressor performance and some generic performance characterizing variables from Rasmussen and Jakobsen (2000) to represent positive displacement compressor performance. Additionally, they indicate if the

variable is an input or an output to the model.

Table 1.1: Displaying different metrics and variables for positive displacement and dynamic compressor types

Variable	**Input / Output**	**Technology Described**
Isentropic Eff.	Output	Both
Adiabatic/Thermal Eff.	Output	Both
Clearance Volume Eff.	Output	Positive Displacement
Polytropic Eff.	Output	Both
Mechanical Eff.	Input/Output	Both
Volumetric Eff.	Output	Positive Displacement
Leakage	Output	Both
Power Consumption	Output	Both
Mass Flow Rate	Output	Both
Fluid Temperature	Input	Both
Fluid Pressure	Input	Both
Polytropic Exponent	Input	Both
Pressure Ratio	Input	Both
Clearance Volume	Input	Positive Displacement
Displaced Volume	Input	Positive Displacement
Displacement Rate	Input	Positive Displacement
Volume Ratio	Input	Positive Displacement

Table 1.1 illustrates that the modeling approaches overlap in a few basic areas, such as efficiencies, however as mentioned above the output of mass flow rate is found using variables that do not overlap with description of the physics of the two technologies. Displacement rate, volume ratio, and swept volume all play into the description

Table 1.2: Displaying different metrics and variables for positive displacement and dynamic compressor types

Variable	**Input / Output**	**Technology Described**
Valve pressure drops	Output	Both
Lubricant properties	Input	Positive Displacement
Volumetric flow rate	Output	Both
Rotational Speed	Input	Both
Torque	Input	Both
Blade angles	Input	Dynamic
Inlet vane angle	Input	Dynamic
Mach number	Input	Dynamic
Impeller Radius	Input	Dynamic
Slip coefficient	Input	Dynamic
Plenum Volume	Input	Both
Stagnation Sonic Velocity	Input	Dynamic
Inertia of Compressor	Input	Dynamic
Specific Heat Ratio	Input	Both
Fluid Friction coefficient	Input	Dynamic
Area of impeller eye	Input	Dynamic
Mean Inducer Radius	Input	Dynamic

of mass flow rate for positive displacement machines and these have no meaning in describing a dynamic compressor. Similarly, blade angle, slip coefficient, impeller radius, and inlet vane angle all are used in modeling the mass flow of a dynamic compressor, but have no meaning in describing a positive displacement compressor. The tables, Table 1.3 and Table 1.4 model is used to further illustrate some key differences

between modeling the positive displacement and dynamic compressor technologies. The tables show model inputs to a positive displacement model and a dynamic model. It is noteworthy that the same authors produced the two studies. One is Popovic and Shapiro (1995) and the other is Popovic and Shapiro (1998) the first being a positive displacement model of a reciprocating compressor and the second being a study pertaining to centrifugal compressor modeling. Table 1.3 shows some of the inputs to the centrifugal study.

Table 1.3: Summary of Inputs from Popovic and Shapiro (1998) dynamic model

Variable	**Type**	**Symbol**
Compressor Shaft Speed	Input	ω
Inlet / Outlet impeller radii	Input	r_1,r_2
Inlet Guide Vane angle	Input	α
Inlet / Outlet Vane tips angles	Input	β
Refrigerant inlet state	Input	P_1,T_1
Impeller and Diffuser exit areas	Input	A_2,A_3
Blockage Factor	Input	k_B
Impeller Slip Factor	Input	σ
Exit Pressure	Input	P_2
Exit Enthalpy	Input	h_2
Mass Flow Rate	Input	$\dot{m}$

It is noted that the mass flow rate of the system is an input into this centrifugal model. That is not at all helpful to the present study, but the inputs still show major differences between dynamic and positive displacement modeling approaches. Slip factor, blockage factor, vane tip angles, impeller angles and diameters, and guide vane positions all have no physical relevance applied to a positive displacement compressor. Table 1.4 displays the inputs to the positive displacement compressor model.

Table 1.4: Summary of Inputs from Popovic and Shapiro (1998) positive displacement model

Variable	**Type**	**Symbol**
Refrigerant inlet state	Input	P_1,T_1
Refrigerant outlet pressure	Input	P_2
Clearance volume / factor	Input	C
Motor speed	Input	ω
Polytropic exponent	Input	n
Effective suction pressure drop	Input	ΔP_{suc}
Effective discharge pressure drop	Input	ΔP_{dis}
Heat Transfer loss coefficient	Input	HT_{loss}

When looking at the inputs for this modeling approach, the variables do not match up well. The study using the inputs in Table 1.4 has the clearance factor as a fundamental starting point for mass flow rate modeling. This parameter has no physical meaning describing a dynamic compressor. This makes it very difficult to combine a model when the first mathematical description of one machine, positive displacement, does not describe any characteristic of the other, dynamic, whatsoever. The effective suction and discharge pressure drops can be related to a dynamic machine, such as the pressure drop as the fluid flows over the inlet guide vanes. The exit pressure drop could be related to the pressure drop occurring when the fluid exits the diffuser and enters the discharge lines. These variables can be related to the different phenomena occurring in compressors, but actually modeling them requires a different characterization of the flow and machine. As mentioned before, the blade angles, slip coefficients, etc., all describe dynamic modeling and have no meaning in a positive displacement machine.

Power consumption modeling in the Popovic and Shapiro (1998) centrifugal study

is a simple function of mass flow and the exit state. The model calculates the mass flow and exit state, and from there the power consumption is found. Relating the mass flow rate and exit state to the power is a good idea, provides simple formulation, and may lessen computational time because of fewer equations. But, as mentioned previously, the mass flow rate derivations are found in very different ways.

In conclusion of the feasibility analysis the fluid mechanics that describes mass flow rate is fundamentally different in the two machines. The physics used to capture mass flow rate behavior in dynamic compressors as compared to positive displacement is different because at the core, pressure energy is generated in entirely differently ways. The flow parameters seem like they could be implemented into a computer program where the user specifies the type of compressor and the program run the appropriate code. However, it would be difficult to derive an equation that describes the mass flow rate of a dynamic and positive displacement compressor utilizing the exact same input terms to describe both. It is easy to think of a formulation where a certain part goes to zero when a centrifugal compressor is selected and the rest of the equation describes positive displacement and vice versa. But the goal of this analysis was to determine if it is possible to come up with a single semi-empirical formulation to describe both technologies. There is also a balance in the semi empirical terms that are determined from experimental data. The dynamic compressor cannot constitute a majority of all the terms that need determined and neither should the positive displacement description. From here semi-empirical compressor models used for predicting positive displacement performance are selected exclusively. Model selection criteria and descriptions follow in the next section.

CHAPTER II

MODEL SELECTION CRITERIA AND DESCRIPTIONS

It is infeasible to formally evaluate all of the variants of compressor models presented here, therefore a subset is selected to encapsulate the general model types and solution modalities. A model that will successfully enable modulation and extrapolation use cases also needs to meet basic performance criteria.

2.1 Selection Criteria and Selected Models

This criteria includes accuracy of 5% or better compared against experimental results, computational speed that is insignificant with modern computers, once trained, and as little proprietary information as possible about the compressor. Lastly, it is desired that a model be applicable to multiple compressor technologies, or at minimum, show potential applicability to others through capturing high-level physics present in the machines. This criteria provided a basis for quantitative and qualitative preliminary selection of models, which resulted in the selection of five models.

The first model is used to baseline the results as the industry-standard approach for system modeling and presentation, AHRI (2020). This model has documented limitations in both extrapolation and modulation modalities but will serve as a basis of comparison. The second model is an Artifical Neural Network (ANN) which has recently shown promise as a black-box alternative for compressor mapping Ma et al. (2020). Another black-box approach by Shao et al. (2004) was selected due to its inclusion of modulation and high-accuracy. Popovic and Shapiro (1995) is a gray-box

model selected due to its inclusion of a thermodynamic reference process and good accuracy. Finally, the Winandy et al. (2002*b*) model is selected because of is high accuracy and high-level of physical phenomenon included. Both Popovic and Shapiro (1995) and Winandy et al. (2002*b*) have not been evaluated in the extrapolation and modulation modalities but the increased physics fidelity made them promising for this study.

2.2 Selected Model Descriptions

This section will provide detailed technical description of each of the five compressor models selected for evaluation. This is split into a baseline model, the AHRI 10-coefficient map AHRI (2020), and four models or approaches from literature, the Artificial Neural Network (ANN) and Shao et al. (2004), Popovic and Shapiro (1995), Winandy et al. (2002*b*). While a compressor model has a large quantity of desired outputs they each need to predict compressor mass flow and power, most fundamentally. Therefore, the descriptions presented will focus on how each model are developed to predict those parameters. All models were codified into the Python programming language.

2.2.1 Baseline Model - AHRI Model

The AHRI model, coming from AHRI (2020), is a mathematically simple third order curve fit with 10 coefficients. While it can be reflected in many forms, most fundamentally it can be presented as functions of mass flow and power. The mass flow rate and power are fit separately as a function of evaporating and condensing temperatures. This results in two equations for performance prediction. The method is very accurate with respect to the data it is fitted to Aute et al. (2015). The computational burden is minimal and requires almost no information about the compressor. It's used extensively in the HVAC&R industry for system level modeling, therefore it is

Table 2.1: Equation used for mass flow rate and power prediction in the AHRI model.

AHRI Formulation
$X = C_1 + C_2T_s + C_3T_d + C_4T_s^2 + C_5T_sT_d + C_6T_d^2 + C_7T_s^3 + C_8T_s^2T_d + C_9T_sT_d^2 + C_{10}T_d^3$

used as a baseline for comparison in the present study. The equation found in Table 2.1 is given by the standard where X is the power input or mass flow rate, T_s and T_d are the suction and discharge dewpoint temperatures, respectively, and C_1-C_{10} are coefficients determined from least squares regression.

In this formulation both mass flow rate and power are fit resulting in 20 total coefficients tuned to data. Once these are known, the model takes inputs of suction and discharge dewpoint temperatures for performance prediction. This model requires no compressor specific information in order to run.

2.2.2 Artificial Neural Network Model

The ANN modeling approach is black-box in nature and is composed of nodes and layers which take numerical inputs. The model formulation requires data to inform an optimization algorithm which adjusts weights and biases within the network based on backpropagation of error determined by a loss function. The optimization algorithm and loss function used for this work were the Adam optimizer, Kingma and Ba (2015), and the MAPE or Mean Squared Error (MSE). These yielded sufficient results during model development. The present study uses evaporating, condensing, suction temperatures, and compressor speed as inputs to the network while mass flow rate and power are outputs. Fully connected dense neural networks are implemented. Each model has one input layer, two hidden, and one output layer. One exception is the model predicting twin screw performance, it had 3 hidden layers. To keep

Table 2.2: Important parameters used during ANN model development

Parameter	Value
Machine Learning Package	Tensorflow 2.5.0
Inputs	4
Outputs	2
Layers	2
Nodes per Layer	10
Activation Function	Rectified Linear
Optimizer	Adam

order of magnitudes for inputs similar, all inputs were normalized between 0.1 and 0.9, Ma et al. (2020). The rectified linear activation function, which sends negative input values to zero and retains the value for positive inputs was chosen for this work. Model formulations are codified in the Python programming language. An open source machine learning package developed by Google, Tensorflow Abadi et al. (2016), is used to initialize, compile, fit, and evaluate models. Data used for model development is split randomly as 80% training data and 20% validation data. To keep the algorithm from overfitting the data, the validation loss metric is monitored via callbacks during training and analyzed visually at the conclusion of a training run. Table 2.2 summarizes the neural network architecture utilized in this study.

2.2.3 The Shao Model

The Shao Model from Shao et al. (2004) is a black-box model that utilizes performance data at different operational frequencies to capture modulation. The equations for mass flow and power are second order functions of evaporation and condensing temperatures. They need six coefficients tuned to data. The variable speed data is

used to fit a second order function to mass flow rate and power ratio. These ratios relate the mass flow and power at the base frequency to performance at different frequencies. The models functional form for mass flow rate, mass flow rate ratio, power, and power ratio are given in Table 2.3.

Table 2.3: Formulations that need tuning in the Shao Model formulation.

Parameter	Equation to be fit
Mass Flow Rate	$a_1 T_c^2 + a_2 T_c + a_3 T_c T_e + a_4 T_e^2 + a_5 T_e + a_6$
Mass Flow Rate Ratio	$c_1(f - f^*) + c_2(f - f^*) + c_3$
Power	$b_1 T_c^2 + b_2 T_c + b_3 T_c T_e + b_4 T_e^2 + b_5 T_e + b_6$
Power Ratio	$d_1(f - f^*) + d_2(f - f^*) + d_3$

In total, there are 18 coefficients needed to run the model. The mass flow rate, power, mass flow rate ratio, and power ratio coefficients are: $a_1 - a_6$, $b_1 - b_6$, $c_1 - c_3$, and $d_1 - d_3$ respectively. The first two coefficient sets (a and b) are fit via least squares regression to T_e and T_c, evaporating and condensing temperature, respectively. The last two sets (c and d) are fitted as functions of compressor frequency, f, and nominal frequency f^* to the mass flow and power ratios. Each equation is fit via least squares. The model inputs are evaporating temperature, condensing temperature, and compressor frequency. There is no compressor specific information needed to run the model. However, with respect to training data, there must be at least three data points measured at variable speed operating conditions to fit the mass flow rate and power ratio equations.

2.2.4 The Popovic and Shapiro Model

The Popovic and Shapiro model from Popovic and Shapiro (1995) is a semi-empirical compressor derived to predict reciprocating compressor performance. The model utilizes an idealized polytropic compression and clearance volume re-expansion with constant pressure suction and discharge processes. This cycle is modified to include phenomena typical to a compressor. This includes utilizing volumetric volumetric efficiency, based on a clearance factor taken as an unknown. The authors then add suction and discharge pressure drop and, for simplicity, set the magnitudes equal. The model utilizes the thermodynamic work rate of a polytropic process as a basis for compressor power requirement. It splits the compressor into three control volumes, a compressor control volume, and two internal control volumes, the motor and the cylinder. Table 2.4 shows the equations for mass flow rate and power consumption used in the model. The mass flow formulation uses the piston displacement rate (RPD), the rotational speed (RPM), the clearance factor (C), suction and discharge pressure (P_{suc}, P_{dis}), suction specific volume (v_{suc}), and the polytropic exponent (n) to predict mass flow. The power formulation uses the mass flow rate ($\dot{m}$), suction and discharge enthalpies (h_{in}, h_{out}), the polytropic work rate ($\dot{W}_{cal}$), and the heat transfer loss coefficient (B_1+B_2 $\dot{Q}_{cyl}$), which is fit to cylinder heat loss ($\dot{Q}_{cyl}$) to predict power consumption.

The heat transfer loss coefficient expression needs two coefficients tuned to data while the polytropic exponent expression needs three. The constant pressure drop term and clearance factor are fitted to data yielding 7 total parameters determined derived data. Once these are known, four inputs are needed to run the model; refrigerant inlet state, outlet pressure, motor speed, and the piston displacement rate. It must be noted that training data for this model must include discharge temperature in order to fit the polytropic exponent expression.

Table 2.4: Popovic and Shapiro model mass flow rate and power formulations.

Parameter	Equation
Mass Flow Rate	$\frac{RPD * RPM}{v_{suc}}(1 + C - C(\frac{p_{dis}}{p_{suc}})^{\frac{1}{n}})$
Power	$\frac{\dot{m}(h_{out} - h_{in}) - \dot{W}_{cal}(B_1 + B_2\dot{Q}_{cyl})}{1 - (B_1 + B_2\dot{Q}_{cyl})}$

2.2.5 The Winandy Model

The Winandy model, presented in Winandy et al. (2002*b*), is a gray-box semi-empirical model derived to predict scroll compressor performance. The model defines an isothermal wall which delivers heat to the suction gas, removes heat from the discharge gas, absorbs electro-mechanical losses, and exchanges heat with ambient. The compression process is broken into two steps, 1) isentropic compression up to the adapted pressure, then 2) adiabatic and isochoric compression to discharge pressure. The adapted pressure represents the pressure during isentropic compression up to the internal volume ratio of the scroll wraps. The mass flow rate is predicted by using a swept volume taken as an unknown in the formulation, the rotational speed, and the suction specific volume evaluated after the suction heat transfer process. All heat transfers to or from the isothermal wall require heat transfer coefficients which are tuned to data. The overall power prediction is the sum of a compression power term, a constant electro-mechanical loss term, and another electro-mechanical loss

Table 2.5: Winandy model mass flow rate and power formulations.

Parameter	Equation	**Heat Transfers**
Mass Flow Rate	$\frac{NV_s}{v_{suc}}$	$\dot{Q}_{suc} = AU_{su}(T_{wall} - T_{suc})$
		$\dot{Q}_{ex} = AU_{ex}(T_{ex} - T_{wall})$
Power	$\dot{W}_{in} + \dot{W}_{loss} + \alpha\dot{W}_{in}$	$\dot{Q}_{amb} = AU_{amb}(T_{wall} - T_{amb})$

term which is proportional to the compression power. Table 2.5 shows the mass flow rate, power, and heat transfer formulations used within the model.

The model needs seven parameters tuned to data. These include the suction, discharge, and ambient heat transfer coefficients (AU_{su}), (AU_{dis}), (AU_{amb}) respectively, the fictitious swept volume (V_s), the volume ratio (ϵ), a work loss term ($\dot{W}_{loss}$), and finally a work loss coefficient (α). There are seven model inputs to calculate mass flow rate and power once the parameters are tuned which are: suction and discharge pressure, suction temperature, a reference mass flow rate, ambient temperature, rotational speed, and refrigerant. This model was codified in Python and applied the Nedler-Mead Nelder and Mead (1965) optimization algorithm to minimize the MAPE between model predicted mass flow rate and power and the data mass flow rate and power.

CHAPTER III

HIGH FIDELITY DATA COLLECTION AND METHODOLOGY

High-fidelity data measured from either a hot-gas-bypass load stand, compressor calorimeter, or a university lab environment was used to train each of the five models presented. The data sets were further used to explore model behavior against three data subsets focused on extrapolation, modulation (variable speed), and variable superheat. Performance data for four different compressor technologies; scroll, screw, reciprocating, and spool compressors are used with four working fluids, R134a, R401A, R1234ze(E), and R32 with a total of 434 data points collected. The compressor types, refrigerant, number of data points, collection standard, reference, and data splits are summarized in Table 3.1. The first three compressor types represent the most common technologies used in commercial and residential heating and cooling equipment today. The fourth technology, spool compressors, represent a novel compression technology that is still in the design optimization phase of development.

Table 3.1 highlights the 7 total data sets collected and used for model testing in this work. Each data set included performance data of the compressor at a variety of saturated suction and discharge temperatures at fixed superheat with measurements of compressor power and mass flow provided. Some of the data sets also included tests which varied the superheat and/or compressor speed/frequency.

Table 3.1: Information on the data sets collected.

Compressor Type	Capacity	Refrigerant	Data Points	Collection Standard	Reference	Splits
Spool	40 tons	R134a	58	ASHRAE 23.1	In House Data	4
Spool	40 tons	R1234ze(E)	44	ASHRAE 23.1	In House Data	4
Scroll	2.5 tons	R410A	196	ASHRAE 23.1	AREP #11	4
Twin screw	75 tons	R134a	13	ASHRAE 23.1	In House Data	2
Reciprocating	2 tons	R32	16	Not Mentioned	AREP #59	2
Scroll	–	R134a	48	Not Mentioned	Cuevas and Lebrun (2009)	3
Reciprocating	–	R134a	59	Not Mentioned	Li (2012)	3

3.1 Data Collection Sources and Standards

Data sets referenced as 'In House Data' came from experimental measurements collected at Oklahoma State University's (OSU) 10-80 ton hot-gas-bypass compressor load stand Schmidt (2018), Singleton et al. (2020). Sets labelled 'AREP' came from a 3 ton compressor calorimeter at the Heat Exchanger Advanced Testing Facility at Oak Ridge National Laboratory. The data collected at Oak Ridge was motivated by an initiative at AHRI called the Low-GWP Alternative Refrigerants Evaluation Program (AREP). Details of the data can be found in Table 3.1. Tests were conducted according to ASHRAE Standard 23.1, ASHRAE (2010) except AREP Report #59, which didn't state a collection standard. Scroll and reciprocating performance data was collected at the Oak Ridge facility while the spool and screw compressor performance originated from OSU's facility. This is additionally summarized in Table 3.1. The scroll compressor utilizing R134a was tested using a calorimeter test bench and the location and testing standard is not mentioned. The swash plate reciprocating compressor utilizing R134a data is from an automotive air-conditioning test

facility at the University of Illinois at Urbana-Champaign and a testing standard is not mentioned.

3.2 Data Subsets (Splits)

Each data set was collected in bulk and had to be split into subsets (splits) for model capability testing. The full data set includes all variations, including testing at various saturated suction temperature, saturated discharge temperature and variable superheat and/or speed/frequency. Baseline data was split from the full data set to include fixed superheat and frequency data. From this two subsets were formed. A training data set to train model parameters with and an extrapolation data set used for testing models at extrapolation scenarios. From the full data set, variable speed and variable superheat data subsets were formed to test the modulation and variable superheat performance of the models. Each full data set collected is somewhat unique in its operating envelope and parameters varied, therefore the number of splits is unique. For example, the data set for the reciprocating compressor utilizing R32 did not include variable superheat or variable speed data. Hence, there are only two splits shown in Table 3.1, these are the training set and extrapolation set. The next sections will describe further the underlying principles of the decision making processes to make the splits.

3.2.1 Baseline and Training Data Sets

Baseline data was split from the full data set to include nominal conditions with respect to the degree of superheat and compressor speed. This data set has in it various saturated suction/discharge temperatures at fixed superheat and compressor speed/frequency. Only the saturated suction/discharge temperatures vary within the baseline data set. Training data points are selected as interior points with respect to the overall envelope present within a data set. These points can be considered

to live in a smaller envelope within the entire envelope present within a data set. Additionally, an extrapolation data set is formed such that all data points are exterior to the training points. These points are used to evaluate extrapolation capabilities and include points at the bounds of the operating envelope present within a data set (*i.e.* most extreme saturated suction and saturated discharge temperatures). Ten data points total were selected as the training data set to train the models. Motivation for this number of training points stems from the AHRI model requirements for ten data points to tune its ten regression coefficients.

Constant Speed Training

Figure 3.1 shows the spool data set collected with R134a. The entire baseline data set (constant speed and superheat) is shown with the selected training data points and the selected extrapolation data points.

Figure 3.2 shows the methodology for selection of constant speed training points. In this case all of the training points come from the baseline data set. The training points are at a constant speed and constant superheat where only the saturated suction and discharge temperatures vary.

Variable Speed and Superheat Training

Figure 3.3 shows the methodology for selection of variable speed and variable superheat training points. In this case, in addition to the data points at the interior envelope - two variable speed points and two variable superheat points are added into the training data set. The reason for these additional points is to ensure a model has seen points at different speeds and superheats before exposing it to the extrapolation, modulation, and variable superheat testing data sets, which are described in detail in Section 3.2.2.

These additional points are selected such that one point is above nominal speed

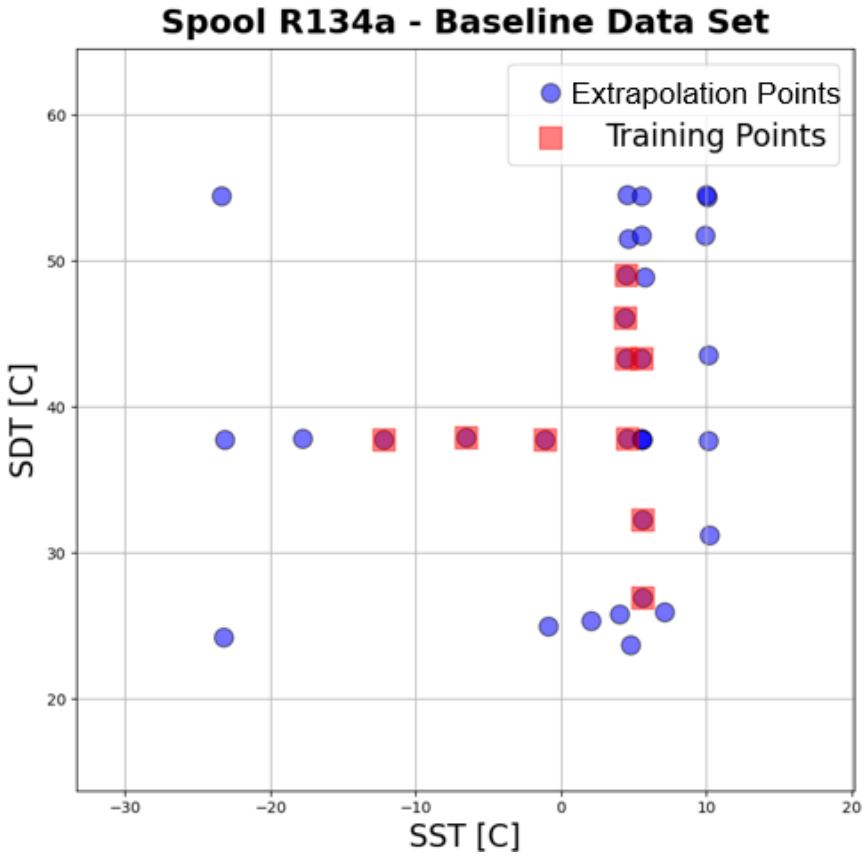

Figure 3.1: Spool R134a data showing points used to train the models and test points used for extrapolation capability testing

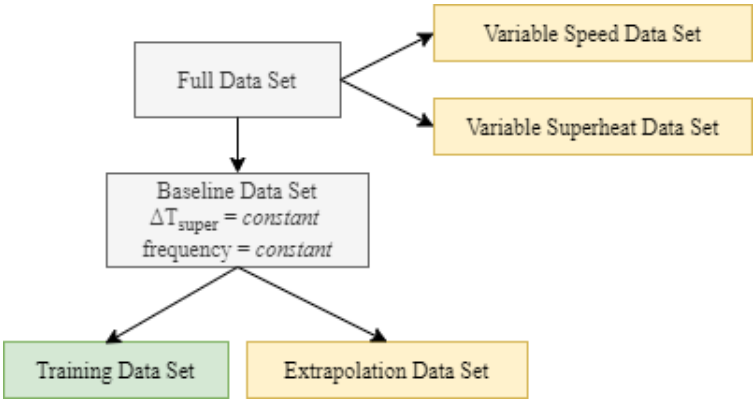

Figure 3.2: Flow chart showing data splits with constant speed training

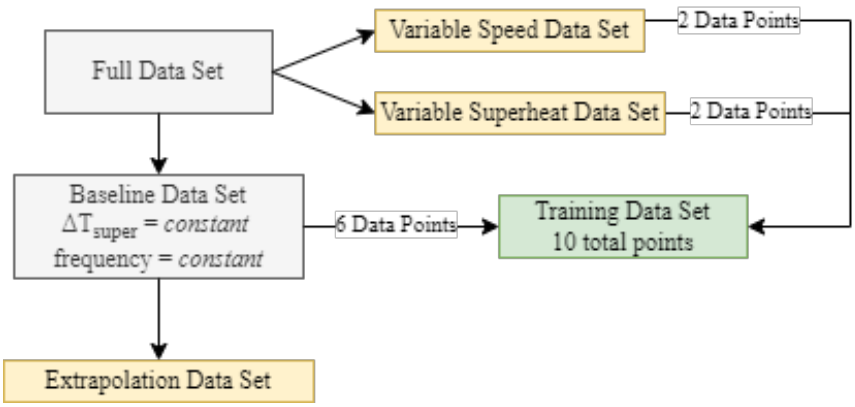

Figure 3.3: Flow chart showing data splits with variable speed and superheat training

and superheat, while the other point is at conditions below nominal speed and superheat. For instance, the Spool compressor utilizing R134a operated at nominal speed of 54 Hz and the two additional training points for speed were at 49 Hz and 59 Hz. The nominal superheat for the data set was 11 K and one point above nominal, at 25 K, and one point below nominal, at 8 K, were selected and used within the training data set. It should be noted that variable speed data and variable superheat data is not present within all data sets collected, therefore when that case arises all training data points come from the baseline data set which contained data at constant speed and constant superheat.

3.2.2 Extrapolation, and Variable Speed/Superheat Data Sets

The extrapolation data set is a subset of the baseline data and includes saturated suction and discharge temperatures that extend beyond the envelope of the training data set. This varied based on compressor technology but extended the saturated suction and discharge temperatures by 10°C and 16°C, respectively, beyond the training envelope, at the most extreme.

The variable speed data was available for the spool with R134a and R1234ze(E), screw, scroll, and reciprocating compressors all using R134a. For the spool and screw compressors, the variable speed data set has a fixed saturated suction and discharge

temperature and superheat with variable operating speed/frequency. For the spool compressor 13 points had speed variation ranging from 1036 - 1790 rpm and for screw compressor there were 7 points with speed ranging from 4300 - 5700 rpm. The saturated suction/discharge and superheat for the compressors is 4 and 16 °C, and 11 K, 4 and 51 °C, and 5 K for the spool, and screw compressor, respectively. The scroll compressor utilizing R134a included 12 variable speed points with speeds ranging from 2100 to 4500 rpm at saturated suction temperatures ranging from 18 - 48 °C, saturated discharge temperatures of 64 - 100 °C, and superheat values ranging from 3 - 8 K. The reciprocating data using R134a included 37 variable speed points with speeds ranging from 1000 - 4000 rpm, at saturated suction temperatures ranging from -14 - 7 °C, saturated discharge temperatures ranging from 42 - 80 °C, and superheats ranging from almost saturated at 0.2 K, up to 23 K. It should be noted for this variable speed data set, the average superheat was 5 K, however it included two outlier superheat points with values of 16 and 23 K at 1000 rpm and 3000 rpm, respectively.

The variable superheat data sets were only available for scroll and spool compressors. The two spool compressor data sets combined have 12 points with fixed speed of 1640 rpm at constant saturated suction and discharge temperatures of 5 and 37 °C with superheats that vary 8 to 27 K. Additionally, 11 points have; fixed suction temperature of 11 °C, saturated suction temperatures ranging from -11 to 10 °C, constant saturated discharge temperature of 37 °C, superheats that vary 8 - 40 K, and a fixed speed of 1640 rpm. Lastly, there are four miscellaneous points at 25 and 33 K superheat, -1 °C and 7 °C saturated suction temperature, respectively, a 51 °C saturated discharge temperature, and again a fixed speed at 1640 rpm. The scroll data set has 64 points at 22 K superheat spanning the entire operating envelope at a constant speed of 3600 rpm. It also included 66 points spanning the envelope at constant suction temperature of 18 °C, with superheats spanning 5 - 30 K, and a

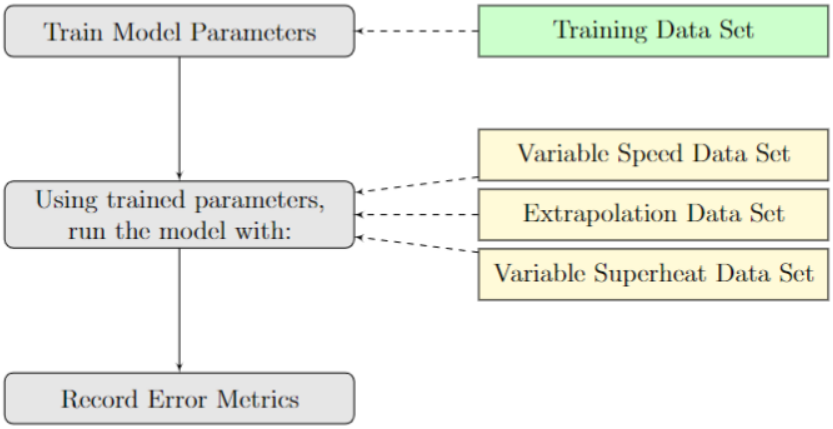

Figure 3.4: Flowchart showing an overview of semi-empirical model testing and data splits

fixed speed of 3600 rpm.

3.3 Model Testing Methodology

Figure 3.4 graphically describes the methodology utilized for this study. For each compressor technology, each of the five models are first trained using their accompanying training data set (which includes 10 points). The trained model is then compared against experimental data from the other three data subsets. The model performance is evaluated using the trained models ability to predict the various subsets of experimental data evaluated using the Mean Absolute Percentage Error,

$$MAPE_{\alpha} = \frac{100}{n}\sum_{i=1}^{n}\left|\frac{Y_{true,i} - Y_{predict,i}}{Y_{true,i}}\right| \tag{3.3.1}$$

where α represents either mass flow rate or power, n is the total number of data points in the data set, i is an individual data point, and $Y_{true,i}$ and $Y_{predict,i}$ are the measured data value and model predicted value, respectively, for mass flow rate or power at a given data point i.

CHAPTER IV

RESULTS

4.1 Constant Speed Training Results

The five models were tested at modulation and extrapolation scenarios following the methodology outlined in above with results presented in this section showing the models ability to predict mass flow rate and compressor power. The screw compressor results are not in shown in Table 4.1 because less than ten points in the set were available to train the models. Six points in the screw data set qualified as training data and therefore those were used to train the models. The AHRI model, requiring a minimum of ten points, could not be evaluated with the screw data available. Therefore, those MAPE values are not shown in Figure 4.1. The models which could be trained with the data yielded results shown in Table 4.1.

4.1.1 Baseline

Figure 4.1 gives two bar charts showing model performances at the training conditions for each data set. The Winandy model does not predict reciprocating compressor performance as shown by MAPEs greater than 15%. The model was derived for scroll compressors and performed under 5% MAPE for power and mass flow rate prediction when applied to spool, screw, and scroll compressor data. The Popovic and Shapiro model did not predict scroll compressor data showing MAPEs above 15%. The model was derived to predict reciprocating compressors, where it performed under 7% MAPE. The black-box models performed well showing a largest MAPE of

6.3% for the ANN at mass flow prediction for screw compressor data. These models showed MAPEs below 1% in 16 out of the 28 cases recorded with the AHRI model performing best overall at training data prediction. Table 4.1 shows MAPE values achieved for all models in numerical format. The mass flow rate error followed by the power error in parenthesis is given for every combination of model and compressor data. Excluding cases where a model didn't predict a certain compressor technology, the largest MAPE was 6.8 and 6.1 % for mass flow rate and power, respectively, coming from the Popovic and Shapiro model.

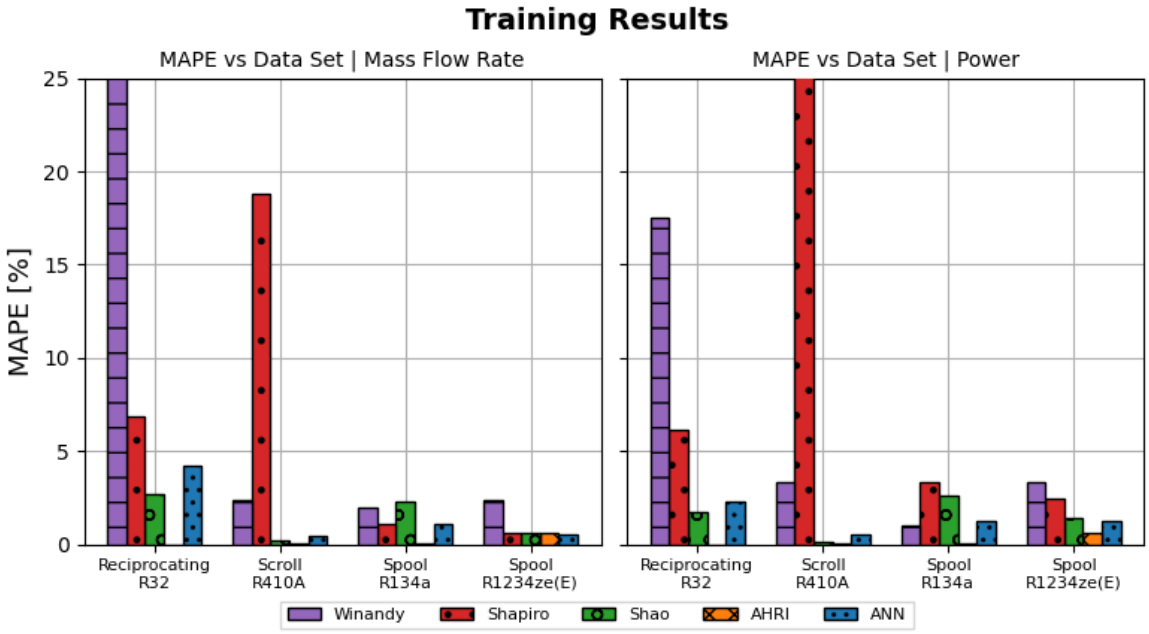

Figure 4.1: Training results at each data set for the five models

4.1.2 Modulation

Figure 4.2 represents the MAPEs of model predicted results for each of the models using the three modulation data sets. In Figure 4.2, the results show the Winandy, Popovic and Shapiro, and the Shao model capture mass flow rate at MAPEs less than 5%. This provides good indication that the aforementioned models could be used to predict mass flow rate at conditions outside that of their training data. The

Table 4.1: Model MAPE results for training data sets

	Model MAPE: Mass Flow Rate, (Power)									
Data Set	Winandy		Popovic & Shapiro		Shao		AHRI		ANN	
Recip. R32	26.5%	(17.3%)	6.8%	(6.1%)	2.7%	(1.7%)	1e-3%	(2e-3%)	4.3%	(2.3%)
Scroll R410A	2.4%	(3.4%)	18.8%	(159%)	0.2%	(0.1%)	6e-2%	(3e-2%)	0.4%	(0.5%)
Spool R134a	2.0%	(1.0%)	1.1%	(3.3%)	2.3%	(2.6%)	6e-2%	(4e-2%)	1.1%	(1.3%)
Spool ze(E)	2.4%	(3.4%)	0.6%	(2.4%)	0.6%	(1.4%)	4e-2%	(0.6%)	0.5%	(1.2%)
Screw R134a	1.2%	(0.6%)	0.2%	(0.2%)	0.1%	(0.4%)	n/a	(n/a)	6.3%	(4.1%)

Table 4.2: Model MAPE results for modulation (variable speed) data sets

	Model MAPE: Mass Flow Rate, (Power)									
Data Set	Winandy		Popovic & Shapiro		Shao		AHRI		ANN	
Spool R134a	3.1%	(2.0%)	2.3%	(4.5%)	3.6%	(2.5%)	20.7%	(20.2%)	19.9%	(19.1%)
Spool ze(E)	3.1%	(3.0%)	2.2%	(2.4%)	2.9%	(2.6%)	20.3%	(21.4%)	19.6%	(20.4%)
Screw R134a	1.7%	(0.7%)	1.1%	(0.4%)	0.8%	(2.6%)	n/a	(n/a)	25.2%	(20.6%)

ANN model produced mass flow rate errors around 20%. The errors achieved for the AHRI model are not shown on Figure 4.2 because, as mentioned before, the screw compressor data did have ten data points at constant superheat and speed to train the model's coefficients. The errors achieved for spool compressor mass flow rate using R134a and R1234ze(E) when running the AHRI model were 20.7% and 20.3%, respectively, as shown in Table 4.2.

For power prediction, Figure 4.2 shows MAPE values were similar to MAPEs achieved for mass flow rate for all models. The Winandy, Popovic and Shapiro,

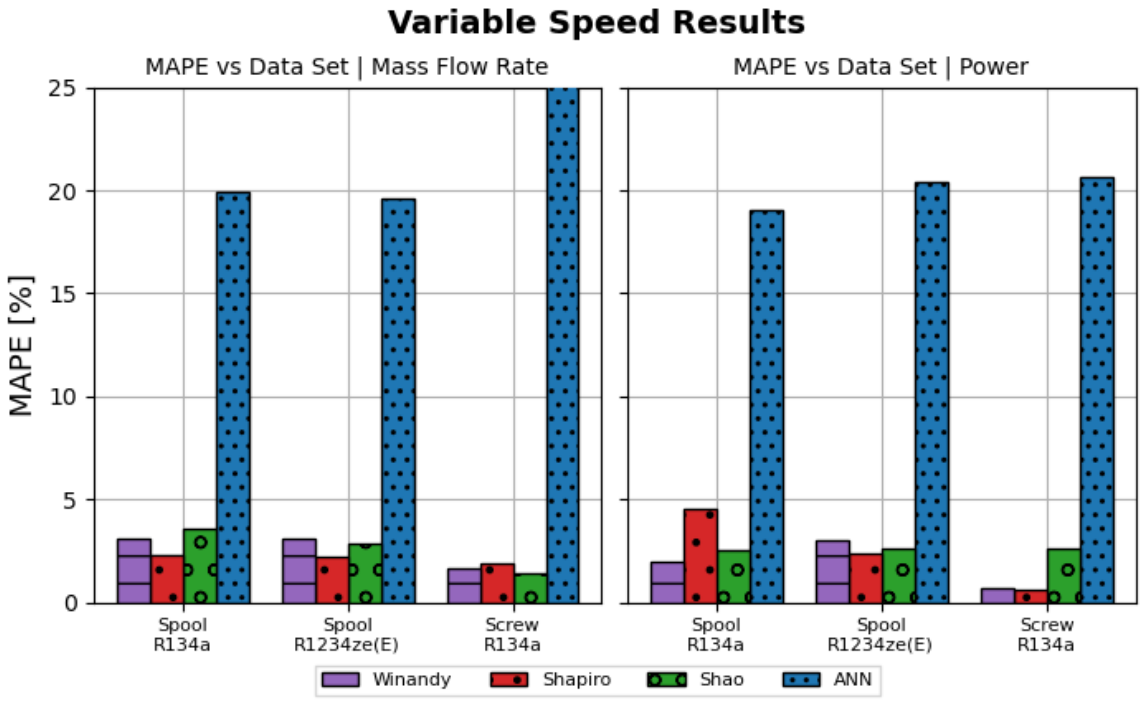

Figure 4.2: Mass flow rate and power results under modulation (variable speed) testing

and Shao model performed under 5% MAPE. The ANN model performs at MAPE's around 20% for power prediction when tested at modulation scenarios. The errors tabulated in 4.2 show the AHRI and ANN models in their present form are not adequate to predict modulation performance for compressors. During training of the ANN, points at variable speed conditions could be included to improve prediction, however the present work studied performance at precise training conditions to examine capabilities and record performance at conditions different to that of the training data.

4.1.3 Extrapolation

Figure 4.3 represents the MAPEs of model predicted results for each of the models using the extrapolation data sets described in Section 3.2.2 with results summarized in Table 4.3. Shown in Figure 4.3, extrapolation is captured by the semi-empirical mod-

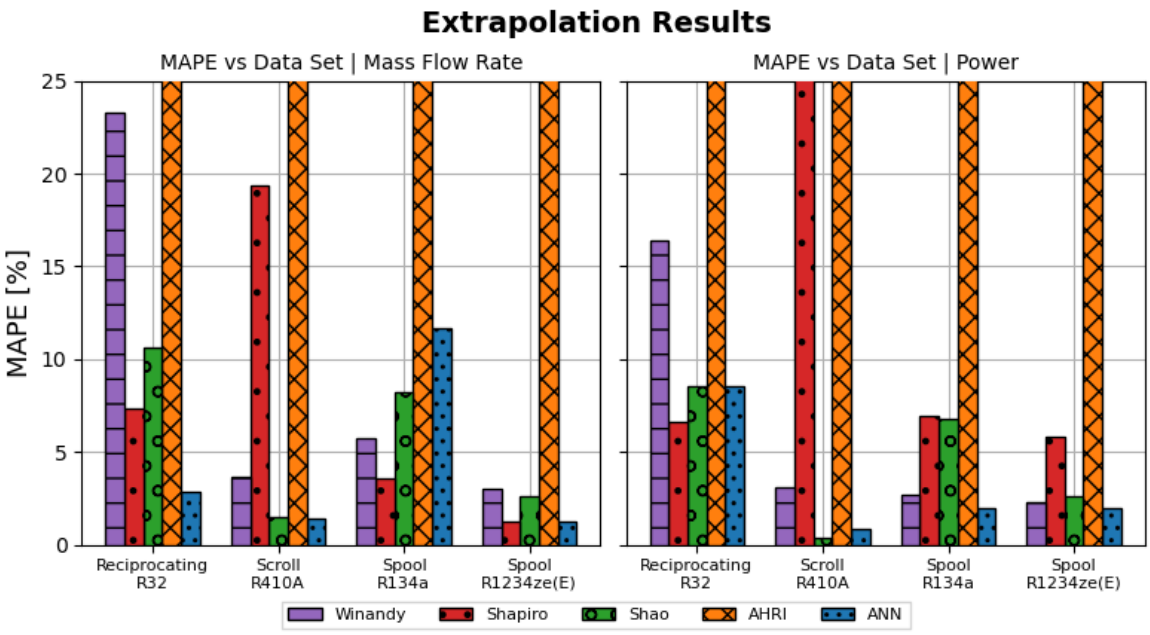

Figure 4.3: MAPE results at extrapolation conditions

els, given that they do predict the compressor technology. The Winandy model performs below 6% for the scroll and spool compressor technologies. The model extrapolated with two different refrigerant data sets for the spool compressor. The model did not capture reciprocating compressor performance. The Popovic and Shapiro model extrapolated below 8% MAPE for the compressor technologies that it predicted. This model however, did not capture scroll compressor technology but performed better at extrapolating spool compressor data than reciprocating data, the latter of which the model was derived initially to predict. The ANN model extrapolated below 3% except in the case of power prediction for the spool compressor utilizing R134a and mass flow rate prediction for the reciprocating compressor using R32. The Shao model performed well when ran with scroll and the spool R1234ze(E) data, however extrapolation errors rose to 8.2% and 10.7% for the reciprocating and spool R134a data respectively. The AHRI model did not perform adequately when extrapolating as can be seen by the errors rising from 45% to 7.0e+6%.

Table 4.3: Model MAPE results under extrapolation scenarios

	Model MAPE: Mass Flow Rate, (Power)									
Data Set	Winandy		Popovic & Shapiro		Shao		AHRI		ANN	
Recip. R32	23.3%	(16.4%)	7.3%	(6.6%)	10.7%	(8.6%)	45.1%	(27.5%)	2.9%	(8.5%)
Scroll R410A	3.6%	(3.1%)	19.3%	(3e3%)	1.5%	(0.4%)	6e5%	(9e5%)	1.4%	(0.8%)
Spool R134a	5.7%	(2.7%)	3.6%	(3.9%)	8.2%	(6.8%)	6e6%	(7e6%)	11.9%	(1.9%)
Spool ze(E)	3.0%	(2.3%)	1.2%	(5.8%)	2.6%	(2.6%)	4e6%	(6e4%)	1.3%	(1.9%)

4.1.4 Variable Superheat

Figure 4.4 shows model performance at variable superheat conditions with results summarized in Table 4.4. The data sets labeled Scroll 1 and Scroll 2 are the two variable superheat data sets described in Section 3.2.2. The first being at a superheat of 22 K, and second a constant suction temperature data set where superheat values range 5 - 30 K. The Winandy model performed at or below 5% for all variable superheat data sets. The Popovic and Shapiro model as mentioned before did not capture scroll performance which is the case here. The model performed better at mass flow prediction than power prediction at variable superheat with the highest error of 18.7% for the spool compressor utilizing R1234ze(E). The opposite is true for the ANN model which performed better at power prediction than mass flow rate for all data sets. The model did not predict below 18% for mass flow rate, while all errors in power prediction were below 6%. The AHRI model performed worst overall with errors ranging from 3e+5% to 2e+6%.

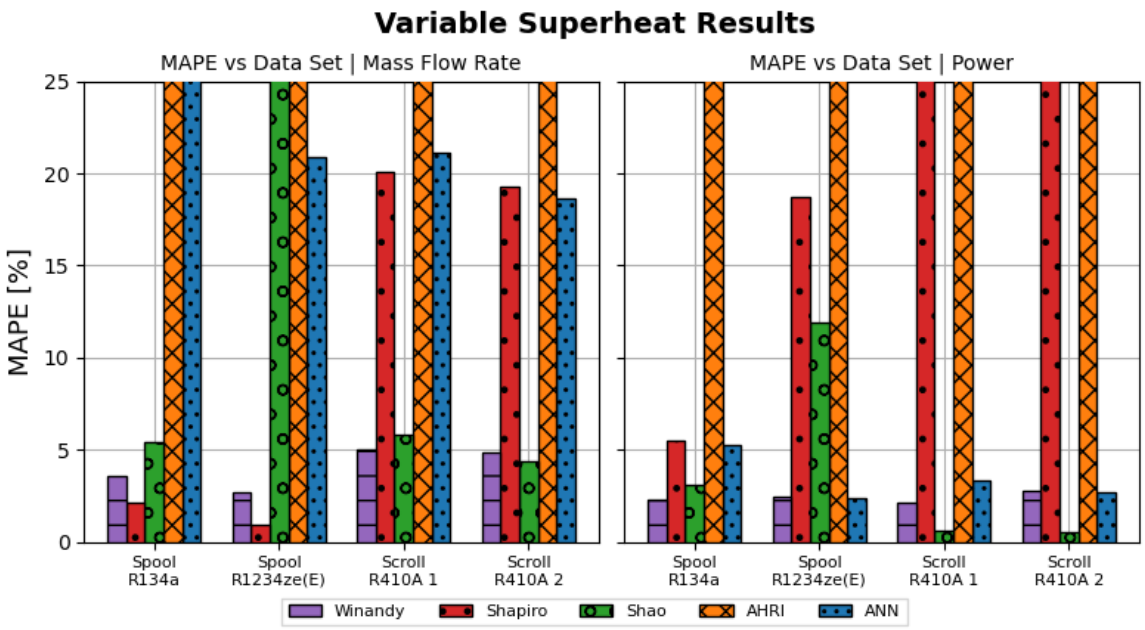

Figure 4.4: Mass flow rate MAPE results at variable superheat conditions

Table 4.4: Mass flow rate results for variable superheat scenarios.

	Model MAPE: Mass Flow Rate, (Power)									
Data Set	Winandy		Popovic & Shapiro		Shao		AHRI		ANN	
Spool R134a	3.6%	(2.3%)	2.1%	(5.5%)	5.4%	(3.1%)	3e5%	(6e5%)	25.5%	(5.3%)
Spool ze(E)	2.7%	(2.5%)	1.0%	(18.7%)	42.2%	(11.9%)	6e7%	(2e6%)	20.9%	(2.4%)
Scroll 1	5.0%	(2.2%)	20.1%	(232%)	5.8%	(0.6%)	7e5%	(9e5%)	21.2%	(3.3%)
Scroll 2	4.9%	(2.8%)	19.3%	(372%)	4.4%	(0.5%)	7e5%	(9e5%)	18.6%	(2.7%)

4.2 Variable Speed Training Results

The five models were tested at modulation and extrapolation scenarios following the methodology outlined in Section 3.2.1 with results presented in this section showing each models ability to predict both mass flow rate and compressor power.

4.2.1 Baseline

Table 4.5: AHRI model results for mass flow rate and power for each data set and their associated subsets.

	AHRI Model MAPE's: Mass Flow Rate, (Power)							
Data Set	Training		Extrapolation		Variable Speed		Variable Superheat	
Spool R134a	6.0e-2%	(4.0e-2%)	6.0e8%	(6.7e8%)	20.7%	(20.2%)	2.9e7%	(5.8e7%)
Spool ze(E)	0.43%	(0.57%)	3.5e6%	(6.3e4%)	20.3%	(21.4%)	6.0e7%	(1.6e6%)
Scroll R410A	5.8e-2%	(3.1e-2%)	6.1e5%	(9.0e4%)	n/a	(n/a)	6.6e5%	(9.2e4%)
Recip. R32	1.0e-3%	(2.0e-3%)	45.1%	(27.5%)	n/a	(n/a)	n/a	(n/a)

The baseline results shown in Table 4.5 represent the AHRI model performance at all compressor data sets that it's coefficients could be trained at (*i.e.*: data sets with ten constant speed and superheat points). The screw, scroll, and reciprocating compressor data, all with R134a, did not have enough constant speed points to adequately train the AHRI model for testing. Therefore, only the data sets shown in Table 4.5 were used for evaluating the model. As can be seen the AHRI model is inadequate in it's mass flow rate and power prediction at extrapolation, variable speed, and variable superheat scenarios. Extrapolation errors rose to 6.0e8% and 6.7e8% for mass flow rate and power, respectively. Variable speed errors were found

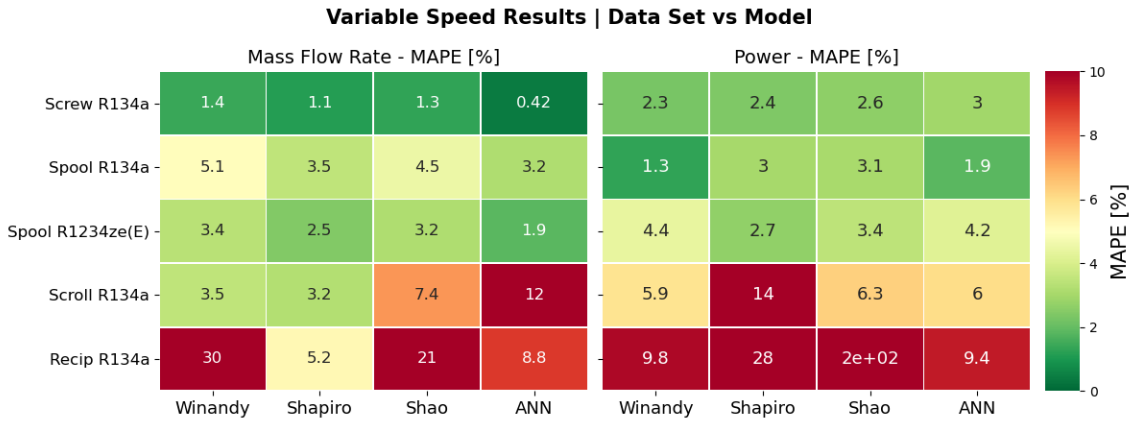

Figure 4.5: Heat map showing modulation (variable speed) MAPE results for mass flow rate and power for each model.

to be 20.7% and 21.4% at the highest for mass flow rate and power, respectively. Variable superheat errors topped out at 5.8e7% and 6.0e7% for mass flow rate and power, respectively. Contrary to extrapolation, variable speed, and variable superheat scenarios, the model showed excellent performance at training data sets with the highest error achieved being 0.43% and 0.57% for mass flow rate respectively. Similar conclusions with respect to training data performance were made by Aute et al. (2015) in their study of the AHRI model. These results provide a baseline to evaluate the semi-empirical models performance in the next sections.

4.2.2 Modulation

Figure 4.5 is a heat map representing the MAPE of model predicted results for each of the models using the five modulation data sets described in above.

The Winandy model failed to predict reciprocating data performance in all situations as the model was derived for scroll machines. This is shown in Figure 4.5 by errors of 30% and 9.8% for the reciprocating compressor using R134a. For the compressor technologies the model does predict, the highest error achieved were 5.1% and 5.9% for mass flow rate and power, respectively.

The Popovic and Shapiro model performance well in predicting mass flow rate at variable speed conditions with errors all below 5.2%. For power, the model struggled in predicting reciprocating and scroll compressor data with R134a where errors reached 28% and 14%, respectively.

The Shao model exhibited highest mass flow rate errors scroll and reciprocating data sets utilizing R134a where 7.4% and 21% MAPE was achieved. For power, the same two data sets showed the highest errors. An error of 200% MAPE was found for power prediction at the reciprocating compressor utilizing R134a. This stems from the quadratic curve fit it utilizes where values outside it's fitting data can lead to unusable results.

The ANN model exhibited a highest error in mass flow rate prediction of 12% for the scroll data set with R134a. In power prediction, the ANN performed worst at the reciprocating data utilizing R134a where a MAPE of 9.4% was achieved. This provides good indication that the aforementioned models could be used to predict mass flow rate at conditions outside the bounds of their training data.

Overall, for both mass flow rate and power prediction, the Winandy model yielded consistent results in modulation scenarios when the model did capture the compressor technology (*i.e.*: in all cases except the reciprocating data). For mass flow rate prediction in modulation scenarios the Popovic and Shapiro model and the ANN performed best overall. In power prediction, the Winandy and the ANN yielded the best result.

4.2.3 Extrapolation

Figure 4.6 is a heat map representing the MAPE for each of the models using the extrapolation data sets described above.

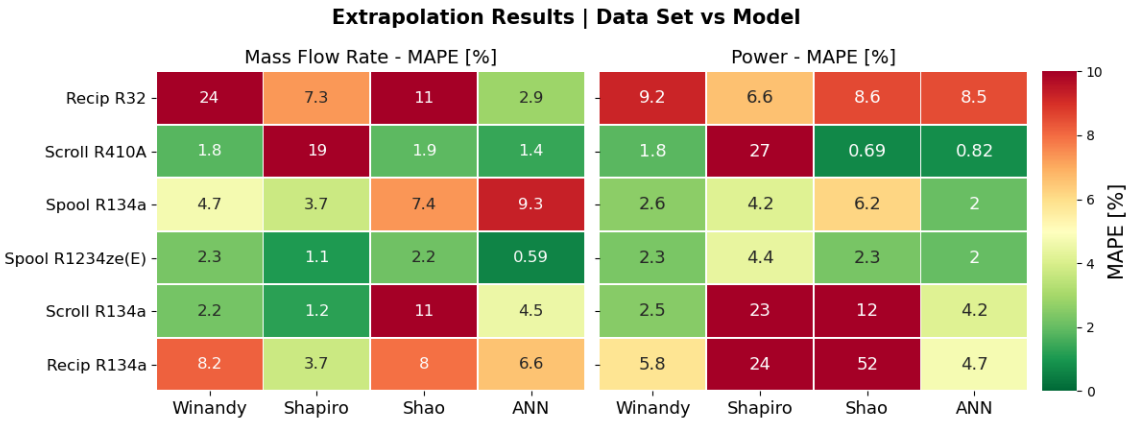

Figure 4.6: MAPE results in extrapolation scenarios for all models.

Results show that extrapolation is captured by the Winandy model given that it does predict the compressor technology. The Winandy model exhibits errors below 5% MAPE in mass flow rate prediction for the scroll and spool compressor technologies. The model extrapolated with two different refrigerant data sets for the spool compressor. For power prediction, the highest MAPE achieved was 2.6% in the spool data set utilizing R134a indicating the model can extrapolate power. The model did not capture reciprocating compressor performance, as mentioned previously.

The Popovic and Shapiro gave varying results in extrapolation scenarios. For reciprocating and spool data sets, the model extrapolated mass flow rate below 8%. In power prediction for the same data sets the model exhibited larger errors, up to 24%. This model, overall, did not capture scroll compressor performance, but did extrapolate mass flow rate to 1.2% MAPE, however power prediction was above 20% for the same data set, the scroll compressor utilizing R134a. The Popovic and Shapiro model performed better at extrapolating spool compressor data than reciprocating data, the latter of which the model was derived initially to predict.

The Shao model performed best when ran with spool data sets and worst with the reciprocating data sets. Mass flow extrapolation errors rose to 11% MAPE for both the reciprocating and scroll data sets utilizing R134a. For the same data sets,

the highest errors in power prediction were found to be 52% and 12%, respectively. The model performed best in the case where scroll data using R410A was predicted.

The ANN model extrapolated mass flow rate below 5% MAPE except in the case of the spool and reciprocating compressors utilizing R134a. For power extrapolation, the ANN model performed below 5% MAPE for all data sets except the reciprocating data with R32. The model extrapolated power better than mass flow rate overall and with respect to black-box models, outperformed it's peers the AHRI and the Shao model in extrapolation scenarios.

The Winandy model out performed the other models in extrapolation scenarios. With the exception of reciprocating compressor data, when exposed to extrapolation scenarios the Winandy model predicted both mass flow and power below 5%.

4.2.4 Variable Superheat

Figure 4.7 shows a heat map with MAPE results given by the models when exposed to variable superheat scenarios. In Figure 4.7 the row second to the bottom labeled 'Scroll R410A 1' is the first variable superheat scroll data set described in 3.2.2 having superheat values of 22 K. The data set labeled 'Scroll R410A 2' in Figure 4.7 is the second variable superheat data set described above having a constant suction temperature of 18 °C. The Winandy model predicted both mass flow rate and power below 4% for all variable superheat scenarios presented to it.

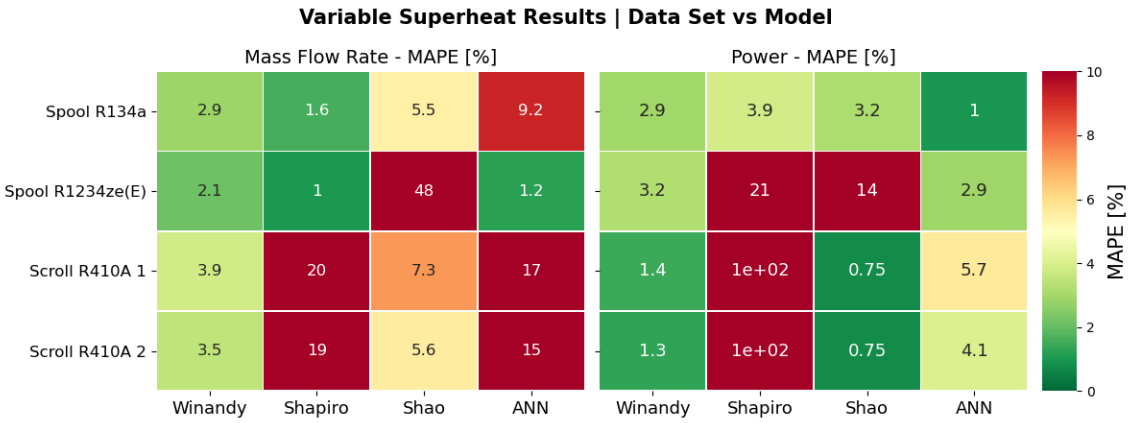

Figure 4.7: MAPE results for models under variable superheat testing.

The Shapiro and Popovic model performs well at mass flow rate prediction in variable superheat scenarios for the spool compressor utilizing R134a and R1234ze(E). Errors are larger in power prediction for the model and only one case, spool compressor utilizing R134a, gave a MAPE below 20%. The Popovic and Shapiro model did not adequately predict scroll compressor performance in variable superheat scenarios.

The Shao model predicts mass flow under 8% for all cases except the spool compressor data set using R1234ze(E) where the error was unacceptably high, 48%. The model showed good power prediction, below 4%, in all cases except the spool compressor using R1234ze(E), where again, the error was unacceptably high at 21%.

Mass flow rate prediction yielded higher MAPE's than power prediction for the ANN model. The scroll compressor data yielded the worst behavior for the ANN model in mass flow rate prediction with errors at or above 15%. The spool compressor with R134a gave 9.2% error while the same compressor with R134a gave 1.2% error in mass flow prediction. Power prediction in variable superheat scenarios yielded errors below 6% for all cases.

4.3 Discussion

The Winandy model failed to predict reciprocating compressor data adequately while the same is said for the Popovic and Shapiro model regarding scroll compressor data. The Popovic and Shapiro model and the Winandy model were each initially derived to predict reciprocating and scroll compressors, respectively. Therefore it is understandable that they perform poorly when applied to other technologies. The semi-empirical models (Winandy model and Popovic and Shapiro model) do capture extrapolation, modulation, and variable superheat scenarios provided the model first predicts that compressor technology. An exception to this is the Popovic and Shapiro model, which in some cases for reciprocating data yielded errors in power prediction at approximately 20%. The AHRI model does not extrapolate, capture modulation or variable superheat data adequately at any point. The Shao model captures modulation to a reasonable level, except for the reciprocating data utilizing R134a. With respect to extrapolation and variable superheat performance, the Shao model showed limited ability in capturing both mass flow rate and power. The ANN model extrapolated to a reasonable level, exhibiting MAPE's below 10% in all cases, however, variable speed and superheat data sets showed inconsistent results in performance prediction where and the highest errors were 12% and 17%, respectively.

4.3.1 Model Capabilities

The Winandy and Popovic and Shaprio models yielded more consistent performance at extrapolation and modulation scenarios than the Shao, ANN and AHRI models. For the scroll, screw, and spool compressors the Winandy model predicted all extrapolation, modulation, and variable superheat scenarios at or below 5.1% and 5.9% MAPE for mass flow rate and power, respectively. The Popovic and Shapiro model demonstrated good results in some situations when applied to screw and spool

compressors data. Due to it's empirical nature the Shao model sometimes exhibited large errors in prediction resulting from inputs beyond that of it's training data. The model does not account for a compression process and only takes data to fit coefficients. Similarly, the ANN and AHRI formulations only require data for tuning parameters. The Winandy model attempts to account for phenomena occurring in the suction line, discharge line, and compression chamber via the isentropic compression assumption and the suction and discharge heat transfer assumptions. The Shapiro and Popovic model does not account for suction and discharge gas heating, but it does model the compression process as polytropic and assumes suction and discharge pressure drops. These two models incorporate more physics into their formulations and the results suggest, particularly for the Winandy model, they are well suited for situations where limited data or model flexibility is desired.

4.3.2 Model Limitations

The five models tested in this work have limitations due to either training data or performance prediction. The training data for a model should require minimal operating conditions and no detailed information derived from comprehensive measurements of the compressor. To this end, the Shao and the Popovic and Shapiro models training data is a limiting factor. Shao requires operating conditions at three different operational speeds to adequately fit the power and mass flow ratios for variable speed prediction. The Shapiro and Popovic model requires discharge temperature measurements to fit the polytropic exponent to pressure ratio. Limitations in performance prediction are exhibited by each model. The Winandy model did not capture reciprocating compressor performance and the Shapiro and Popovic model did not capture scroll compressor performance. Other models exhibited limitations during specific testing scenarios. The ANN model did not predict predict compressor behavior during variable superheat testing. The AHRI model exhibited large errors throughout

testing.

4.3.3 Future Model Development

Future work based on the results presented herein will be developing a compressor model to capture multiple compressor technologies and adequately capture modulation and extrapolation. The model will be tested subject to the same methodology as used here. The Winandy model offered good results during testing of the compressors that it predicted. With its performance here and the body of literature showing modifications, it is selected as the basis for future model development.

CHAPTER V

SELECTED MODEL

From the above results and discussion, the Winandy Model is chosen to move forward with model development. It performed adequately in capturing extrapolation, variable speed, and variable superheat for scroll, screw, and spool compressor technologies.

5.1 Additional Compressor Technology Prediction

The Winandy Model is the backbone of a rotary piston compressor model where additional phenomena occurring throughout the compression process are modeled Molinaroli et al. (2017). The additional fidelity not found in the original model comes in the form of leakage and re-expansion modeling. A portion of the discharge mass flow gets diverted back to suction mass flow through two streams, leakage and re-expansion mass flows. Isobaric mixing occurs and mass and energy balances are applied. An additional difference between the study's model and the original Winandy Model comes from compression process modeling. The authors use isentropic compression instead of two-step compression, isentropic to the adapted pressure and then constant volume compression to discharge pressure.

The detail added yielded sufficient results for the authors in their application to one compressor technology, rolling piston type. It is a goal of this study to remain broad in terms of the type of compressor the selected model can predict. In that spirit, the original Winandy Model, which adequately predicted scroll, screw, and spool

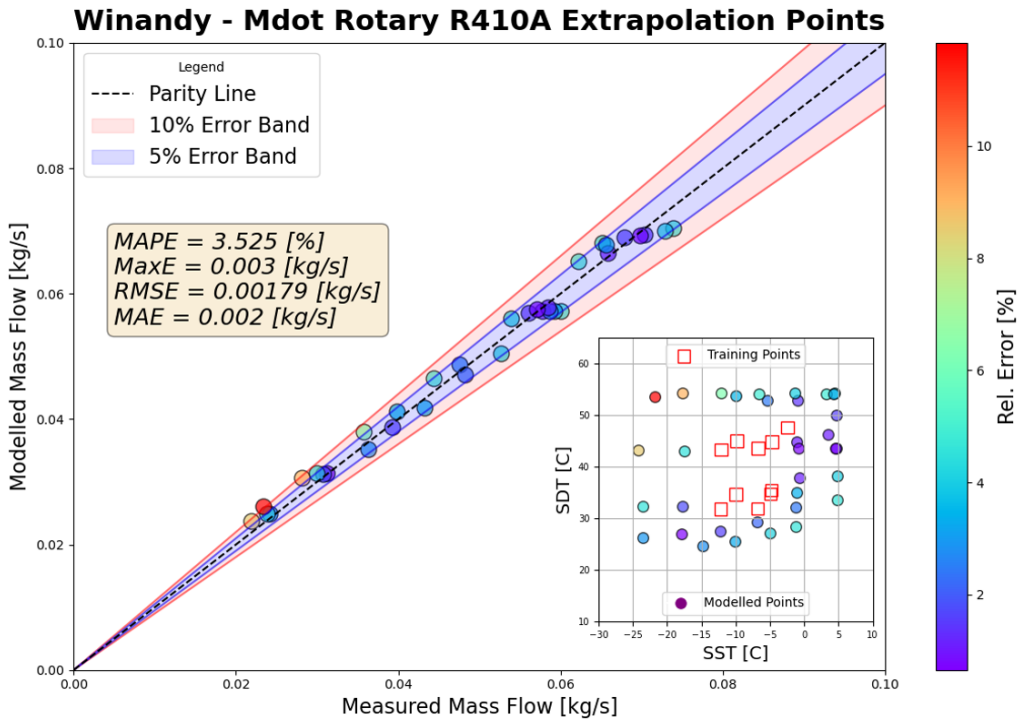

Figure 5.1: Parity plot showing extrapolation results for the Winandy Model predicting rotary compressor mass flow rate

technologies, is tested with rotary piston compressor data. The data was acquired through an industry partner. The reason this data is not included in Chapter IV is because it was given after extrapolation, variable speed, and variable superheat testing had been completed and a model selected.

To further test the Winandy Model predictive capabilities the model was applied to data coming from a commercially available 4 ton dual rotary compressor made by Highly. The data was collected Purdue University using a compressor calorimeter Rohleder (2019). The refrigerant utilized is R410A and the compressor operated at 60 Hz during experiments. The data set contained 44 test points that ranged from -25 - 5 °C and 25 - 55 °C for evaporating and condensing temperature respectively. The target superheat was 11 K for the data set. Values varied slightly, 1-2 K, but no data points were directly taken at variable superheat conditions. Therefore, from

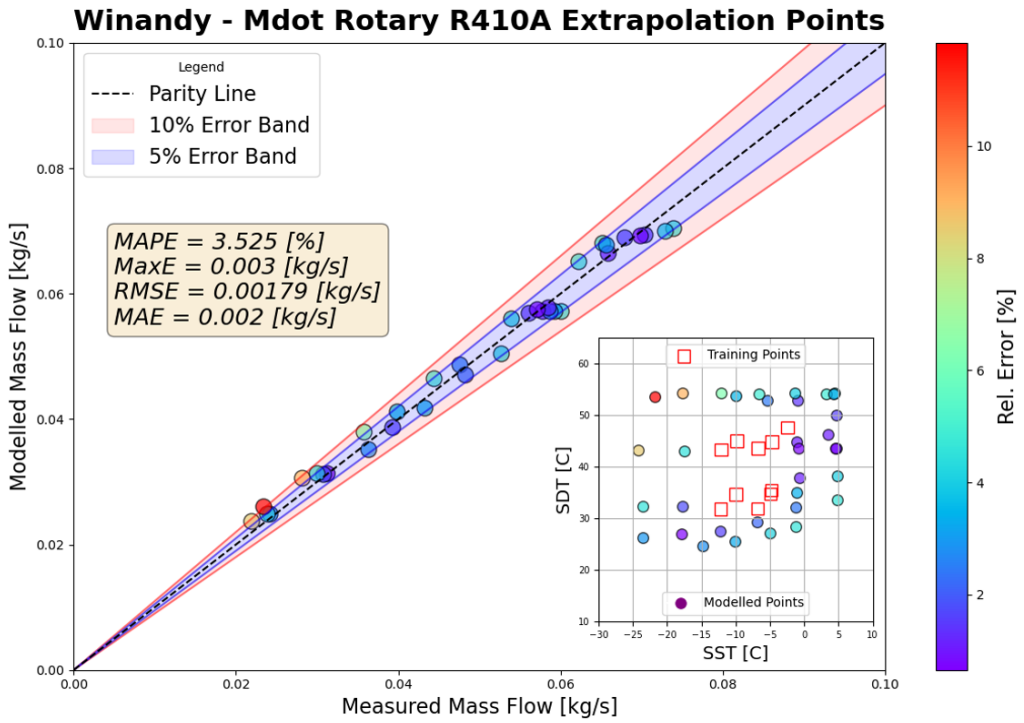

Figure 5.2: Parity plot showing extrapolation results for the Winandy Model predicting rotary compressor power consumption

this data set only general model performance and extrapolation performance can be analyzed.

Training and extrapolation data was selected following the same methodology outlined in Section 3.2.1. For the training data, the model yielded MAPEs of 1.24 % and 1.26 % for mass flow rate prediction and power prediction, respectively. Figure 5.1 shows a parity plot for mass flow rate prediction in extrapolation testing. The subplot within the figure shows points used to train the model and points that modeled. The main plot shows how predicted results differ from measured values. The MAPE for mass flow rate prediction is 3.5%. Figure 5.2 shows the power prediction results. The MAPE yielded by the Winandy Model in power prediction at extrapolation is 3.5%. These results indicate that the Winandy Model in its original form can predict rotary compressor performance and capture extrapolation within 5% MAPE. This is

a positive attribute and further demonstrates the models utility. The result brings the total number of compressor technologies predicted by the model to 4; scroll, screw, spool, and rotary.

5.2 Initial Modifications to Selected Model

Since the Winandy Model will predict all compressor types it's been applied to by this study, except reciprocating, it is necessary to investigate the possibility of making a modification to the model that may successfully enable adequate performance. There are studies that use the Winandy formulation to predict reciprocating machines Winandy et al. (2002*a*), Duprez et al. (2006). However, they modify the mass flow rate and power formulation provided by the original work. The prediction for mass flow rate in the original work utilizes a fictitious volume ratio that is a parameter to be found by the optimizer. The reciprocating compressor is not a fixed volume ratio machine contrary to scroll compressors. The volume ratio in reciprocating compressors is variable because as the piston rises and compresses mass, the gas will flow once cylinder pressure exceeds discharge pressure. The crank angle, and therefore piston position and internal volume, at which in-cylinder pressure exceeds discharge pressure is dependent on operating conditions.

Another difference found in reciprocating compressors is the presence of valves at the suction and discharge. In scroll, screw and spool compressors there are typically no suction valves, however discharge valves are usually present. With the no such a valve in a reciprocating machine there is inherent pressure drop as a fluid flows through. Subsequently, a model that predicts this drop may have the potential to be more accurate in prediction. The Winandy Model in its original form has no suction or discharge pressure losses.

5.2.1 Pressure Drop

In order to test for model improvements with constant suction and discharge pressure drop, one term was added to parameters which were solved for by the optimization algorithm. This term was a constant pressure drop factor that subtracted from the suction pressure and added to the discharge pressure. Figure 5.3 show an overall schematic of Winandy model. Included in the figure is the pressure drop at the suction and discharge to illustrate the modification made.

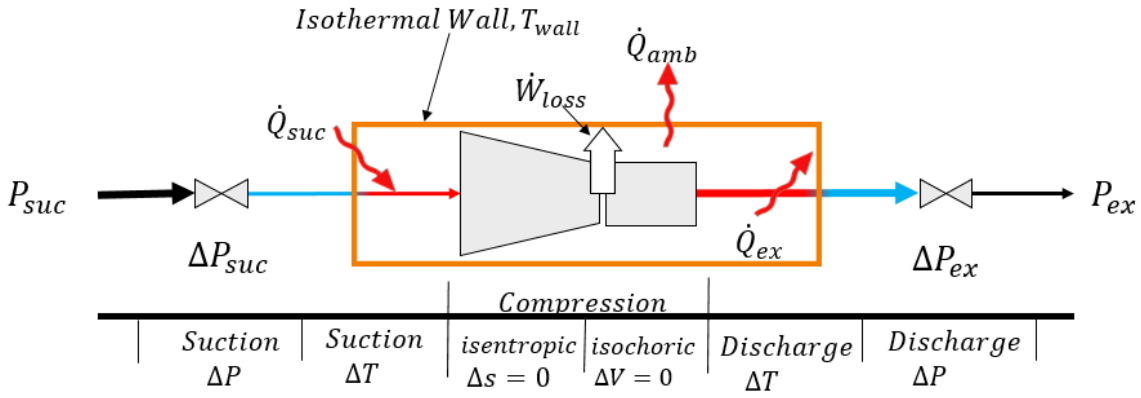

Figure 5.3: Schematic of the Winandy model with ΔP_{suc} and ΔP_{dis} modification added

The model was then ran with all data sets and MAPE recorded. Table 5.1 shows the change in MAPE for extrapolation cases. The negative values indicate that the MAPE went down for a given data set while positive changes indicate the MAPE increased. Table 5.2 and Table 5.3 show the resulting changes in MAPE for variable speed and variable superheat, respectively.

The model performance with respect to scroll compressors improved overall showing negative values in all cases. The spool and screw compressor predication showed improvements in some cases, but other cases, MAPE increased slightly. With respect to reciprocating compressors, the MAPEs again showed improvements in some cases and in others, slightly larger errors. It must be noted, however, that in order

to capture reciprocating compressor performance to the standard set forth by this work, the improvements should be on or close to the order of magnitude of 10. This is because results shown in Chapter IV includes errors that can range up to 30% MAPE. Ultimately, the constant pressure drop modification did not allow the model to adequately capture reciprocating compressor performance.

Table 5.1: Change in MAPE for extrapolation cases with constant pressure drop at suction and discharge

Extrapolation ΔMAPE		
Data Set	$\dot{m}$	$\dot{W}$
Scroll R134a	-0.55	-0.49
Spool R134a	-1.12	-0.68
Spool R1234ze(E)	0.19	0.15
Scroll R410A	-0.27	-0.18
Recip. R134a	0.12	2.240
Recip. R32	-1.93	0.12

5.2.2 Reciprocating Compressor Prediction Modifications

The Winandy Model as tested will not predict reciprocating compressor performance. Modifying the model slightly improved results with respect scroll, screw, and spool compressors, but some errors increased. No errors for these compressors increased beyond reason. The largest single increase was in the spool compressor utilizing

Table 5.2: Change in MAPE for variable speed cases with constant pressure drop at suction and discharge

Variable Speed ΔMAPE		
Data Set	$\dot{m}$	$\dot{W}$
Scroll R134a	-0.03	-0.80
Screw R134a	0.08	-1.05
Spool R134a	-1.06	0.17
Spool R1234ze(E)	-0.66	-1.32
Recip. R134a	0.25	1.86

R134a in extrapolation. That error was in mass flow rate prediction and increased by 0.2%. It is desired to have a model that can predict reciprocating performance while retaining accuracy in the other technologies.

Mass Flow Rate Modification

The mass flow rate formulation for the Winandy Model is shown in Equation 5.2.1, where the swept volume, V_s, is a parameter determined by the optimizer, N is the rotational speed, and ν_{suc} is the suction specific volume evaluated after suction heat transfer and pressure drop. It is desired that this formulation be modified such that it can capture reciprocating compressor performance. In order to do this, a formulation that includes a clearance factor that represents the percentage of total gas volume that remains in the cylinder after the discharge valve has closed is pursued. The

Table 5.3: Change in MAPE for variable superheat cases with constant pressure drop at suction and discharge

Variable Superheat ΔMAPE		
Data Set	$\dot{m}$	$\dot{W}$
Spool R134a	-1.07	-0.97
Spool R1234ze(E)	-0.74	-0.34
Scroll R410A	-0.28	-0.11
Scroll R410A constant T_{suc}	-0.43	-0.08

formulation is shown in Equation 5.2.2

$$\dot{m} = N \frac{V_s}{\nu_{suc}} \tag{5.2.1}$$

The aspirations for using this formula come from the prospect that one single representation can hold for all compressor types. Since the clearance factor is multiplied by the fictitious swept volume, it is reasonable to think that factor could go to 0 for non reciprocating compressors and retain a value for reciprocating compressors. This could account for the cylinder volume leftover after the discharge valve closes and therefore more accurately predict mass flow rate.

$$\dot{m} = N \frac{V_s - CV_s}{\nu_{suc}} \tag{5.2.2}$$

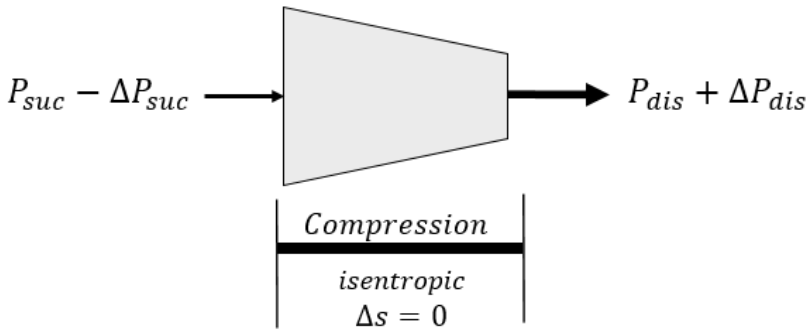

Figure 5.4: Schematic of the isentropic compression process utilized in initial modifications to the Winandy model

Compression Process Modification

As mentioned at the beginning of this chapter, some studies have used isentropic compression to eliminate a volume ratio dependence in the Winandy Model. This assumption has proved fruitful for reciprocating performance prediction. Additionally, polytropic compression has been utilized in a modification to Winandy Model Byrne et al. (2014). The study, however, applies that compression process model to scroll compressors, but one may assume that as long as the compression is modeled without the input of volume ratio, it may predict reciprocating performance more adequately. For the present study, isentropic compression is introduced to the model and applied to the reciprocating data utilizing R32 as a test case. Figure 5.4 shows the compression process of the modified model. The pressure at which isentropic compression begins is evaluated after the suction pressure drop is applied. The gas is compressed up to a final pressure equal to the discharge pressure plus the discharge pressure drop.

Training Data Investigation

For testing the model modifications in prediction of reciprocating compressor performance the modifications in the three previous sections were implemented. The model was then applied to the reciprocating compressor data utilizing R32. This gives a baseline as to how the model will perform with respect to this technology. Initially, when applied to the training data, the model performed poorly with mass flow rate and power MAPEs at greater than 20%. It was noticed, however, that two points within the training data set were yielded unreasonably high errors that brought the overall errors up. In an attempt to see if the model could perform adequately on the rest of the training data, these two points were removed and the model was retrained. Figure 5.5 and 5.6 show the parity plots and MAPE for mass flow rate and power, respectively, achieved when using only the 8 remaining training data points after the two outliers were removed.

Results show that errors become much closer to those desired by this work. The modifications bring the errors down to 4.99% and 6.89% for mass flow rate and power, respectively. This indicates the model has improved with respect to performance prediction of reciprocating compressors.

However, when the model is evaluated at the two outlier points the results resume to their high error values with magnitude similar to before, approximately 20% MAPE. Again these two points showed the highest errors of the whole training data set. This fact points toward the model being incapable of extrapolating to new points once trained. The outlier points require different parameter values than what has been achieved by the minimization algorithm. Parameter values that predict the other 8 points semi-adequately do not yield sufficient results when the model is ran at the other two. This implies that the modifications do not allow for extrapolation to other operating conditions which is a core requirement of this work.

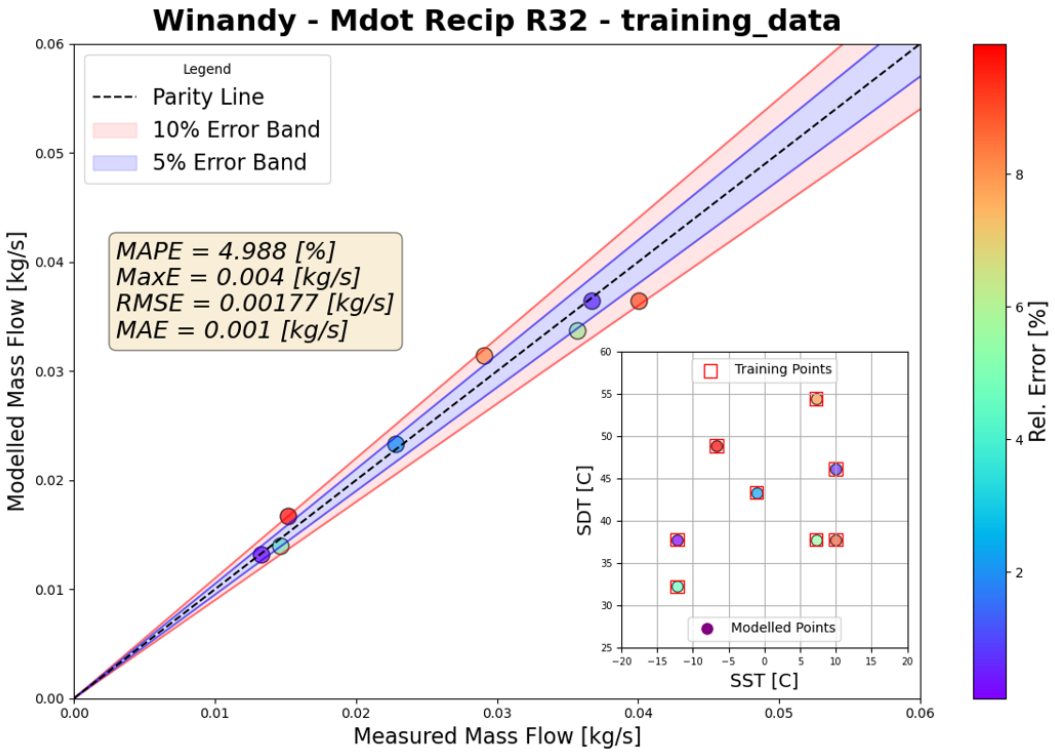

Figure 5.5: Parity plot showing the mass flow rate results using modified model and 8 training points

5.3 Overall Modification Results

Modifications made to the original model include adding pressure drops at the suction and discharge, changing the mass flow rate formulation to account for clearance volume, and changing the compression process model to an isentropic compression assumption. The first modification increased model fidelity and improved performance in most cases for scroll, screw, and spool compressor performance prediction. The reciprocating compressor prediction improved in some cases, but did not reduce to an acceptable level. The next modifications, being mass flow rate and compression process, were aimed at enabling the model to adequately capture reciprocating compressors. Results indicated that the proposed changes do enable the model to better capture the technology, but not it is not a sufficient enough reduction in error

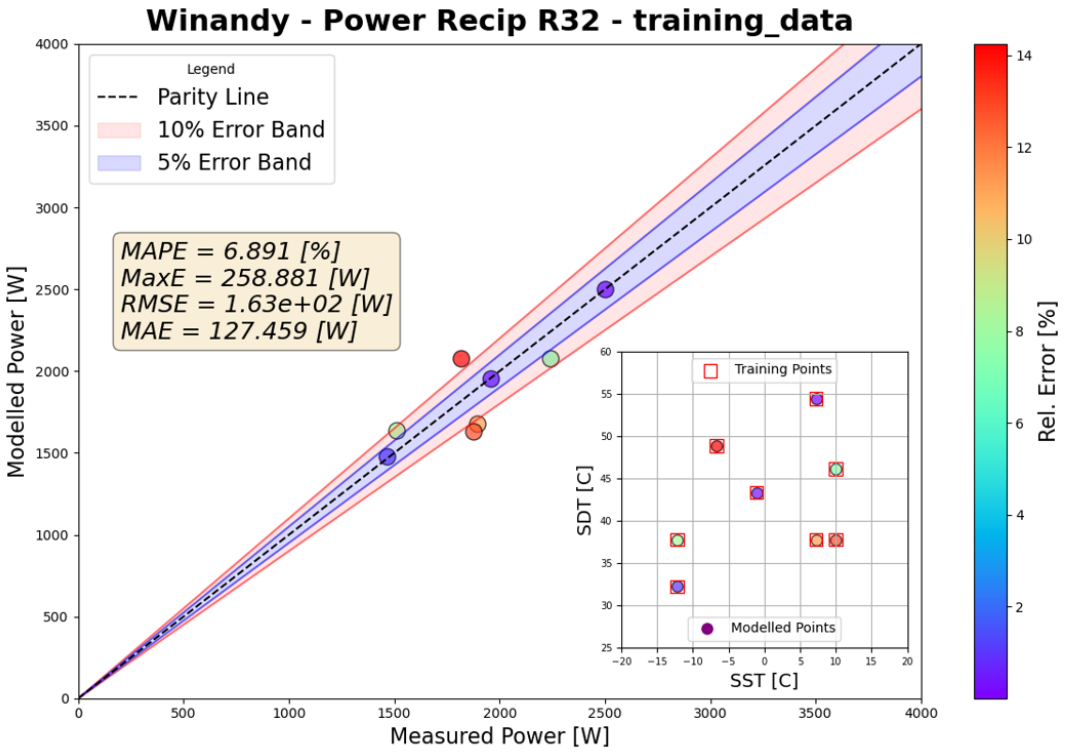

Figure 5.6: Parity plot showing the power results using modified model and 8 training points

to warrant keeping the change. From here, the model will be kept with pressure drops at the suction and discharge and the requirement for predicting reciprocating compressor performance is removed.

CHAPTER VI

CONCLUSIONS AND FUTURE WORK

6.1 Conclusions

This thesis studies semi-empirical compressor models and their ability to extrapolate, modulate, and capture variable superheat conditions. A feasibility analysis on combining positive displacement and dynamic compressor models into one was performed. It was determined that the physical mechanisms generating pressure energy present in the machines are far different and require different modeling approaches. From there five positive displacements compressor models were identified and tested; the industry standard AHRI model, an artificial neural network (ANN) model, and lastly, three models from literature, the Shao model Shao et al. (2004), Popovic and Shapiro model Popovic and Shapiro (1995), and the Winandy model Winandy et al. (2002*b*). Data sets selected for model testing were of high fidelity experimental data to ensure model prediction is accurate. Experimental data for scroll, spool, screw, and reciprocating compressors is collected totalling 434 data points including four refrigerants; R134a, R410A, R32, and R1234ze(E). These data sets were split to enable training model parameters at constant conditions, then test the model using data outside the conditions of the training data. Four different data subsets were identified and used: the training data set, extrapolation data set, variable speed data set, and variable superheat data set. Models were trained using the training data set then tested at the others to examine performance. The mean absolute percentage

error (MAPE) was used to quantify prediction capability of the models in the various scenarios. From the results some conclusions can be made regarding the performance of the semi-empirical and empirical models.

- The Winandy model, as tested, will capture extrapolation, modulation, and variable superheat scenarios in scroll, screw, and spool compressors
- The Winandy model outperforms the Popovic and Shapiro model when compared head to head
- The ANN model performed its worst at predicting mass flow rate during variable superheat scenarios
- Of the literature models tested, the Shao model yielded the largest single error value for both mass flow and power prediction
- The AHRI model will not predict compressor performance under extrapolation, modulation, or variable superheat scenarios

The Winandy model performed the best overall when considering all aspects desired by the authors which included: limited training data, low computational cost, accurate performance at extrapolation and modulation scenarios, and applicability to multiple compressor technologies. The model captured performance with four different refrigerants at extrapolation, modulation, and variable superheat performance yielding a maximum error of 5.1% and 5.9% MAPE for mass flow rate and power prediction, respectively. This model is chosen as a formulation with promising attributes for future model development. As cited in the literature survey, this formulation has been modified to capture a range of compressors and will be the basis for a new model desired to capture multiple compressor technologies and exhibit strong extrapolation and modulation capabilities. After selection, the model was tested with an additional

compressor technology, rotary piston. The data had 44 total test points and utilized R410A as the refrigerant. Performance was adequate and the model captured extrapolation to below 5% MAPE for mass flow rate and power prediction. Initial modifications were done to the Winandy model in an attempt to improve overall performance. Pressure drop at the suction and discharge was added resulting in slightly better performance, but the modification did not enable reciprocating compressor prediction. To this end, a mass flow rate and compression process modification was made to the model. The results improved performance from approximately 20% MAPE for mass flow rate and power to 5% and 7%, respectively. However, in extrapolation cases the errors rose above the standards set forth by this work. This leads to the reciprocating performance prediction requirement to be removed and focus solely on scroll, screw, spool, and rotary technologies.

6.2 Future Work

Future work from this study should focus on a few main topics: model prediction capability, parameter conversion methods, training data, optimization methods, and further extrapolation testing. Regarding the prediction capability, it would be beneficial to modify the model such that it can capture vapor-injected compressor performance. This technology currently used in heat pump applications and a model that can accurately predict injection compressors is of value to manufactures who lack resources to test systems at a range of conditions. A study of methods to convert parameters achieved by the optimization with one refrigerant to those with another should be pursued. Enabling this conversion would allow new refrigerants to be evaluated without needing extensive test data. Another study should consider different optimization algorithms for determining parameters. There are a number of algorithms available and while the Nelder-Meade method yielded satisfactory results for this study, different algorithms should be sought and tested for better results. Addi-

tionally, other objective functions which the algorithm minimizes should be studied in conjunction. Minimizing the MAPE of power and mass flow rate yielded the results shown in the study, however, other error metrics and algorithm combinations may give satisfactory results. To that end, a systematic approach to providing initial guesses to the algorithm should be investigated. Good guesses are those that are close to final minimized values and may be difficult to estimate accurately. A study should investigate methods to ensure that good guesses given to the algorithm lead to global minimum of the objective function. Lastly, to continue extrapolation capability testing, the model should tested a varying ambient temperatures to ensure accurate results. This includes pursuing high-fidelity data that contains test points with ambient temperature variation. Model prediction capability could then be evaluated to determine if performance in these situations is adequate.

REFERENCES

Abadi, M., Agarwal, A., Barham, P., Brevdo, E., Chen, Z., Citro, C., Corrado, G. S., Davis, A., Dean, J., Devin, M., Ghemawat, S., Goodfellow, I. J., Harp, A., Irving, G., Isard, M., Jia, Y., Józefowicz, R., Kaiser, L., Kudlur, M., Levenberg, J., Mané, D., Monga, R., Moore, S., Murray, D. G., Olah, C., Schuster, M., Shlens, J., Steiner, B., Sutskever, I., Talwar, K., Tucker, P. A., Vanhoucke, V., Vasudevan, V., Viégas, F. B., Vinyals, O., Warden, P., Wattenberg, M., Wicke, M., Yu, Y. and Zheng, X. (2016), 'Tensorflow: Large-scale machine learning on heterogeneous distributed systems', *CoRR* **abs/1603.04467**.
URL: *http://arxiv.org/abs/1603.04467*

AHRI (2020), 'ANSI/AHRI standard 540:2020 standard for performance rating of positive displacement refrigerant compressors and compressor units', *Air Conditioning and Refrigeration Institute Arlington, VA, USA* .

Aprea, C. and Renno, C. (2008), 'Experimental model of a variable capacity compressor', *Archives of Thermodynamics* **33**, 29–37.

ASHRAE (2010), 'Methods for Performance Testing Positive Displacement Refrigerant Compressors and Condensing Units that Operate at Subcritical Pressures of the Refrigerant', *American Society of Heating Refrigeration and Air Conditioning Engineers Atlanta, GA, USA* .

Aute, V., Martin, C. and Radermacher, R. (2015), 'Ahri project 8013 : A study of methods to represent compressor performance data over an operating envelope

based on a finite set of test data', *Air-Conditioning, Heating, and Refrigeration Institute* .

Barroso-Maldonado, J. M., Belman-Flores, J. M., Ledesma, S., Rangel-Hernández, V. H. and Cabal-Yépez, E. (2017), 'Predicting the energy performance of a reciprocating compressor using artificial neural networks and probabilistic neural networks', *Revista Mexicana de Ingeniera Quimica* **16**, 679–690.

Braun, J., Mitchell, J., Klein, S. and Beckman, W. (1987), 'Models for variable speed centrifugal chillers'.

Brondum, D., Materne, J., Biancardi, F. and Pandy, D. (1998), 'High-speed, direct-drive centrifugal compressors for commercial hvac systems'.
URL: *http://docs.lib.purdue.edu/cgi/viewcontent.cgi?article=2358&context=icec*

Byrne, P., Ghoubali, R. and Miriel, J. (2014), 'Scroll compressor modelling for heat pumps using hydrocarbons as refrigerants', *International Journal of Refrigeration* **41**, 1–13.

Cheung, H., Sarfraz, O. and Bach, C. K. (2018), 'A method to calculate uncertainty of empirical compressor maps with the consideration of extrapolation effect and choice of training data', *Science and Technology for the Built Environment* **24**, 743–758.

Cheung, H. and Wang, S. (2018), 'Performance comparison of empirical and semi-empirical compressor models with uncertainty analysis and probabilistic forecasting techniques'.

Corber, J. M., Navarro, E. and Urchueguı, J. F. (2007), 'Performance analysis of a series of hermetic reciprocating compressors working with r290 (propane) and r407c', *International Journal of Refrigeration* **30**, 1244–1253.

Cuevas, C. and Lebrun, J. (2009), 'Testing and modelling of a variable speed scroll compressor', *Applied Thermal Engineering* **29**, 469–478.

Dabiri, A. E. and Rice, C. K. (1981), 'A compressor simulation model with corrections for the level of suction gas superheat', *ASHRAE Transactions* **87**.

Demierre, J., Rubino, A. and Schiffmann, J. (2015), 'Modeling and experimental investigation of an oil-free microcompressor-turbine unit for an organic rankine cycle driven heat pump', *Journal of Engineering for Gas Turbines and Power* **137**, 1–10.

Duprez, M.-E., Dumont, E. and Frè, M. (2006), 'Modelling of reciprocating and scroll compressors'.

Fang, X., Chen, W., Zhou, Z. and Xu, Y. (2014), 'Empirical models for efficiency and mass flow rate of centrifugal compressors'.
URL: *http://dx.doi.org/10.1016/j.ijrefrig.2014.03.005*

Giuffrida, A. (2016), 'A semi-empirical method for assessing the performance of an open-drive screw refrigeration compressor', *Applied Thermal Engineering* **93**, 813–823.

Jahnig, D. I., Reindl, D. T. and Klein, S. A. (2000), 'Semi-empirical method for representing domestic refrigerator/freezer compressor calorimeter test data', *ASHRAE Transactions* **106**.

James, N. A., Braun, J. E., Groll, E. A. and Horton, W. T. (2016), 'Semi-empirical modeling and analysis of oil flooded r410a scroll compressors with liquid injection for use in vapor compression systems', *International Journal of Refrigeration* **66**, 50–63.

Kingma, D. P. and Ba, J. L. (2015), 'Adam: A method for stochastic optimization',

3rd International Conference on Learning Representations, ICLR 2015 - Conference Track Proceedings pp. 1–15.

Kurz, R. (2004), 'The physics of centrifugal compressor performance', pp. 1–15.

Ledesma, S., Belman-Flores, J. M. and Barroso-Maldonado, J. M. (2015), 'Analysis and modeling of a variable speed reciprocating compressor using ann', *International Journal of Refrigeration* **59**, 190–197.

Li, W. (2012), 'Simplified steady-state modeling for hermetic compressors with focus on extrapolation', *International Journal of Refrigeration* **35**, 1722–1733.

Ma, J., Ding, X., Horton, W. T. and Ziviani, D. (2020), 'Development of an automated compressor performance mapping using artificial neural network and multiple compressor technologies', *International Journal of Refrigeration* **120**, 66–80.

Mackensen, A., Klein, S. A. and Reindl, D. T. (2002), 'Characterization of refrigeration system compressor performance', *International Refrigeration and Air Conditioning Conference* p. Paper 567.

Molinaroli, L., Joppolo, C. M. and Antonellis, S. D. (2017), 'A semi-empirical model for hermetic rolling piston compressors', *International Journal of Refrigeration* **79**, 226–237.

Navarro, E., Granryd, E., Urchueguía, J. F. and Corberán, J. M. (2007), 'A phenomenological model for analyzing reciprocating compressors', *International Journal of Refrigeration* **30**, 1254–1265.

Nelder, J. A. and Mead, R. (1965), 'A Simplex Method for Function Minimization', *The Computer Journal* **7**(4), 308–313.

Popovic, P. and Shapiro, H. (1995), 'A semi-empirical method for modeling a reciprocating compressor in refrigeration systems'.

Popovic, P. and Shapiro, H. (1998), 'A modeling study of a centrifugal compressor'.

Qiao, H., Kwon, L., Aute, V. and Radermacher, R. (2014), 'Transient modeling of a multi-evaporator air conditioning system and control method investigation', *IEA Heat Pump Conference* pp. 1–12.

Rasmussen, B. and Jakobsen, A. (2000), 'Review of compressor models and performance characterizing variables.', *International Compressor Engineering Conference* pp. 515–522.

Rohleder, C. S. (2019), 'Experimental analysis of positive displacement compressors for domestic refrigerator freezer and air conditioning application'.

Sanaye, S., Dehghandokht, M., Mohammadbeigi, H. and Bahrami, S. (2010), 'Modeling of rotary vane compressor applying artificial neural network', *International Journal of Refrigeration* .

Schmidt, D. D. (2018), 'Development of a light-commercial compressor load stand to measure compressor performance using low-gwp refrigerants'.

Shao, S., Shi, W., Li, X. and Chen, H. (2004), 'Performance representation of variable-speed compressor for inverter air conditioners based on experimental data', *International Journal of Refrigeration* **27**, 805–815.

Singleton, J., Schmidt, D. and Bradshaw, C. R. (2020), 'Control and commissioning of a hot-gas bypass compressor load stand for testing light-commercial compressors on low-gwp refrigerants', *International Journal of Refrigeration* **112**, 82–89.

Tello-Oquendo, F. M., Navarro-Peris, E. and Gonzálvez-Maciá, J. (2019), 'Comparison of the performance of a vapor-injection scroll compressor and a two-stage scroll compressor working with high pressure ratios', *Applied Thermal Engineering* **160**.

Wan, H., Cao, T., Hwang, Y., Chang, S.-D. and Yoon, Y.-J. (2021), 'Machine-learning-based compressor models: A case study for variable refrigerant flow systems', *International Journal of Refrigeration* **123**, 23–33.

Weisner, F. (1960), 'Practical stage correlations for centrifugal compressors'.

Weisner, F. and Caswell, H. (1959), 'How refrigerant properties affect impeller dimensions'.

Winandy, E. and Lebrun, J. (2002), 'Scroll compressors using gas and liquid injection: Experimental analysis and modelling', *International Journal of Refrigeration* **25**, 1143–1156.

Winandy, E., O, C. S. and Lebrun, J. (2002*a*), 'Simplified modelling of an open-type reciprocating compressor', *International Journal of Thermal Sciences* **41**, 183–192.

Winandy, E., O, C. S. S. and Lebrun, J. (2002*b*), 'Experimental analysis and simplified modelling of a hermetic scroll refrigeration compressor', *Applied Thermal Engineering* **22**, 107–120.

Yang, L., Zhao, L. X., Zhang, C. L. and Gu, B. (2009), 'Loss-efficiency model of single and variable-speed compressors using neural networks', *International Journal of Refrigeration* **32**, 1423–1432.

Zendehboudi, A., Li, X. and Wang, B. (2017), 'Utilization of ann and anfis models to predict variable speed scroll compressor with vapor injection', *International Journal of Refrigeration* **74**, 475–487.

Zhao, D., Xu, L., Huangfu, Y., Dou, M. and Liu, J. (2017), 'Semi-physical modeling and control of a centrifugal compressor for the air feeding of a pem fuel cell'.
URL: *https://doi.org/10.1016/j.enconman.2017.11.030*

Ziviani, D., Bahman, A. M., James, N. A., Lumpkin, D. R., James, E. and Groll, E. A. (2018), 'Machine learning applied to positive displacement compressors and expanders performance mapping', pp. 1–10.

APPENDICES

APPENDIX A

Winandy Model Results

The Winandy results are shown in this appendix while the results for the AHRI, ANN, Shao, and Popovic and Shapiro model can be found at the following link: `https://github.com/KalenGabel/Semi-Emp-Model-Eval.git`

0.1 Reciprocating Data utilizing R134a

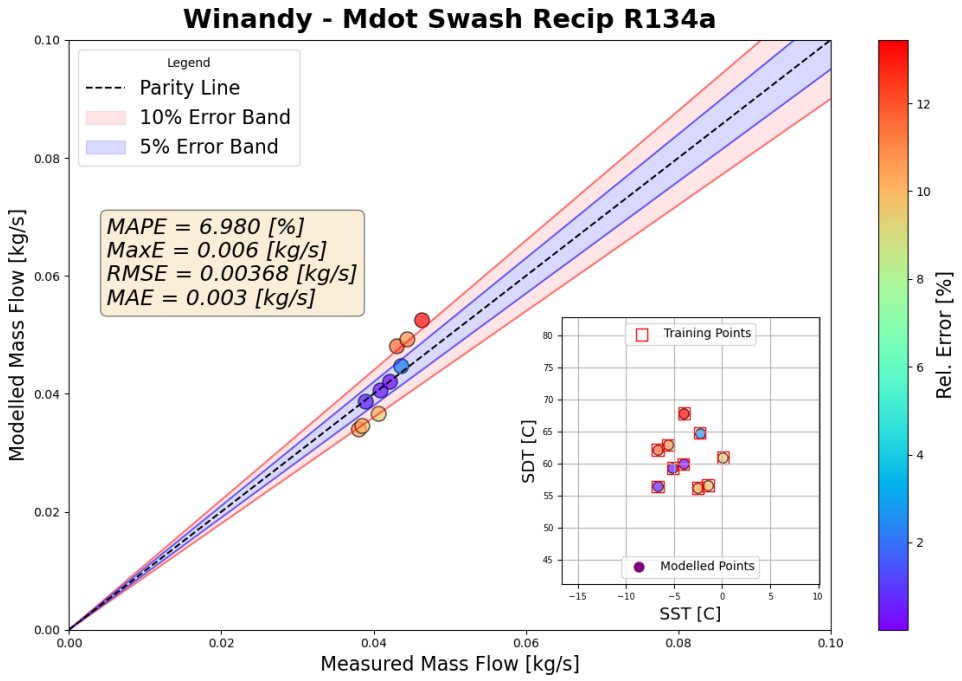

Figure A.1: Winandy model mass flow rate results for training data with reciprocating compressor utilizing R134a

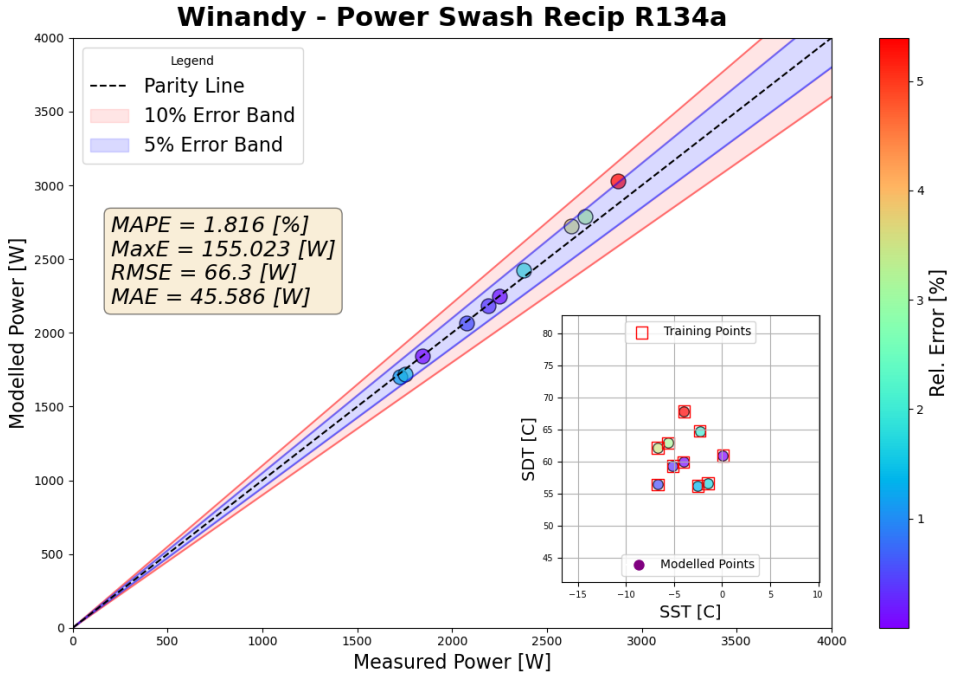

Figure A.2: Winandy model power results for training data with reciprocating compressor utilizing R134a

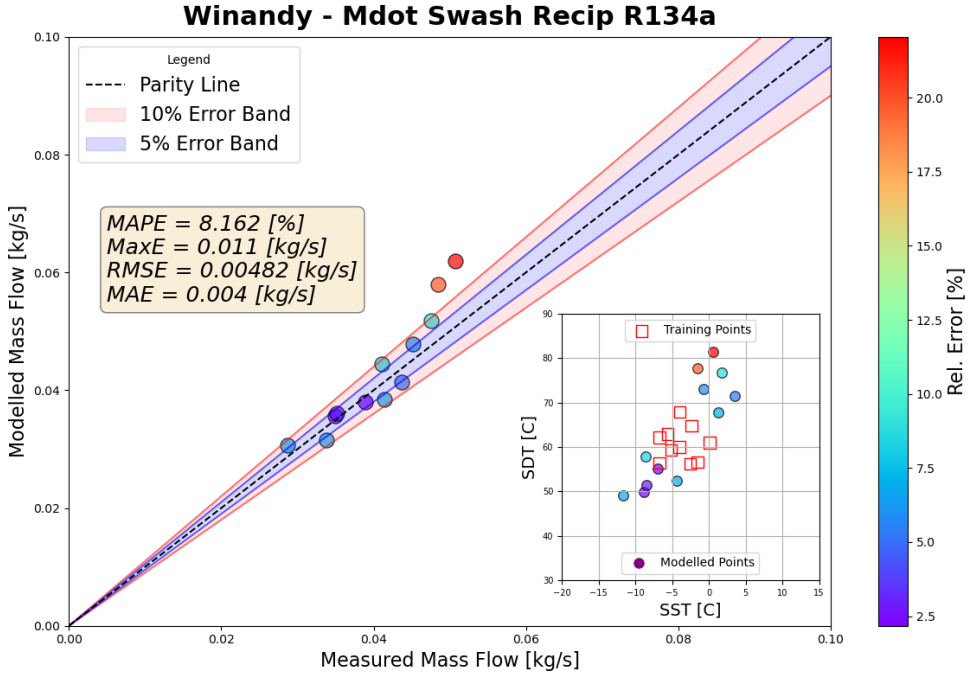

Figure A.3: Winandy model mass flow rate results for extrapolation data with reciprocating compressor utilizing R134a

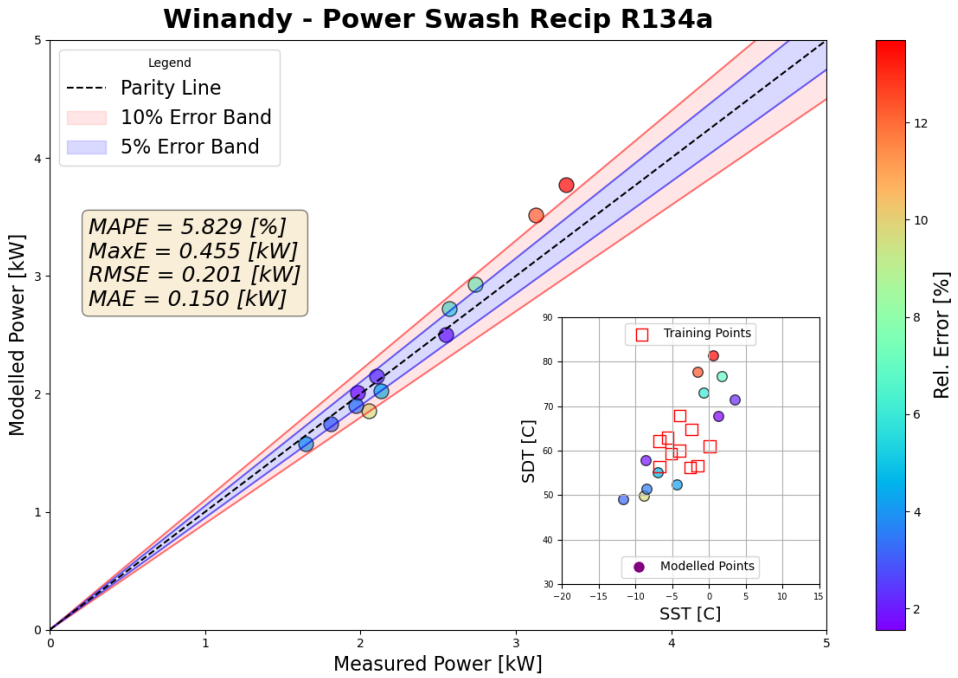

Figure A.4: Winandy model power results for extrapolation data with reciprocating compressor utilizing R134a

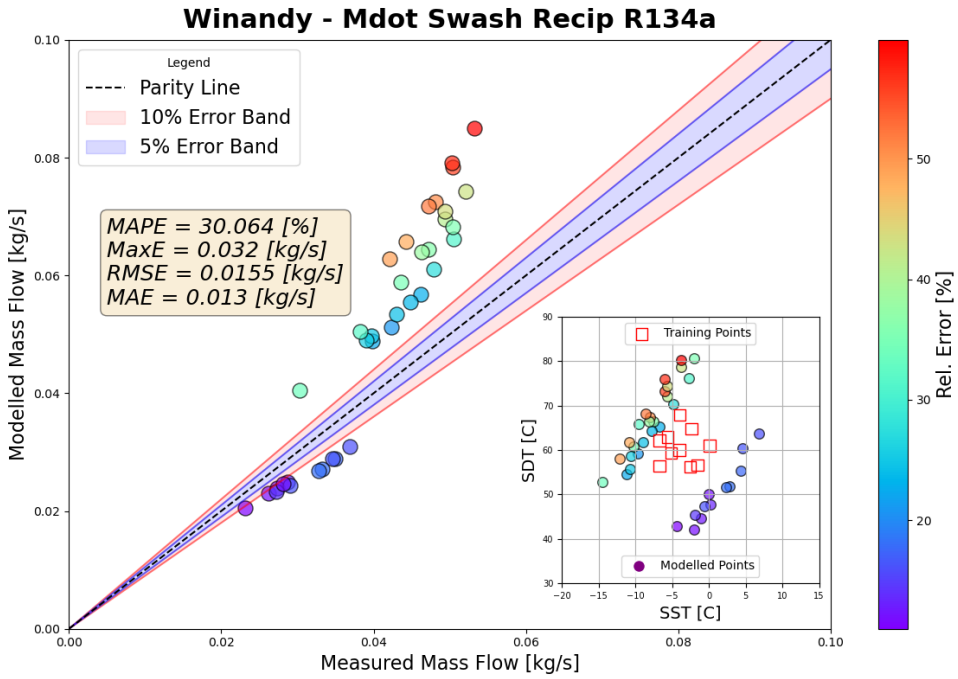

Figure A.5: Winandy model mass flow rate results for variable speed data with reciprocating compressor utilizing R134a

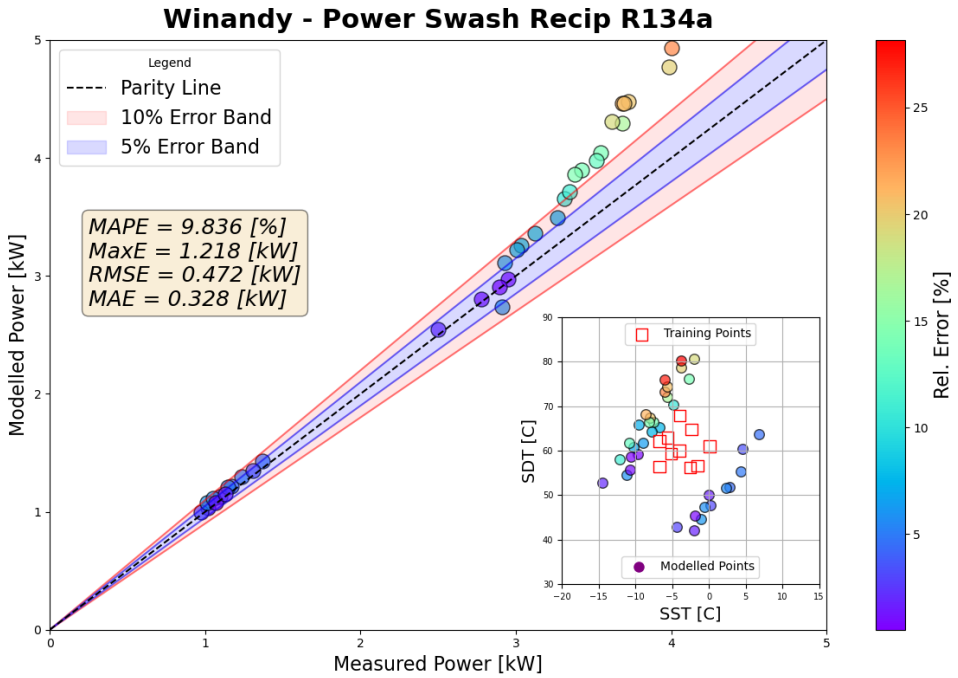

Figure A.6: Winandy model power results for variable speed data with reciprocating compressor utilizing R134a

0.2 Screw Compressor Data utilizing R134a

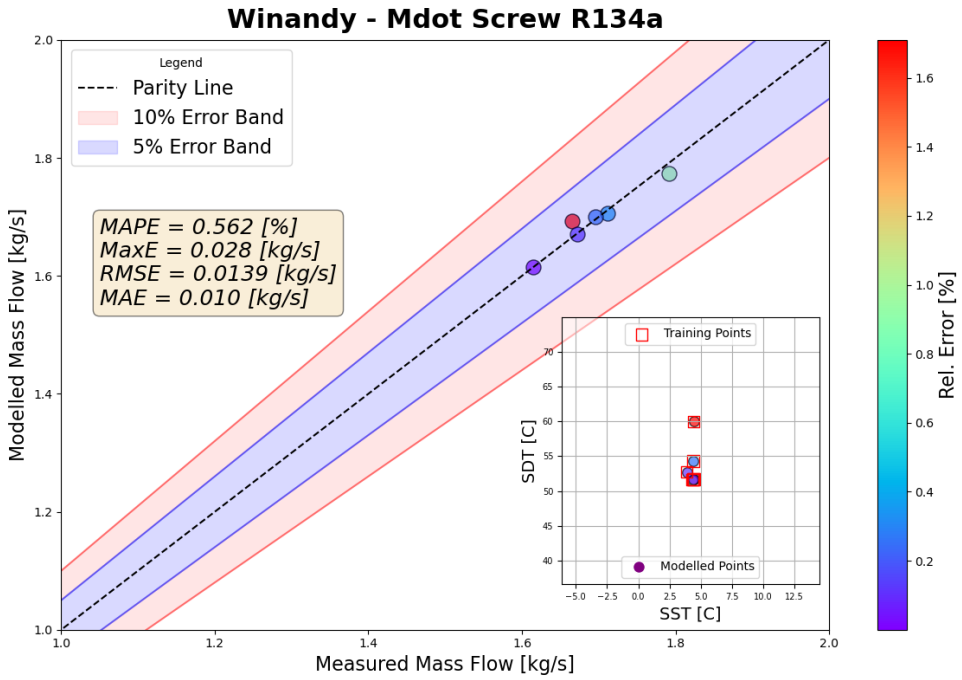

Figure A.7: Winandy model mass flow rate results for training data with screw compressor utilizing R134a

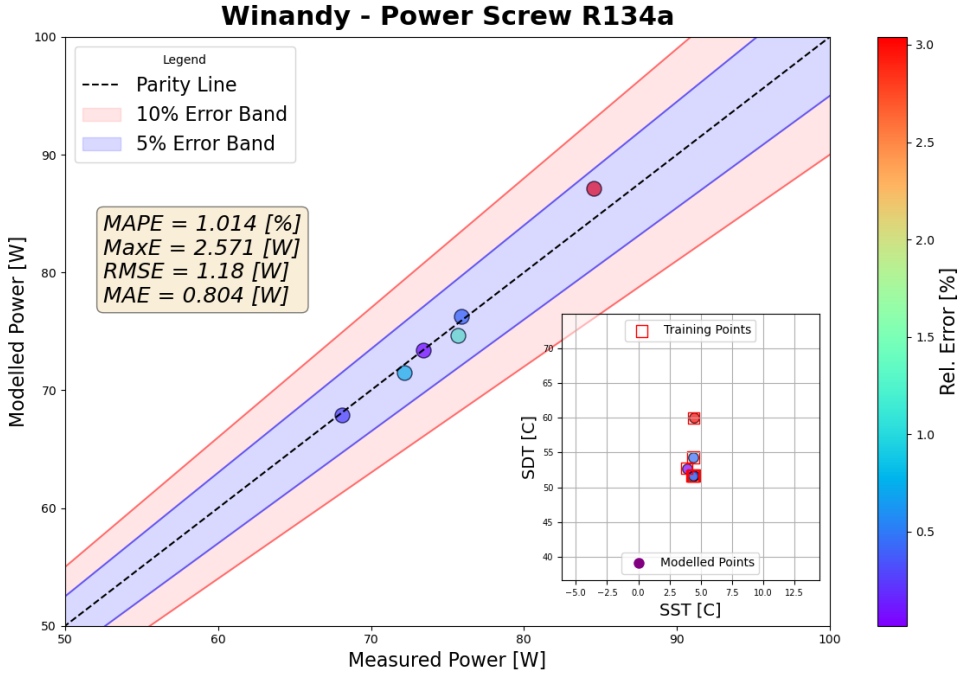

Figure A.8: Winandy model power results for training data with screw compressor utilizing R134a

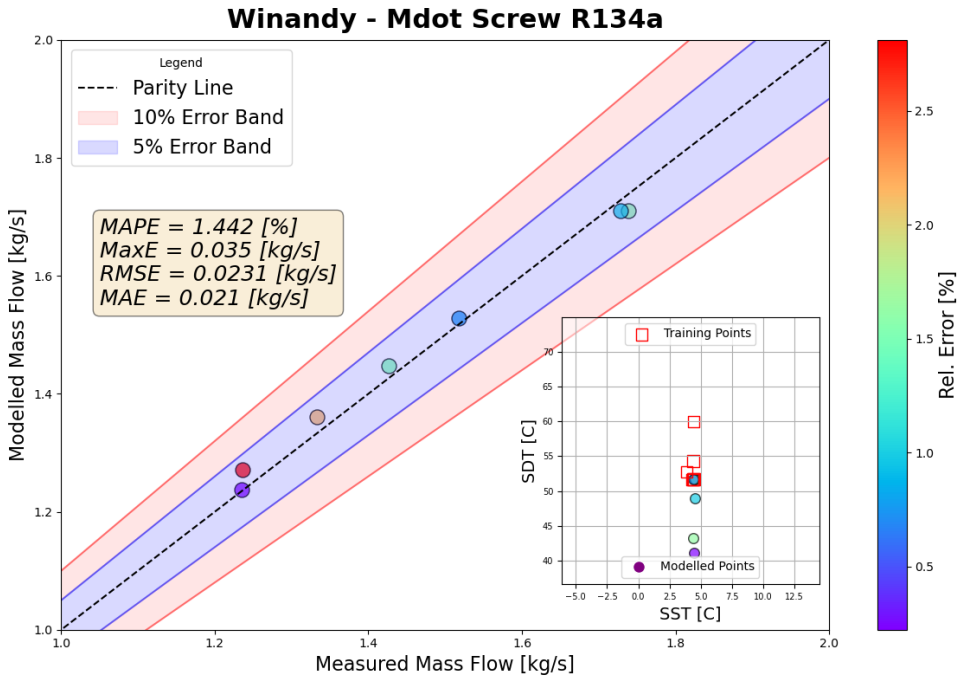

Figure A.9: Winandy model mass flow rate results for variable speed data with screw compressor utilizing R134a

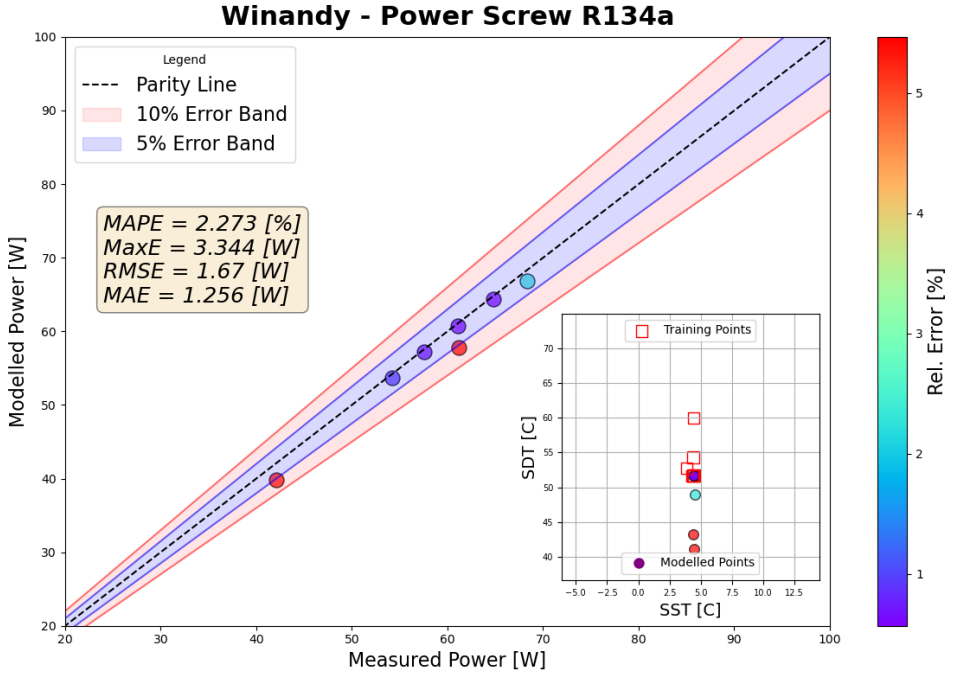

Figure A.10: Winandy model power results for variable speed data with screw compressor utilizing R134a

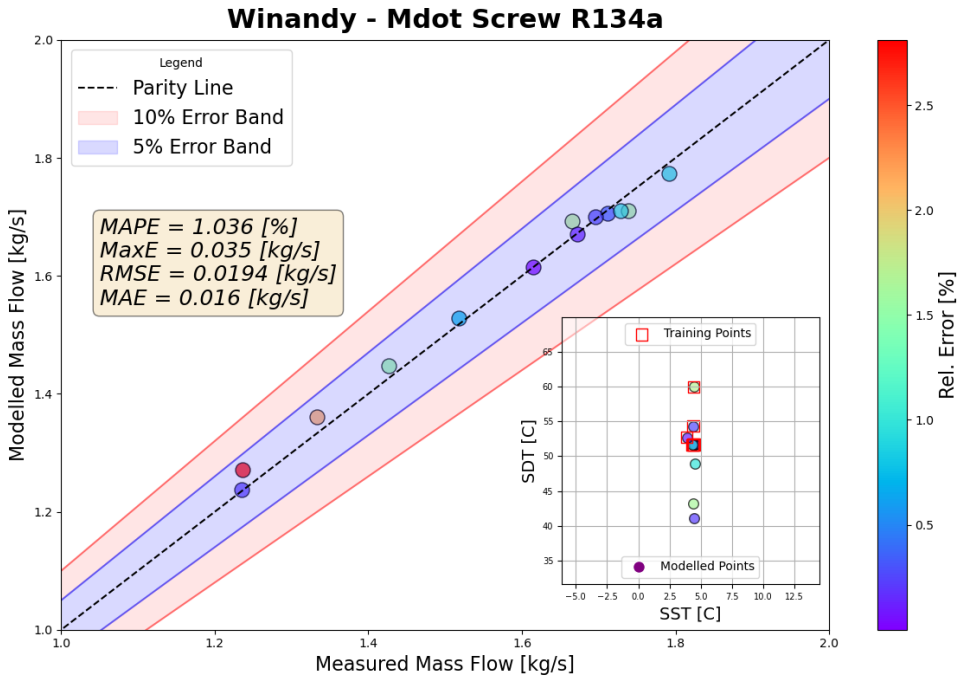

Figure A.11: Winandy model mass flow rate results for full data with screw compressor utilizing R134a

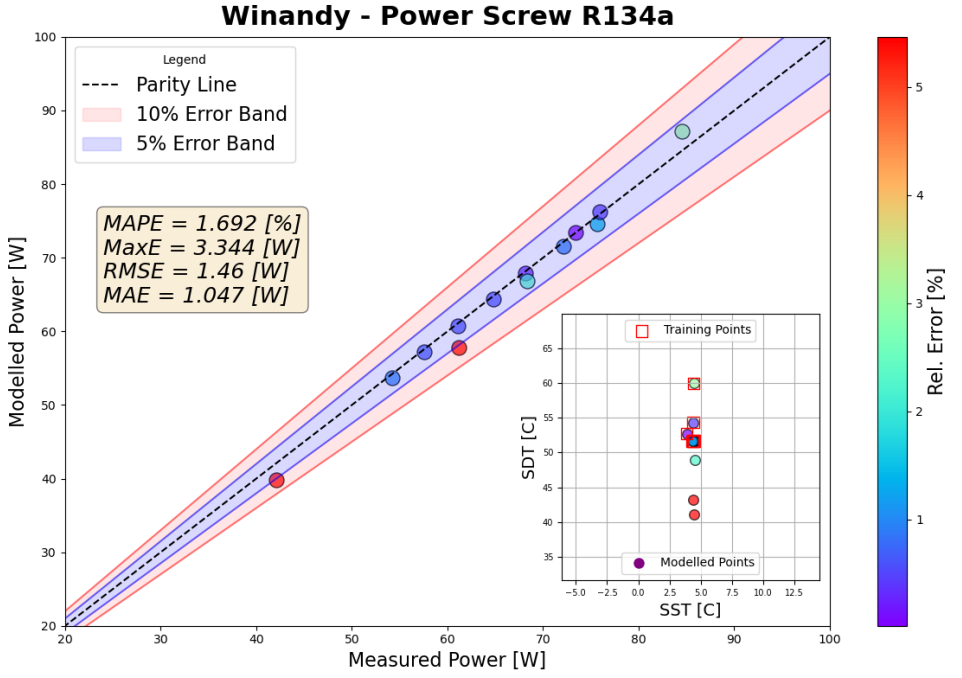

Figure A.12: Winandy model power results for full data with screw compressor utilizing R134a

0.3 Scroll Compressor Data utilizing R134a

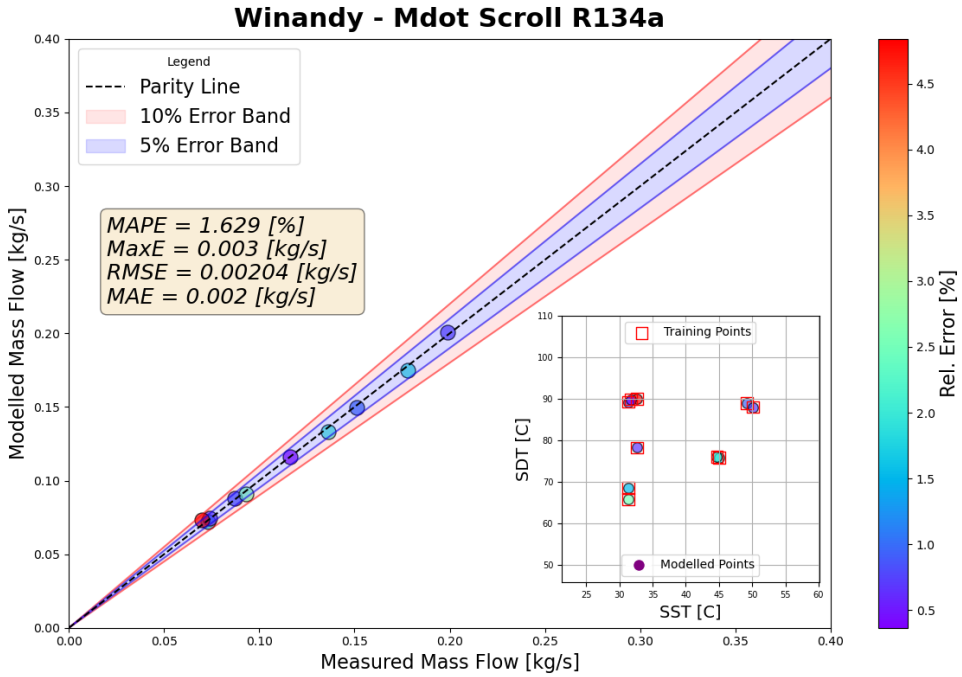

Figure A.13: Winandy model mass flow rate results for training data with scroll compressor utilizing R134a

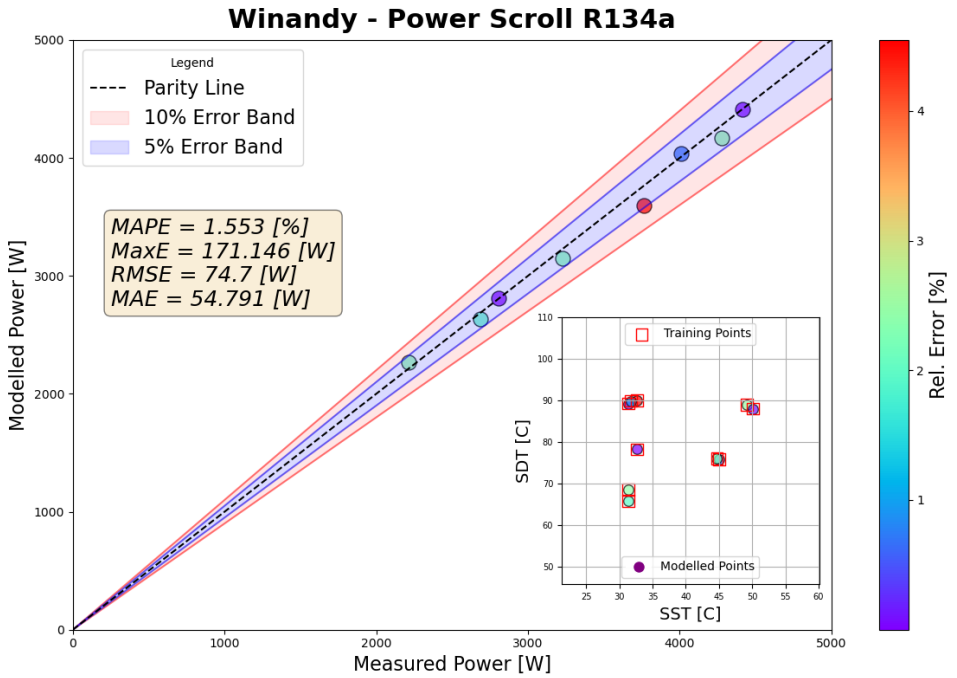

Figure A.14: Winandy model power results for training data with scroll compressor utilizing R134a

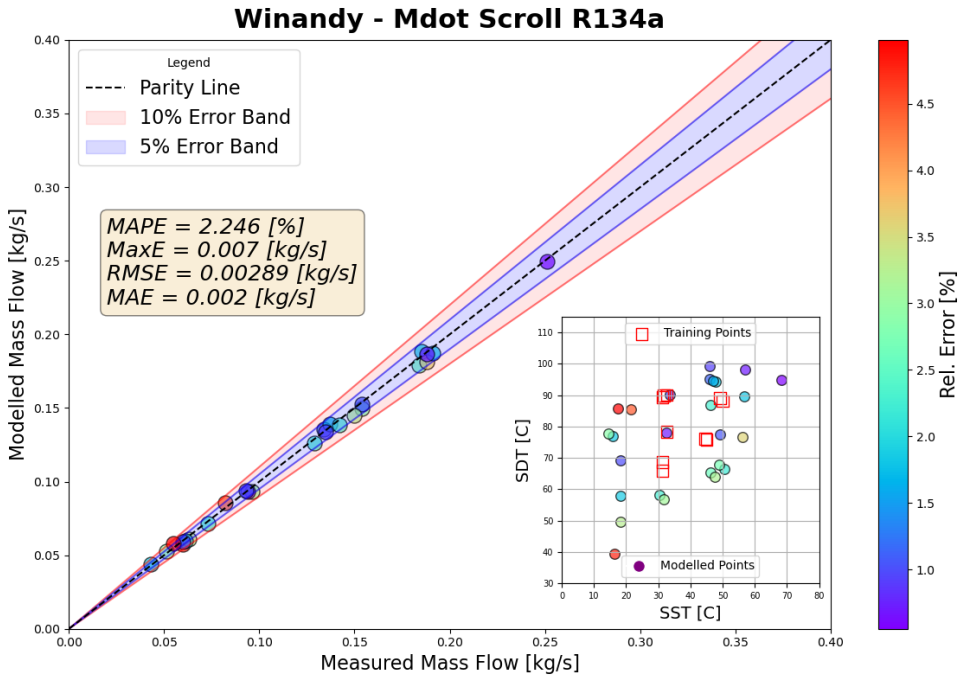

Figure A.15: Winandy model mass flow rate results for extrapolation data with scroll compressor utilizing R134a

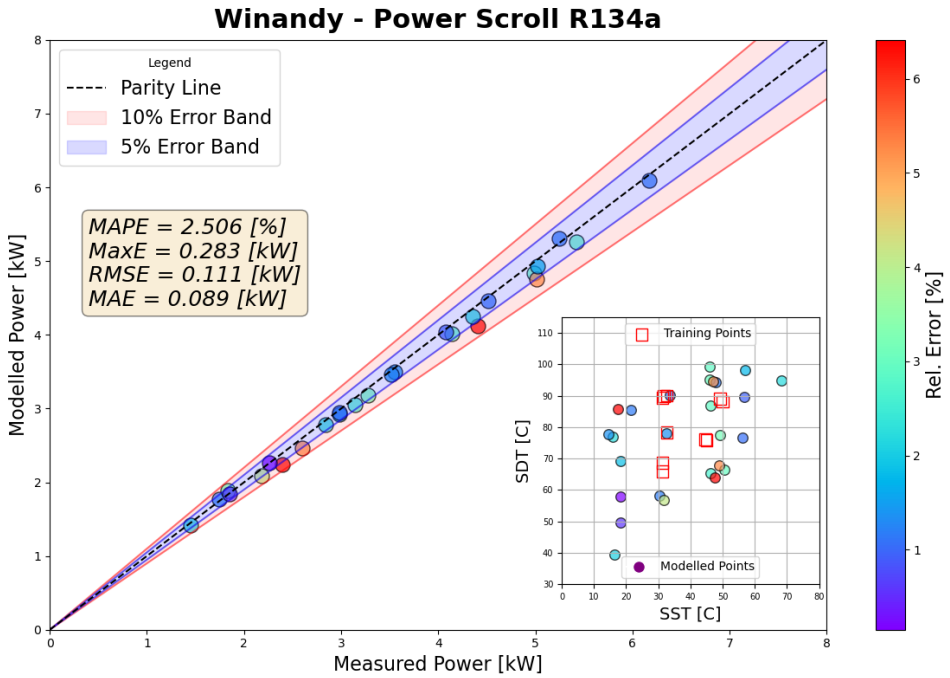

Figure A.16: Winandy model power results for extrapolation data with scroll compressor utilizing R134a

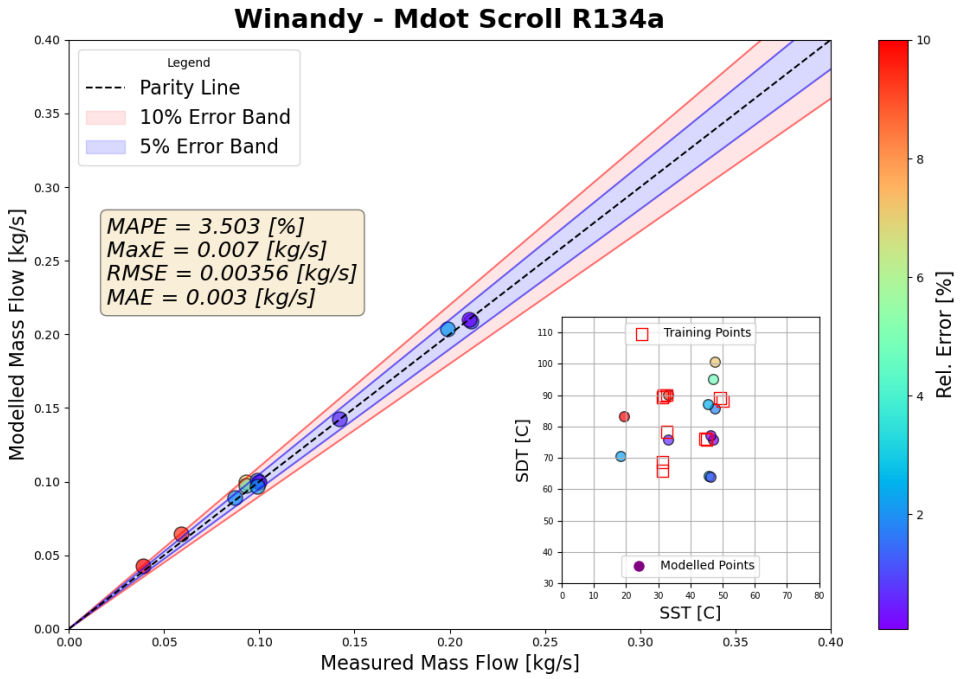

Figure A.17: Winandy model mass flow rate results for variable speed data with scroll compressor utilizing R134a

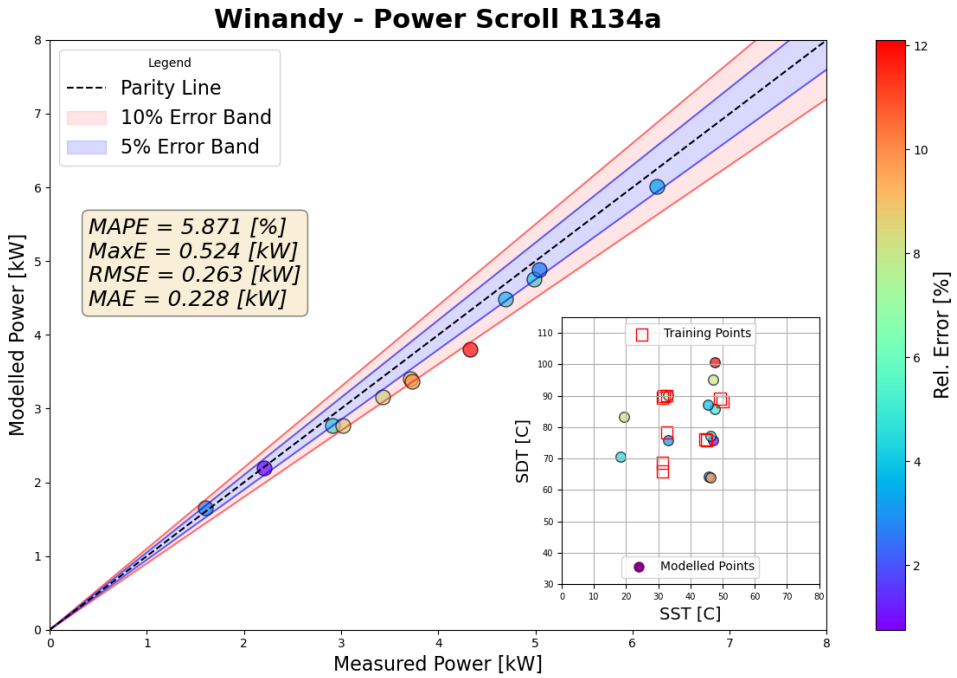

Figure A.18: Winandy model power results for variable speed data with scroll compressor utilizing R134a

0.4 Scroll Compressor Data utilizing R410A

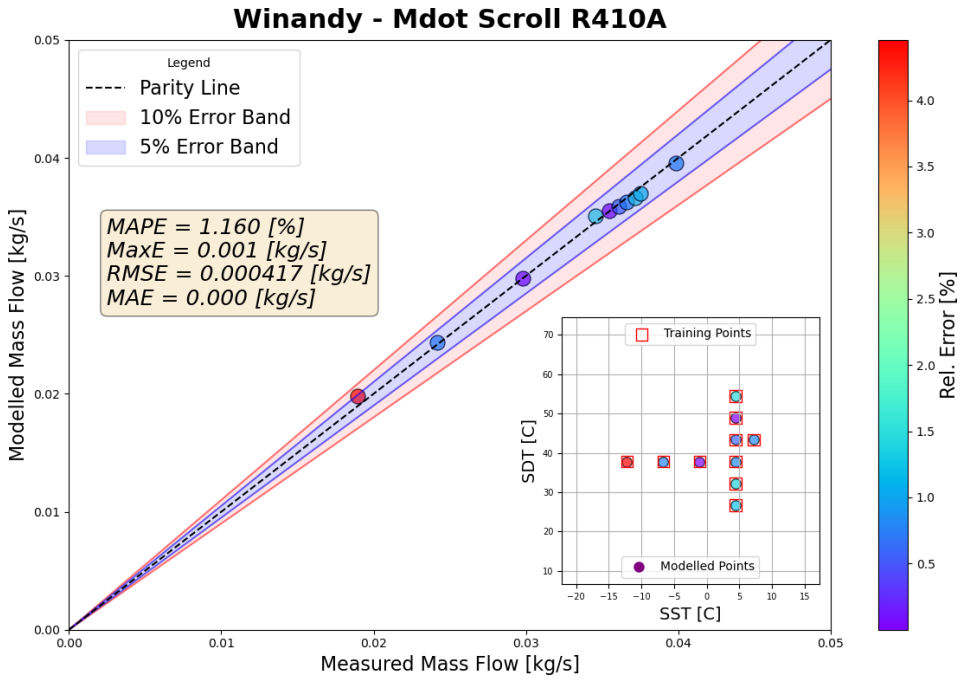

Figure A.19: Winandy model mass flow rate results for training data with scroll compressor utilizing R410A

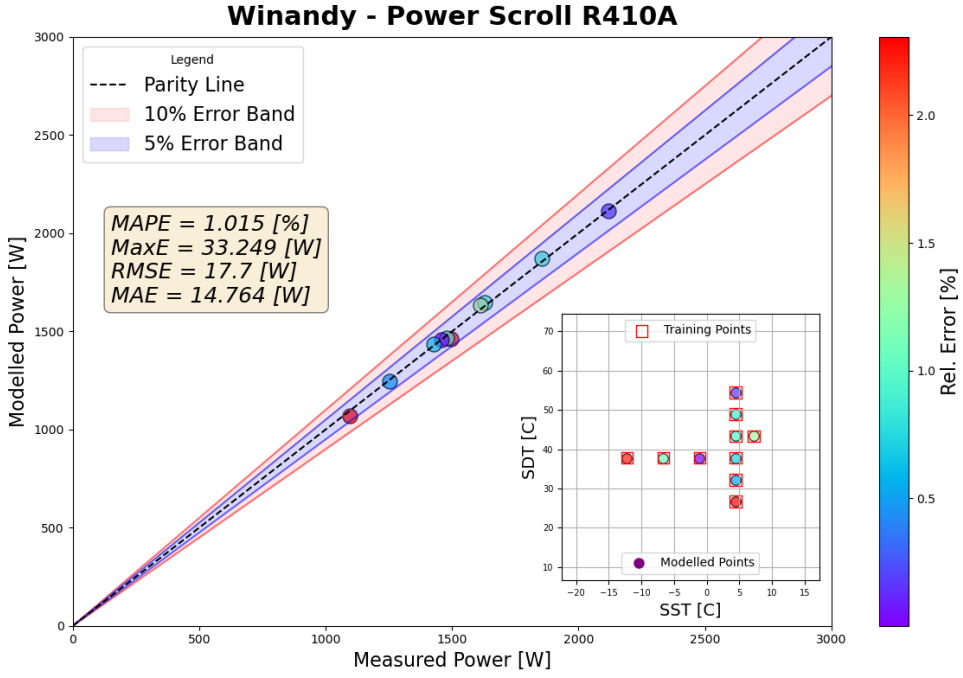

Figure A.20: Winandy model power results for training data with scroll compressor utilizing R410A

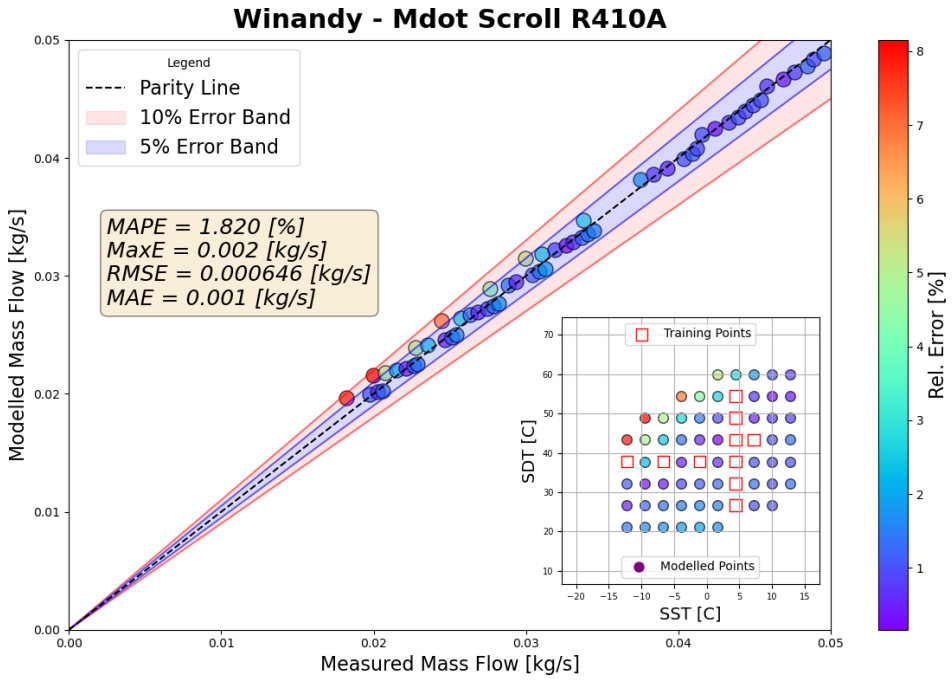

Figure A.21: Winandy model mass flow rate results for extrapolation data with scroll compressor utilizing R410A

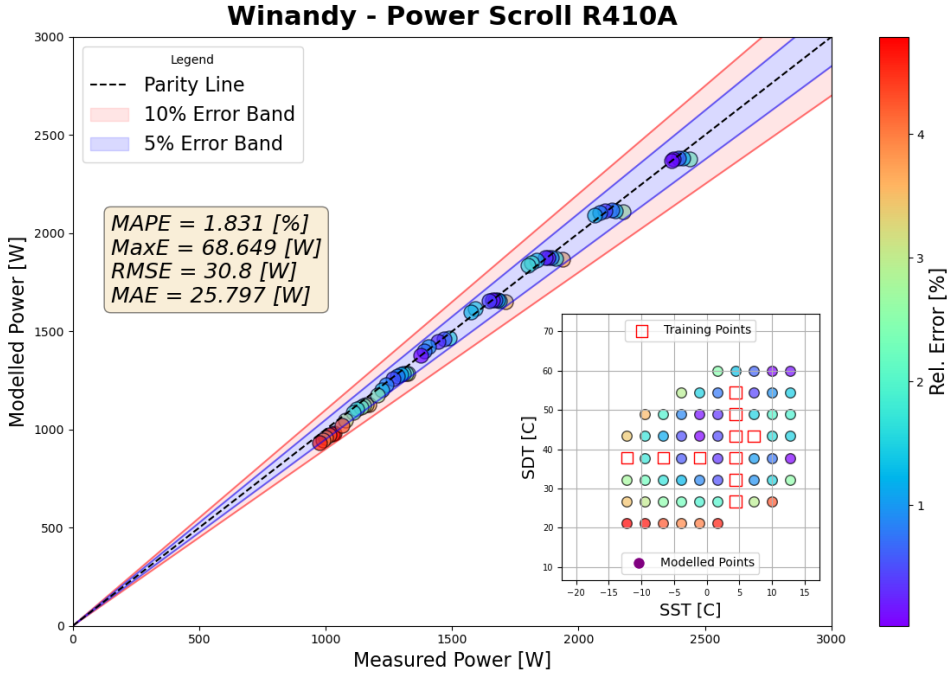

Figure A.22: Winandy model power results for extrapolation data with scroll compressor utilizing R410A

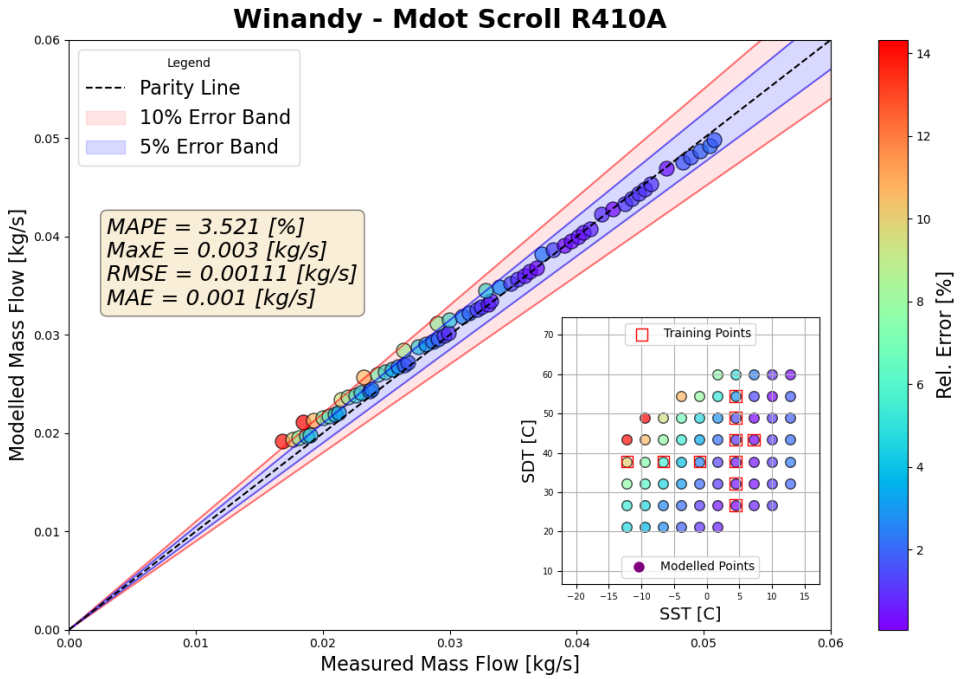

Figure A.23: Winandy model mass flow rate results for constant suction temperature data with scroll compressor utilizing R410A

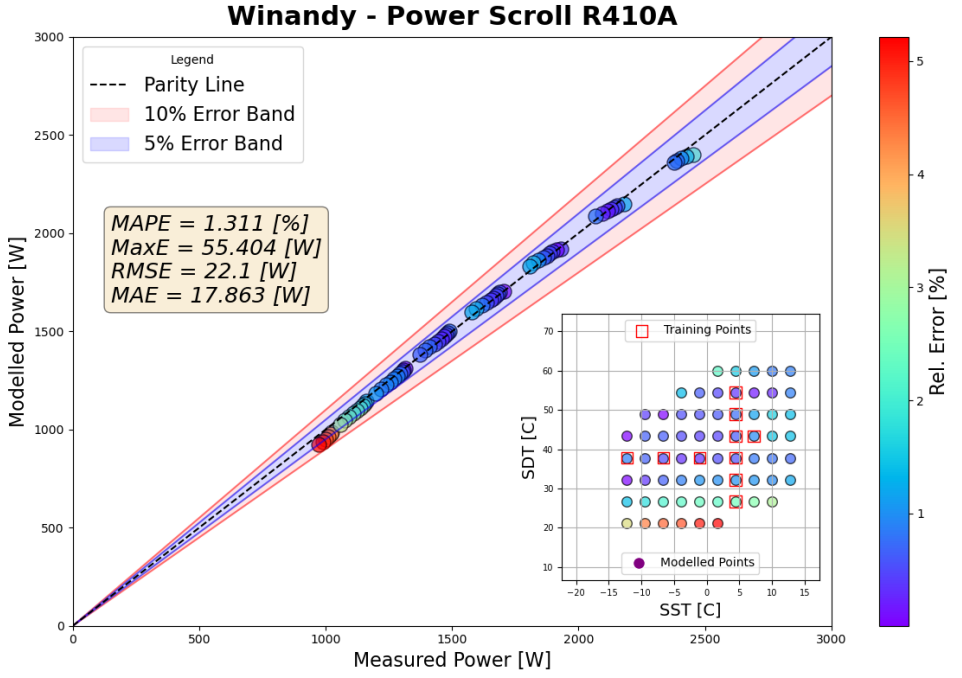

Figure A.24: Winandy model power results for constant suction temperature data with scroll compressor utilizing R410A

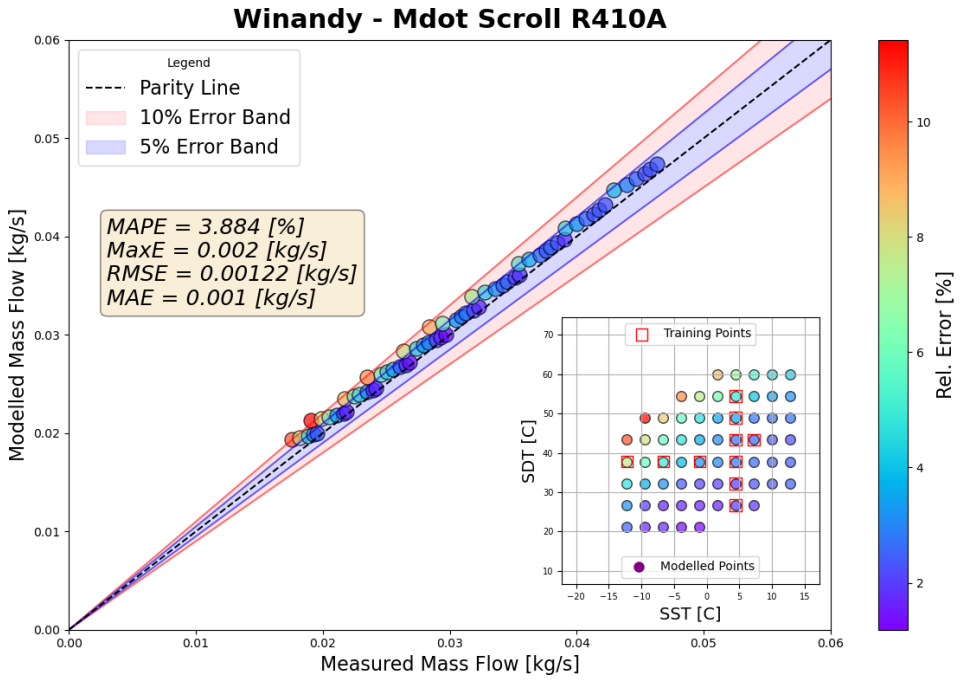

Figure A.25: Winandy model mass flow rate results for variable superheat data with scroll compressor utilizing R410A

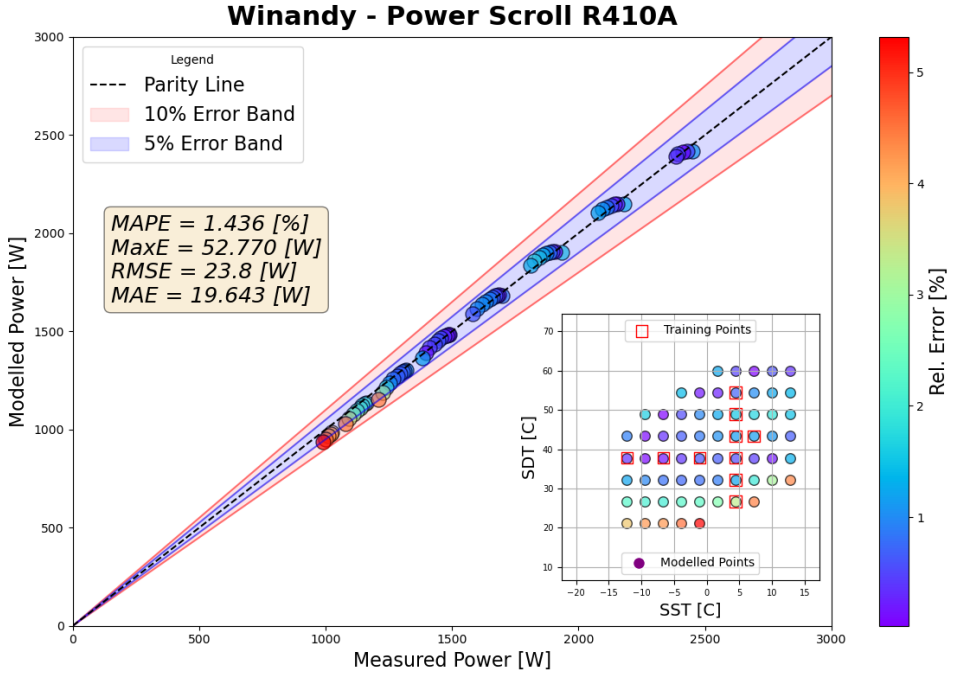

Figure A.26: Winandy model power results for variable superheat data with scroll compressor utilizing R410A

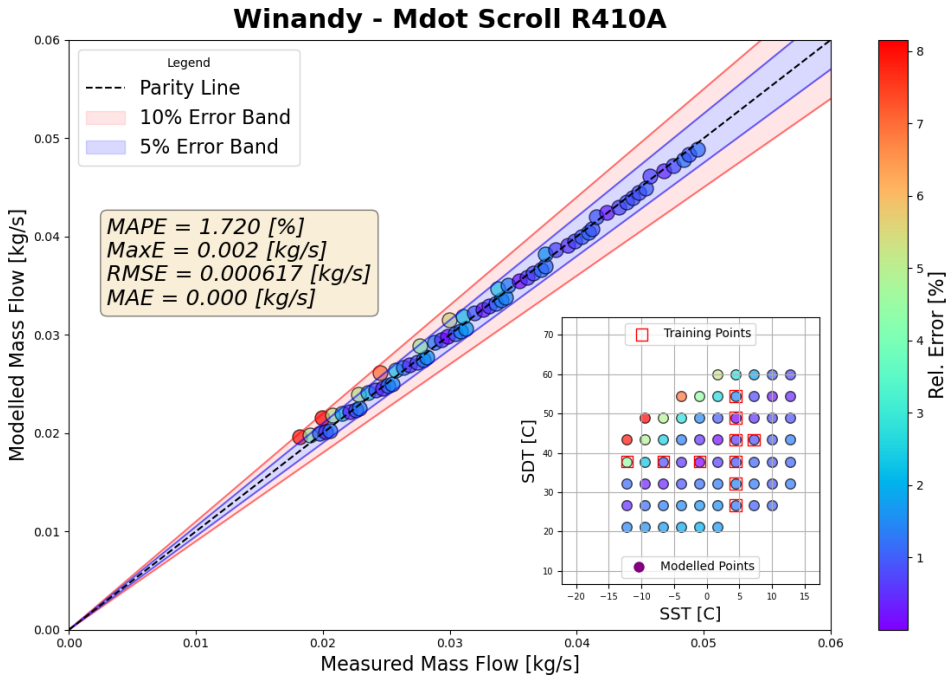

Figure A.27: Winandy model mass flow rate results for full data with scroll compressor utilizing R410A

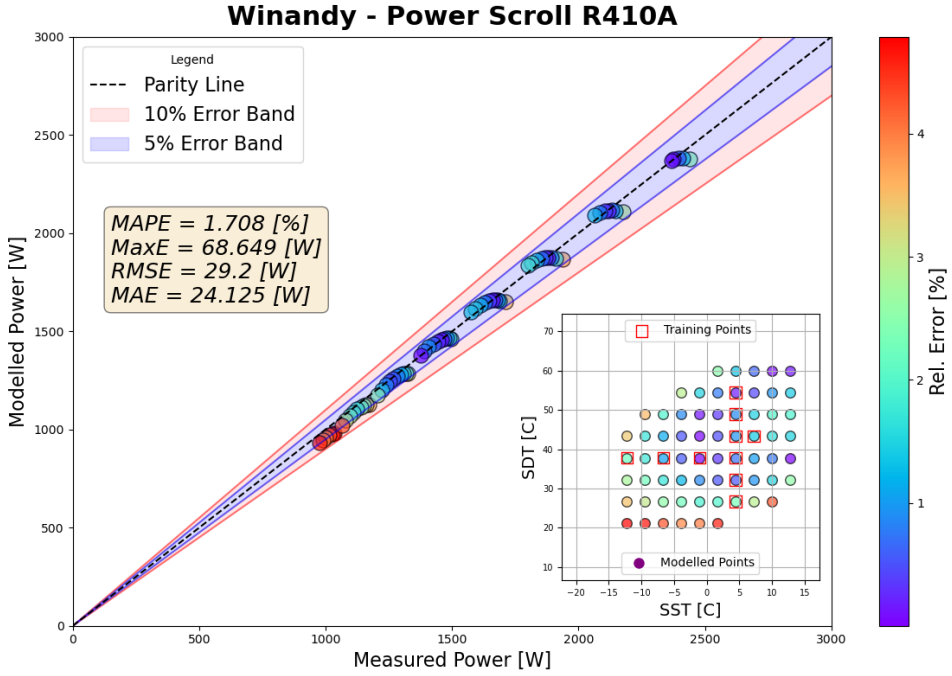

Figure A.28: Winandy model power results for full data with scroll compressor utilizing R410A

0.5 Spool Compressor Data utilizing R134a

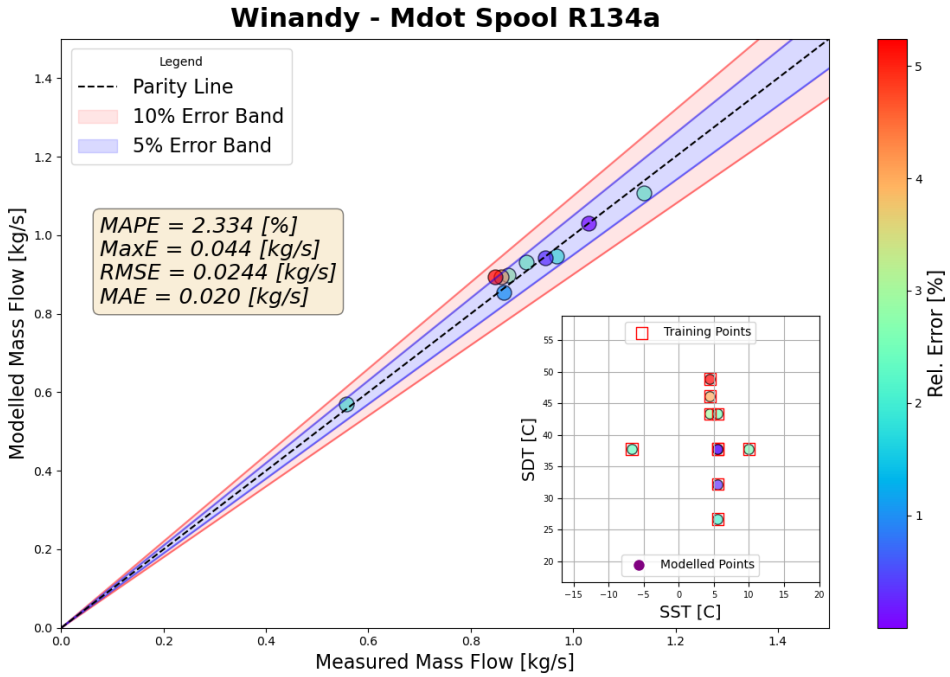

Figure A.29: Winandy model mass flow rate results for training data with spool compressor utilizing R134a

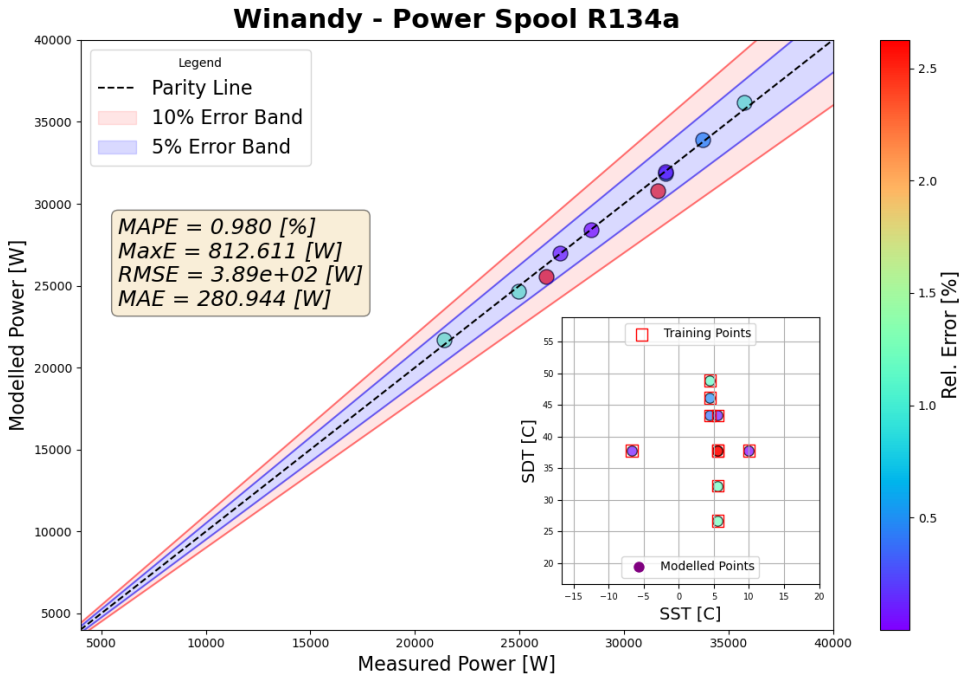

Figure A.30: Winandy model power results for training data with spool compressor utilizing R134a

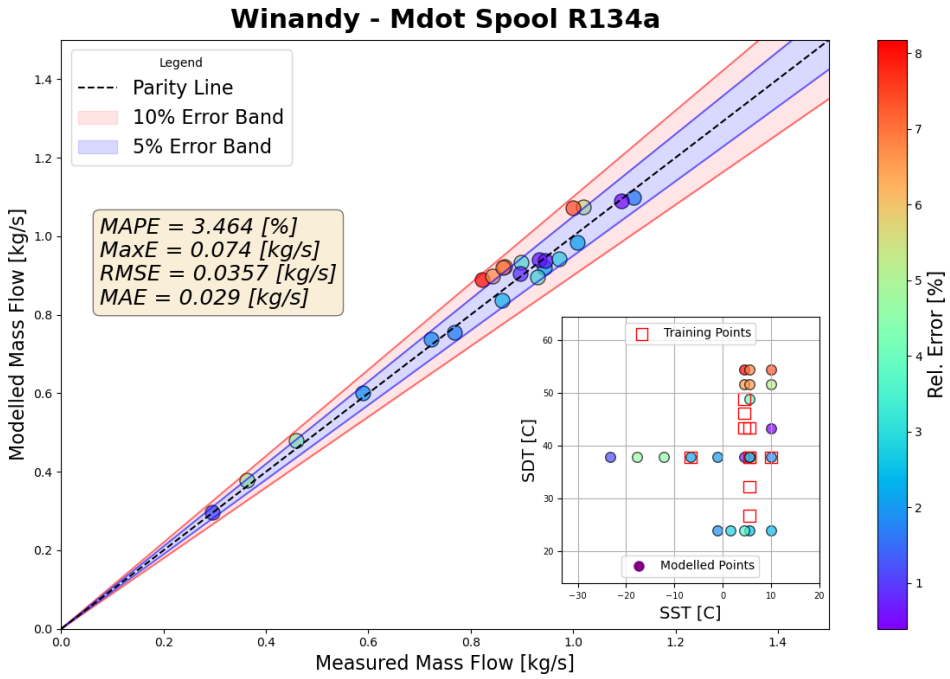

Figure A.31: Winandy model mass flow rate results for extrapolation data with spool compressor utilizing R134a

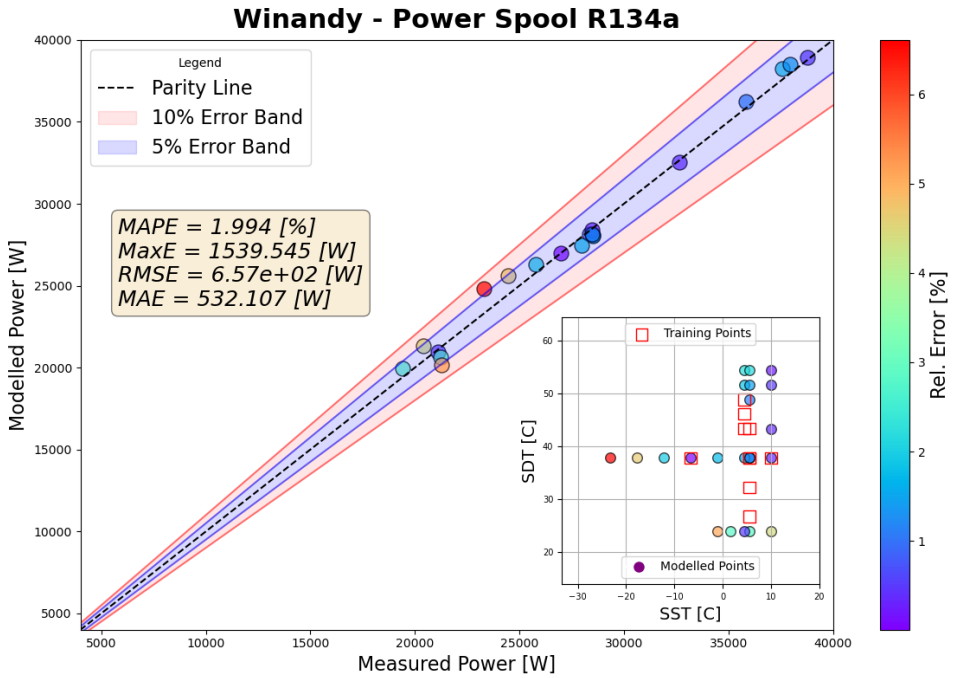

Figure A.32: Winandy model power results for extrapolation data with spool compressor utilizing R134a

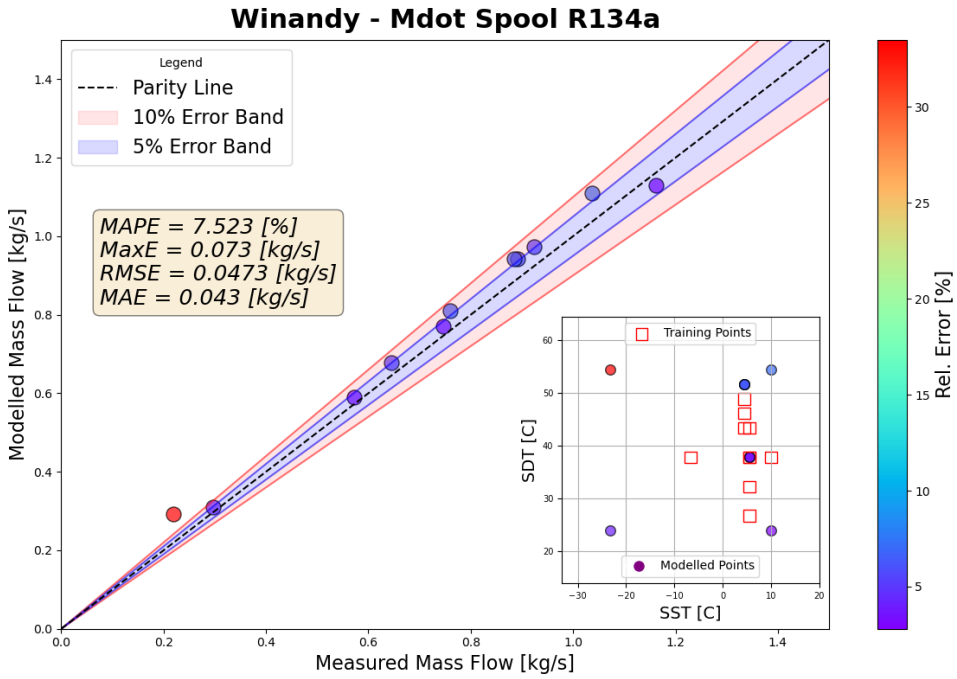

Figure A.33: Winandy model mass flow rate results for variable speed data with spool compressor utilizing R134a

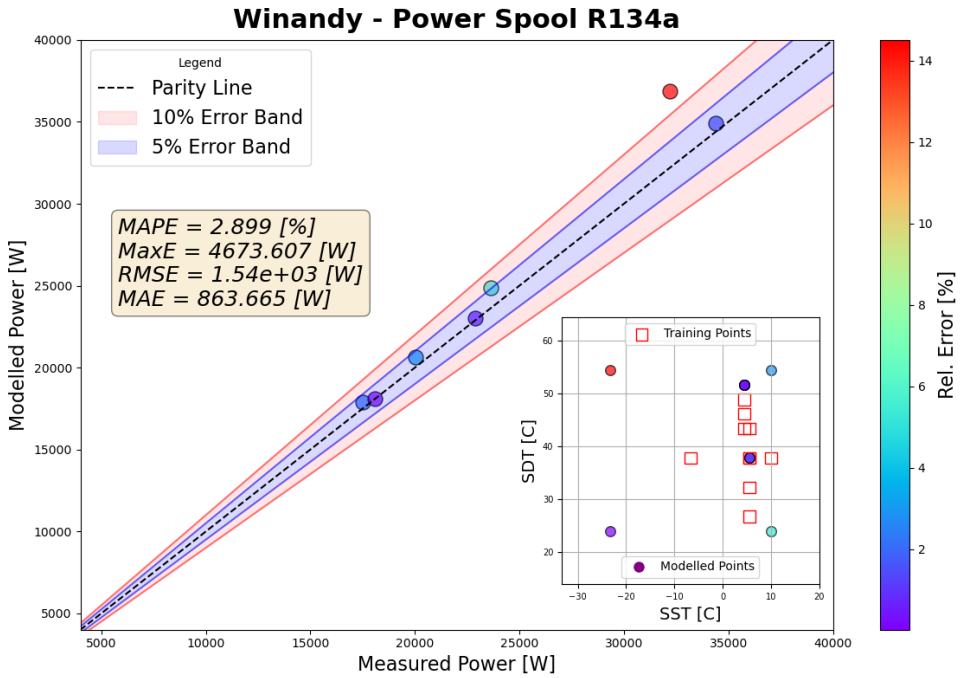

Figure A.34: Winandy model power results for variable speed data with spool compressor utilizing R134a

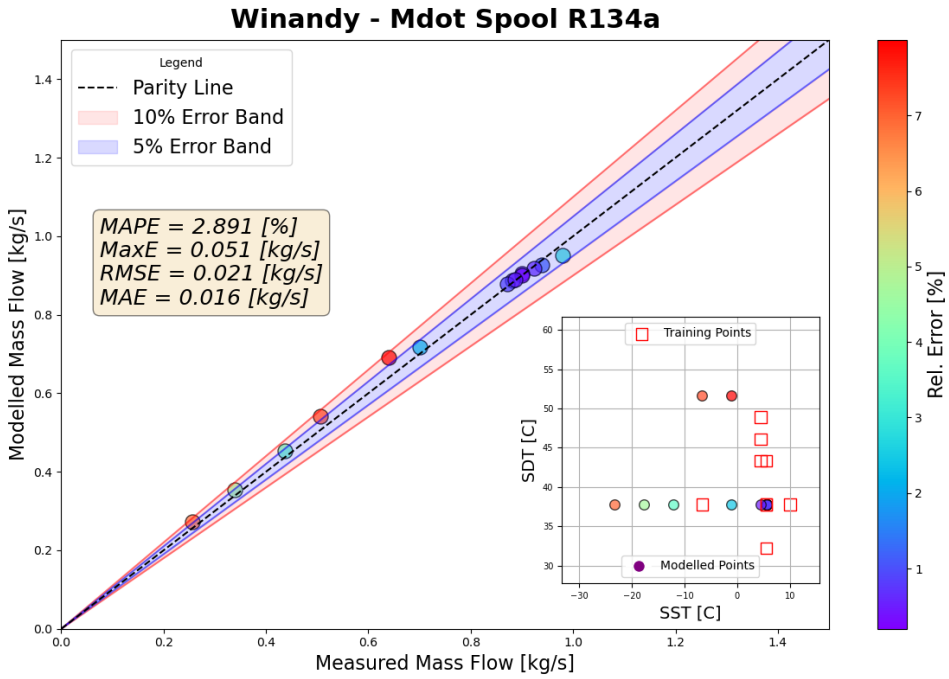

Figure A.35: Winandy model mass flow rate results for variable superheat data with spool compressor utilizing R134a

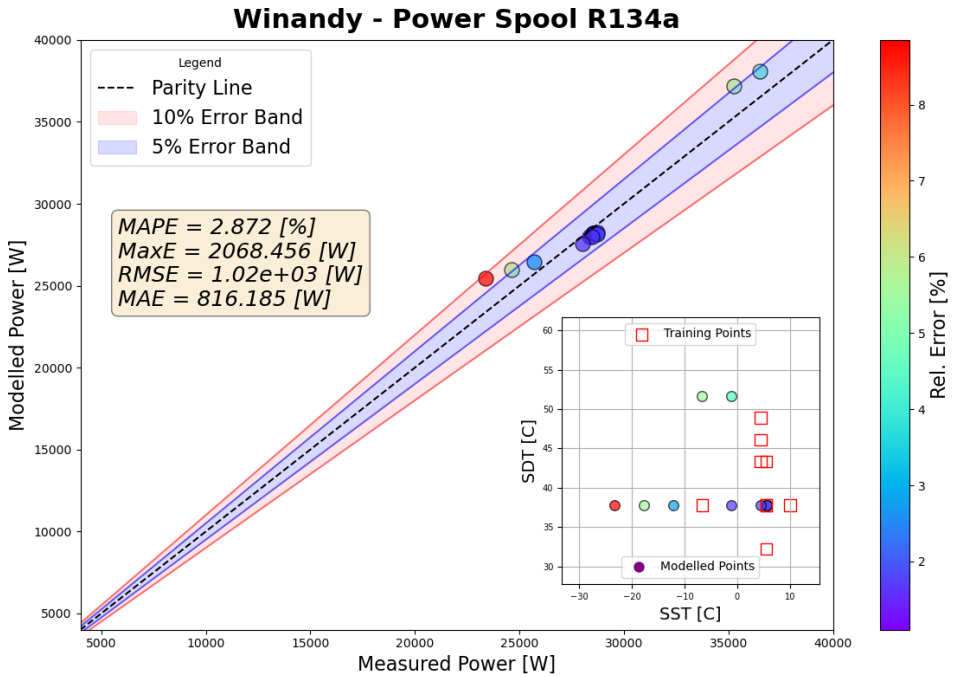

Figure A.36: Winandy model power results for variable superheat data with spool compressor utilizing R134a

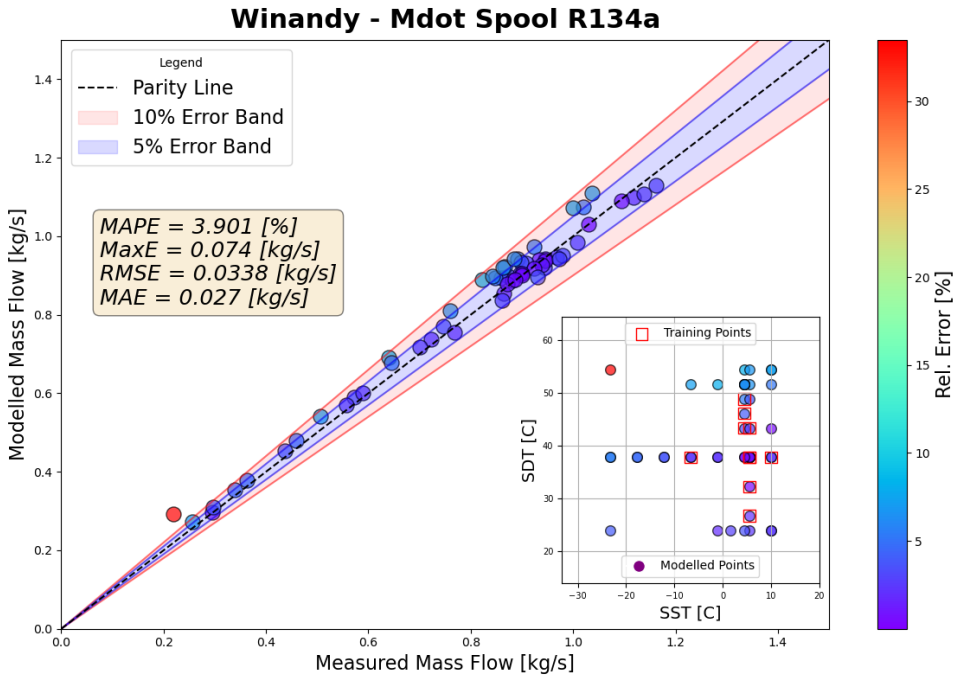

Figure A.37: Winandy model mass flow rate results for full data with spool compressor utilizing R134a

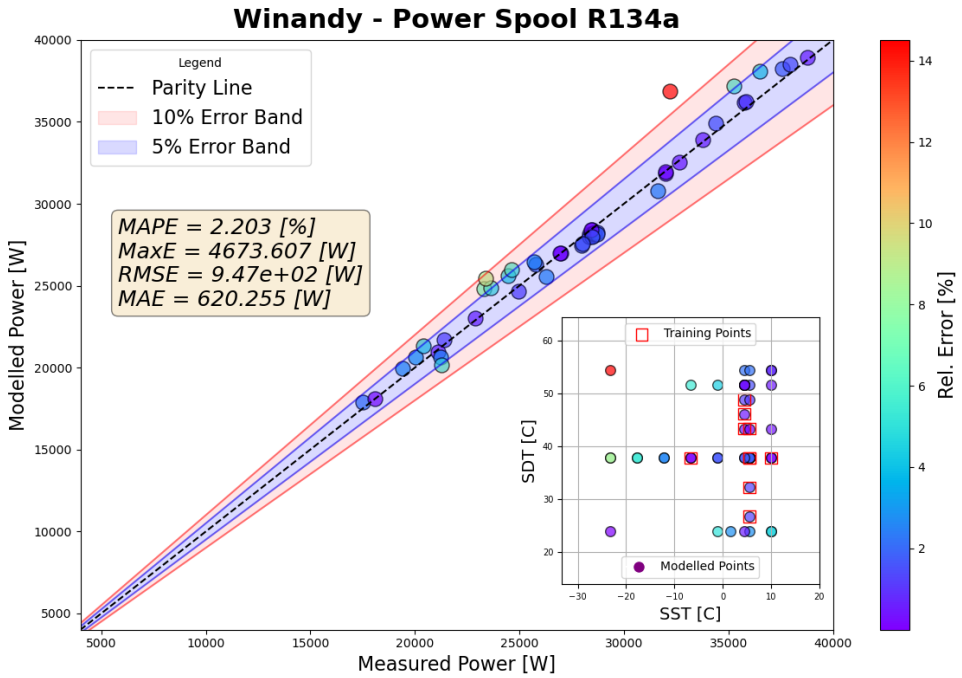

Figure A.38: Winandy model power results for full data with spool compressor utilizing R134a

0.6 Spool Compressor Data utilizing R1234ze(E)

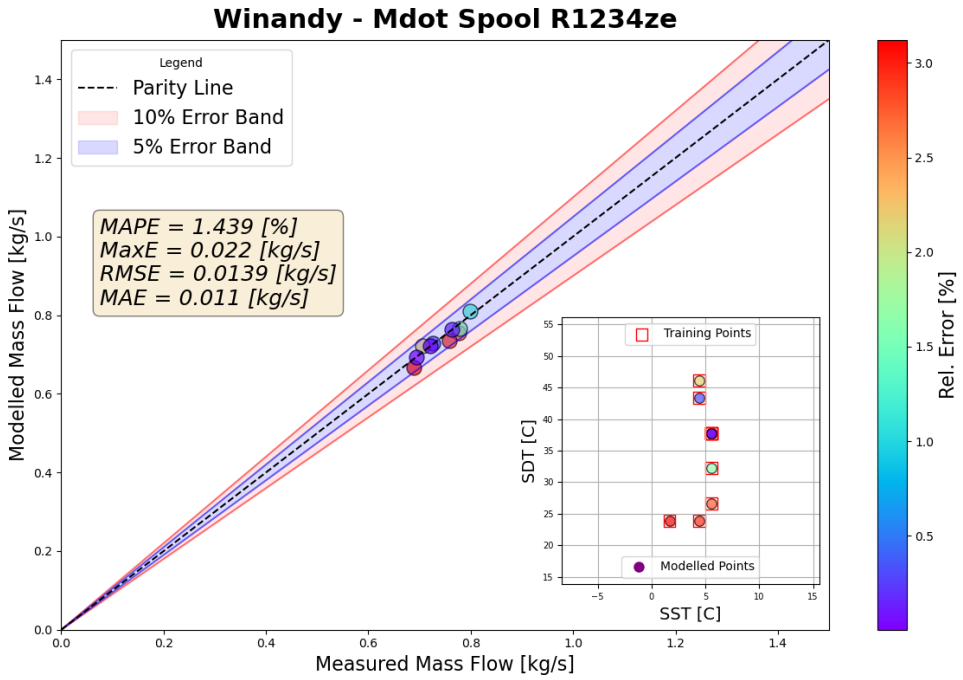

Figure A.39: Winandy model mass flow rate results for training data with spool compressor utilizing R1234ze(E)

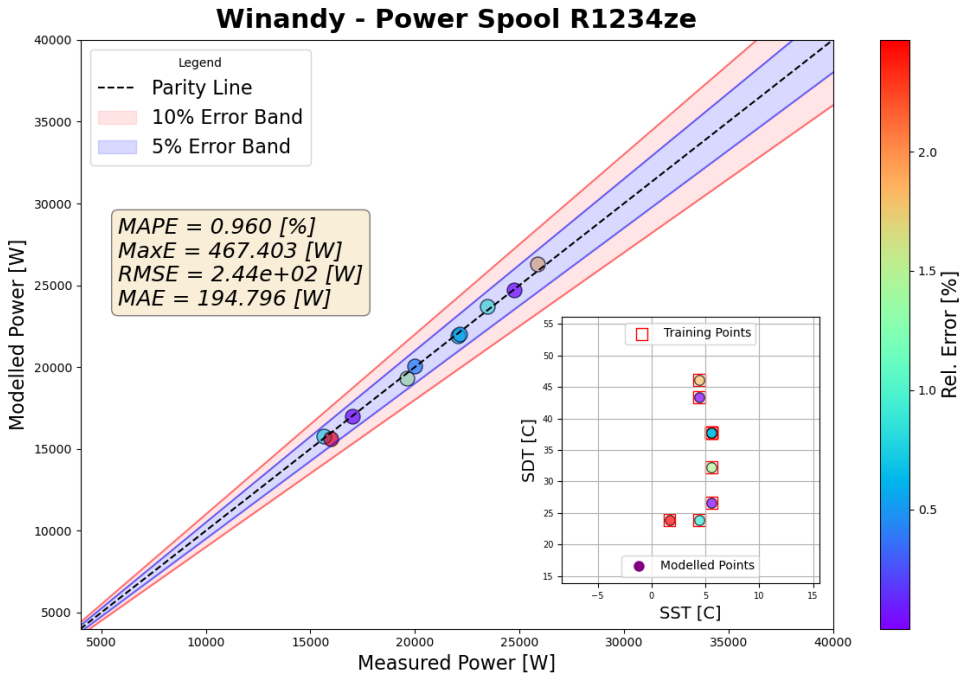

Figure A.40: Winandy model power results for training data with spool compressor utilizing R1234ze(E)

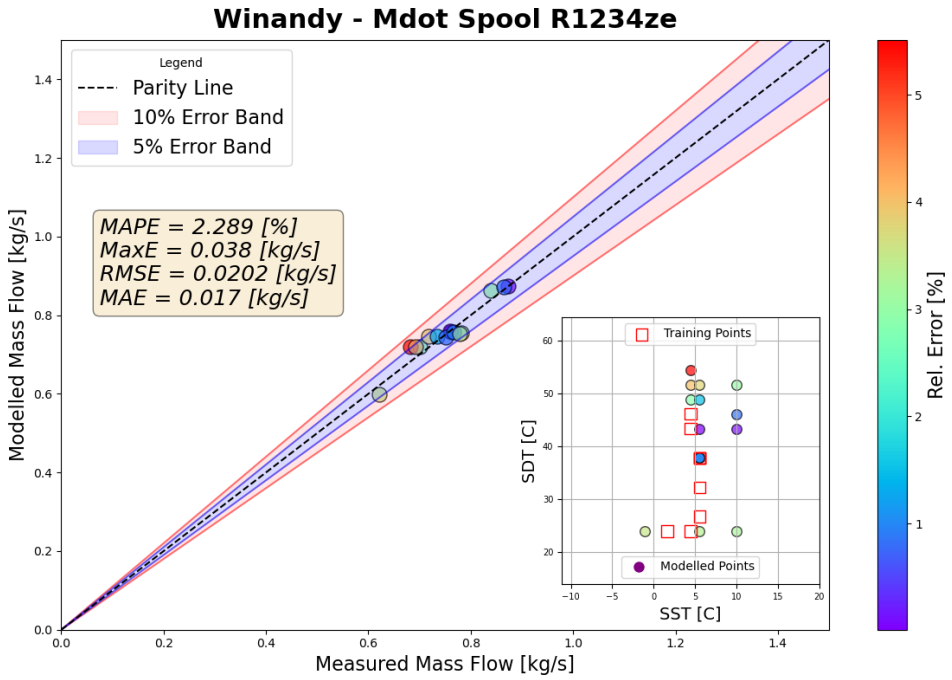

Figure A.41: Winandy model mass flow rate results for extrapolation data with spool compressor utilizing R1234ze(E)

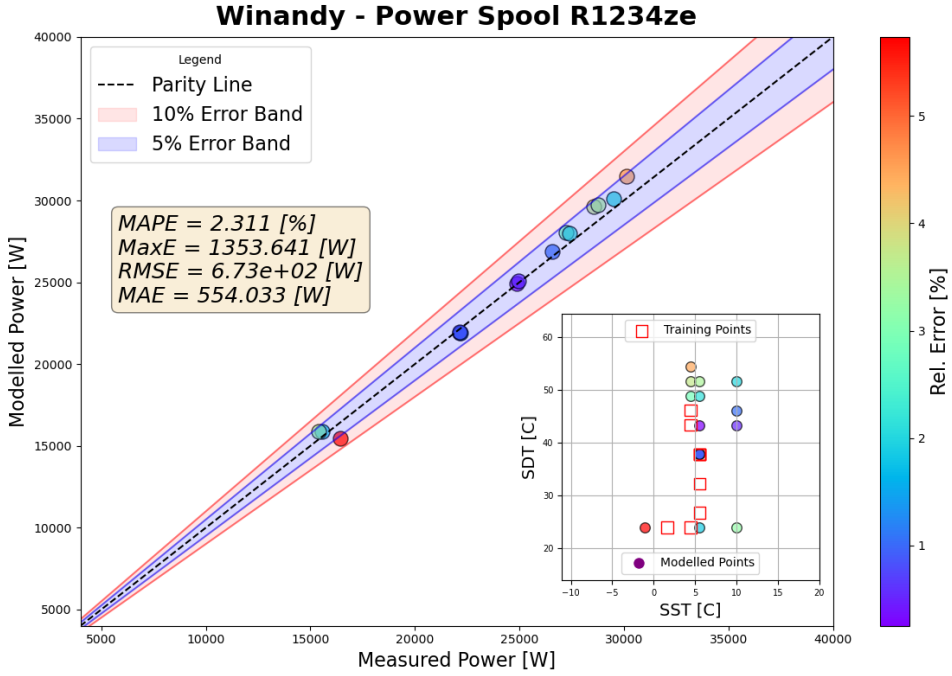

Figure A.42: Winandy model power results for extrapolation data with spool compressor utilizing R1234ze(E)

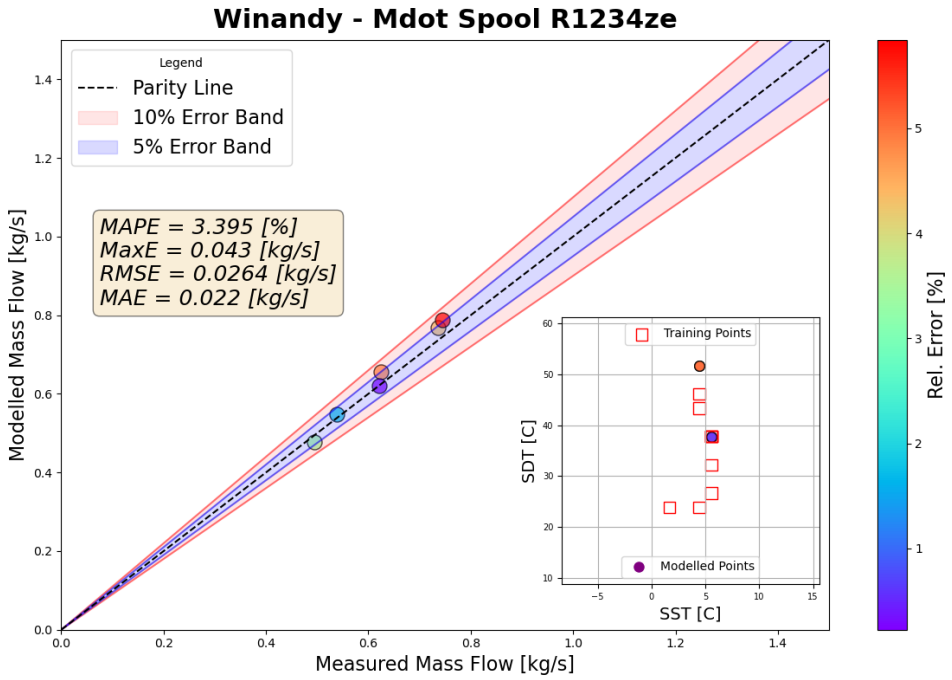

Figure A.43: Winandy model mass flow rate results for variable speed data with spool compressor utilizing R1234ze(E)

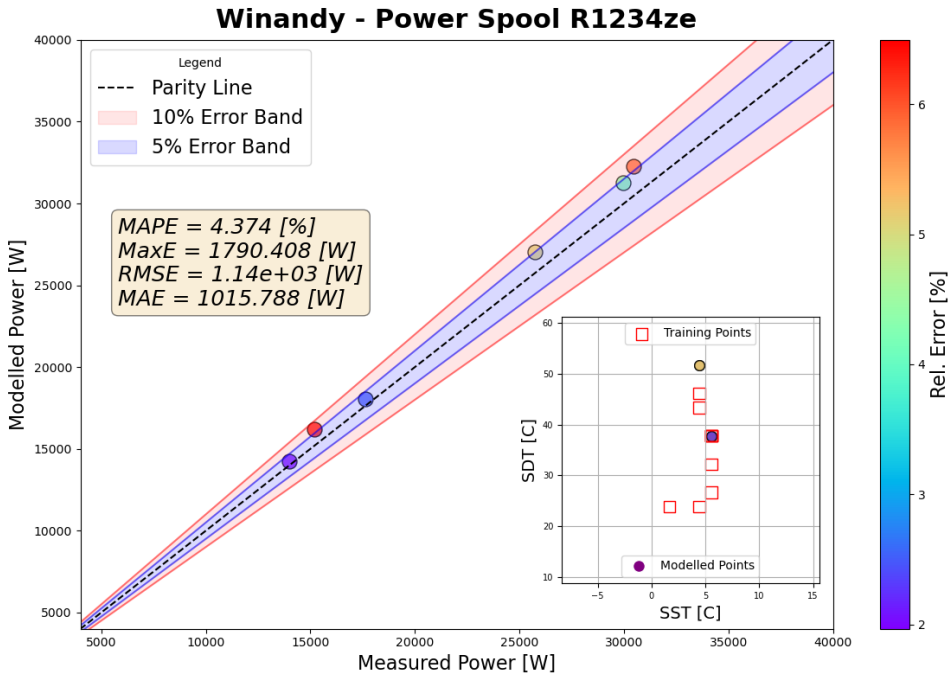

Figure A.44: Winandy model power results for variable speed data with spool compressor utilizing R1234ze(E)

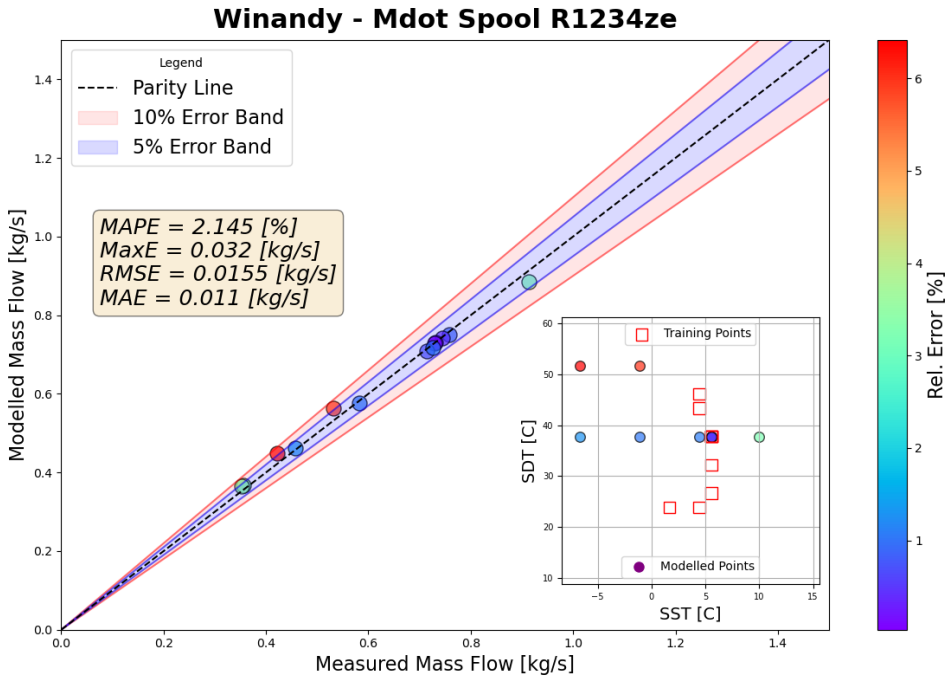

Figure A.45: Winandy model mass flow rate results for variable superheat data with spool compressor utilizing R1234ze(E)

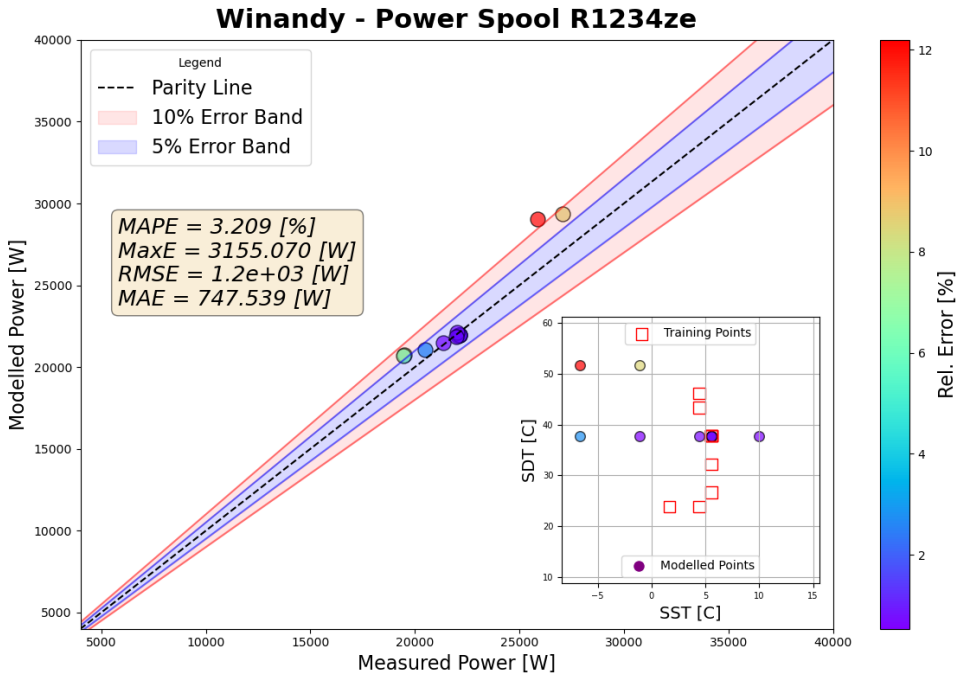

Figure A.46: Winandy model power results for variable superheat data with spool compressor utilizing R1234ze(E)

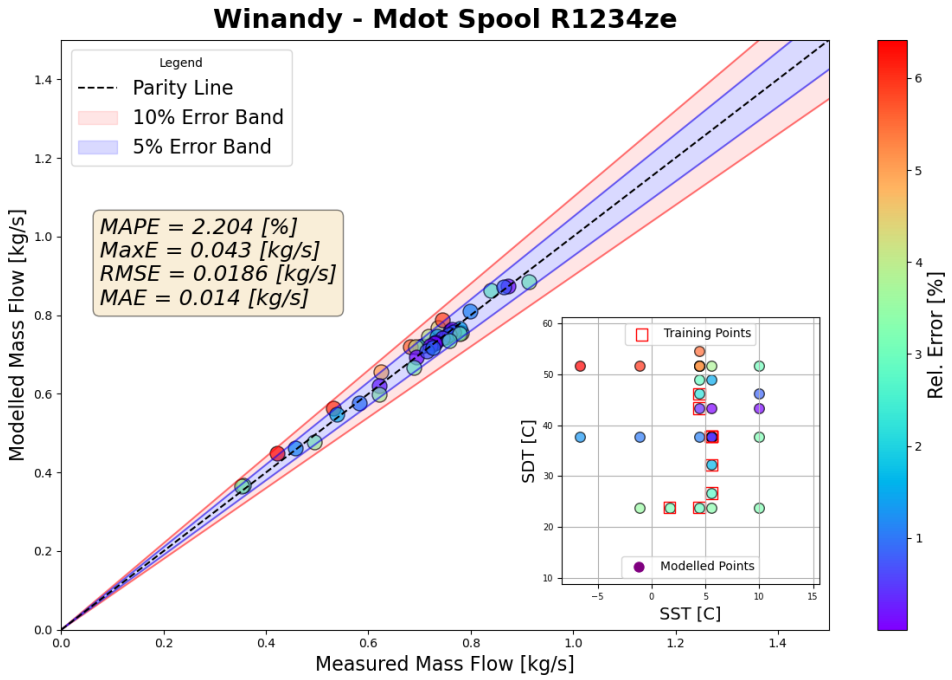

Figure A.47: Winandy model mass flow rate results for full data with spool compressor utilizing R1234ze(E)

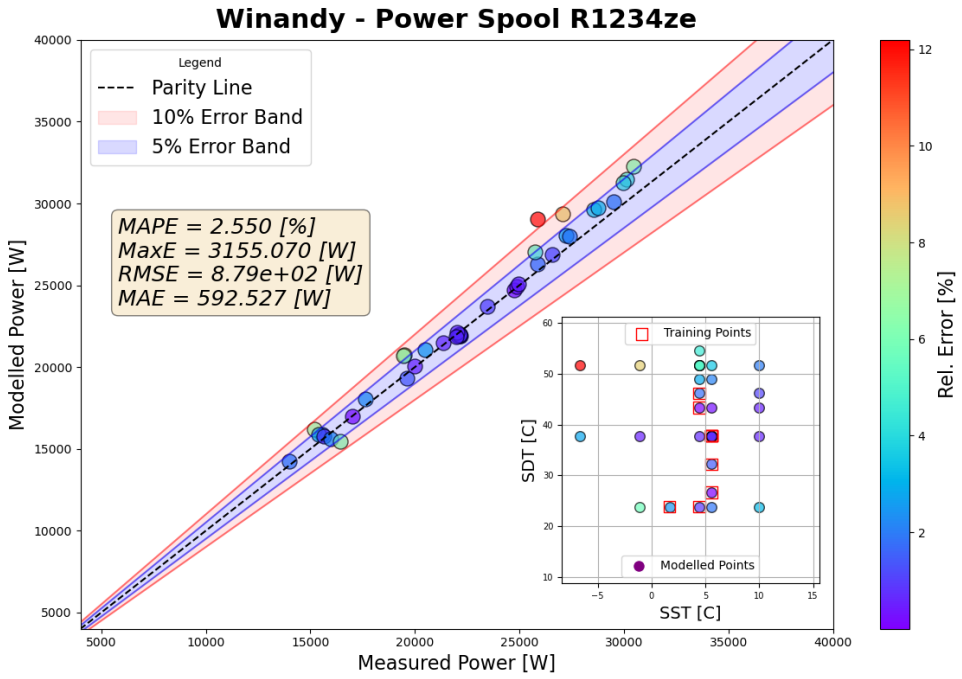

Figure A.48: Winandy model power results for full data with spool compressor utilizing R1234ze(E)

0.7 Reciprocating Compressor Data utilizing R32

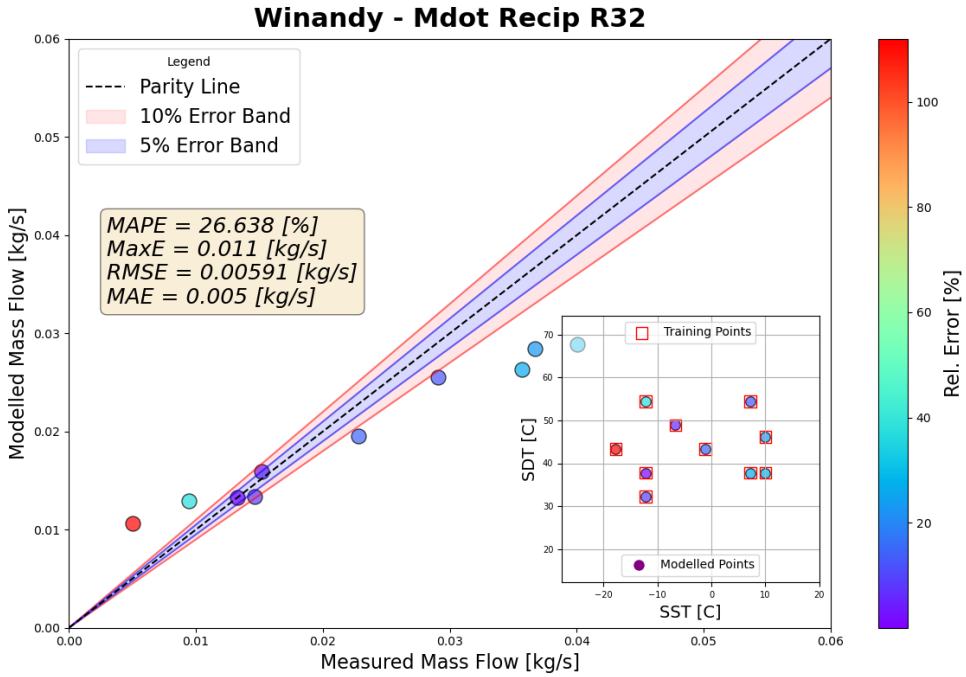

Figure A.49: Winandy model mass flow rate results for training data with reciprocating compressor utilizing R32

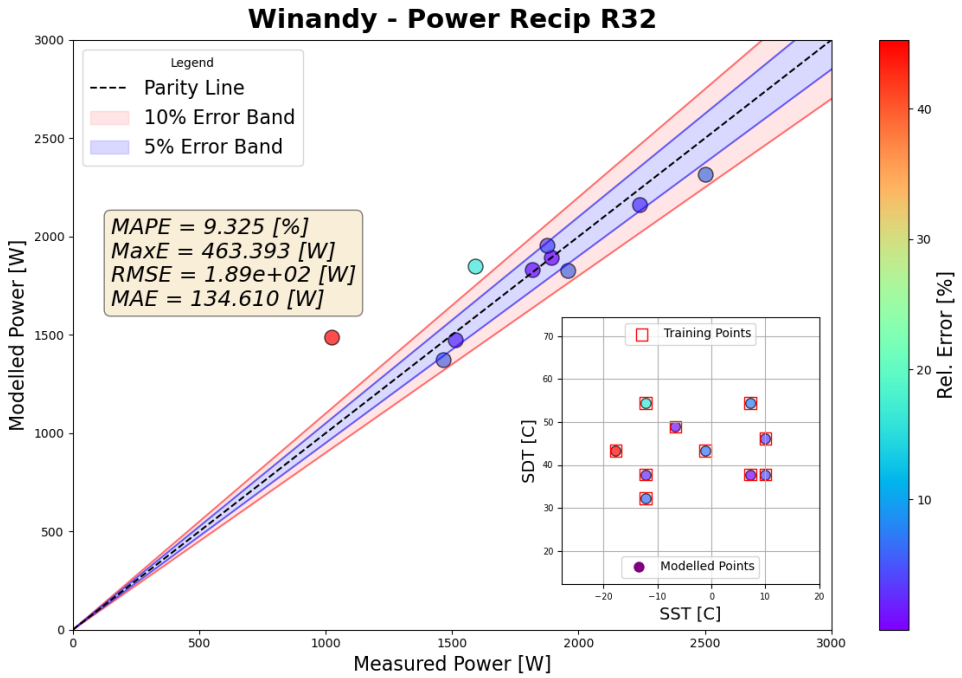

Figure A.50: Winandy model power results for training data with reciprocating compressor utilizing R32

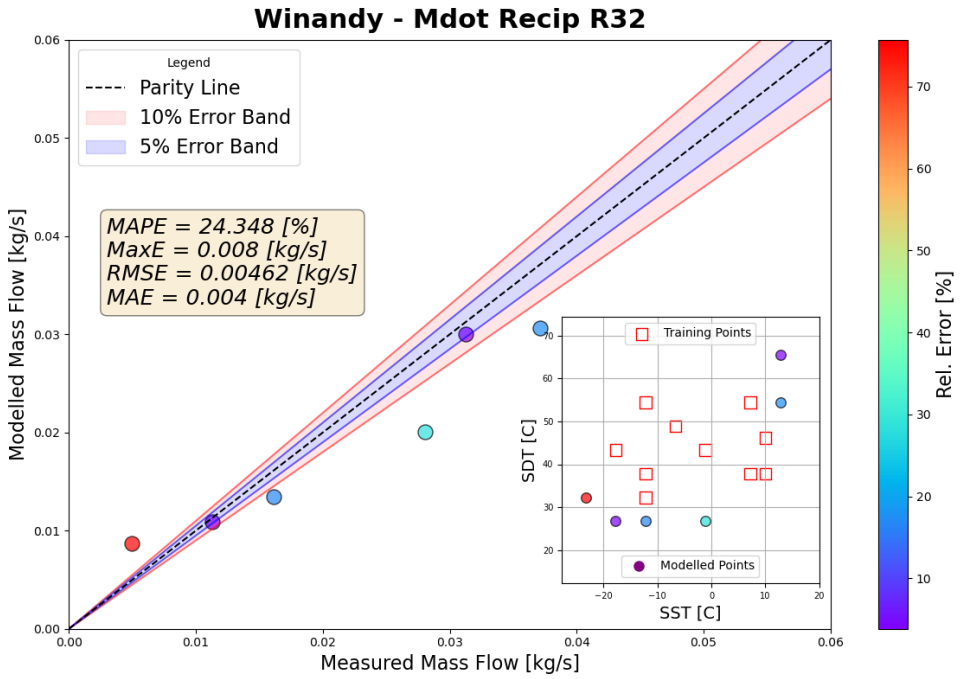

Figure A.51: Winandy model mass flow rate results for extrapolation data with reciprocating compressor utilizing R32

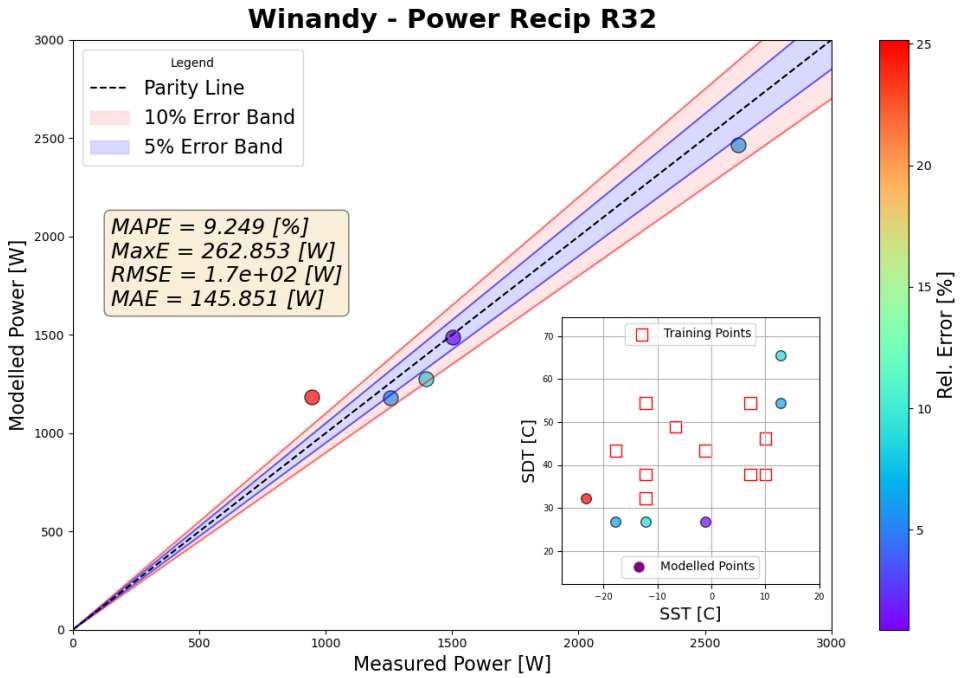

Figure A.52: Winandy model power results for extrapolation data with reciprocating compressor utilizing R32

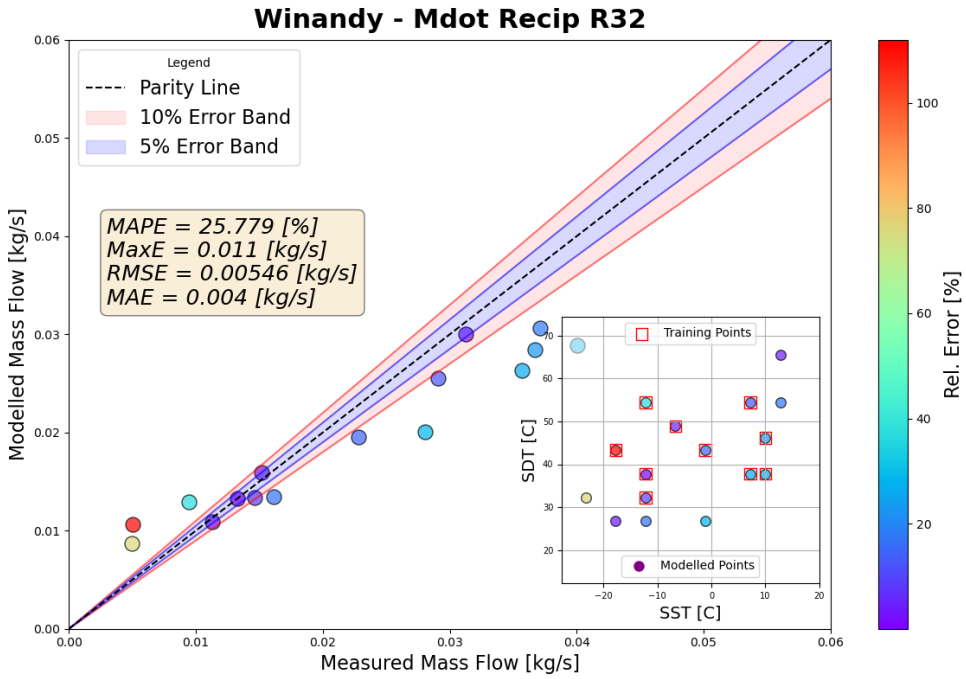

Figure A.53: Winandy model mass flow rate results for full data with reciprocating compressor utilizing R32

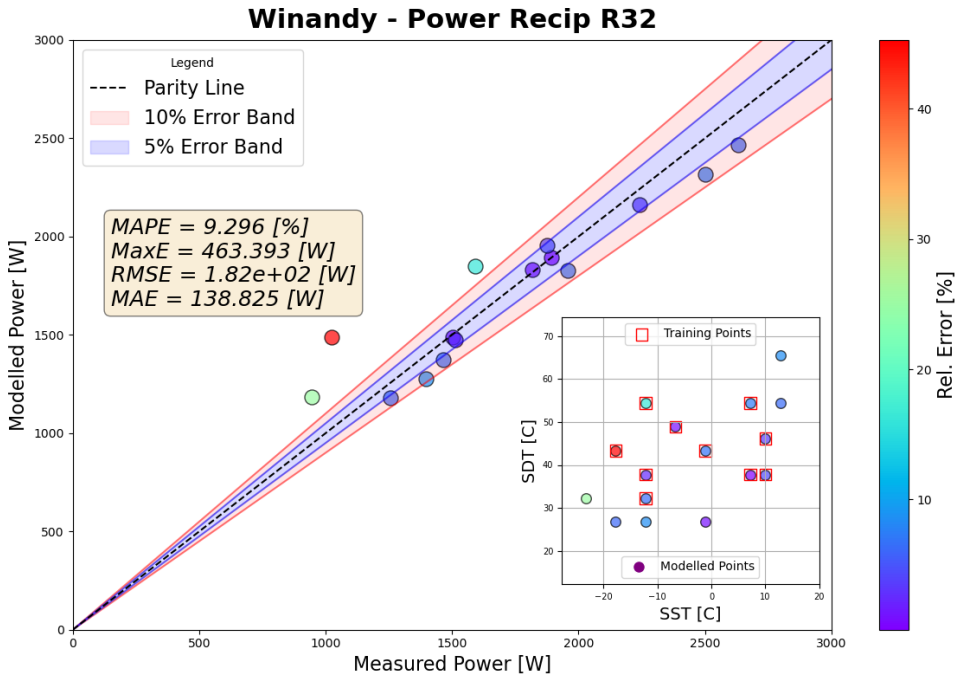

Figure A.54: Winandy model power results for full data with reciprocating compressor utilizing R32

0.8 Rotary Compressor Data utilizing R410A

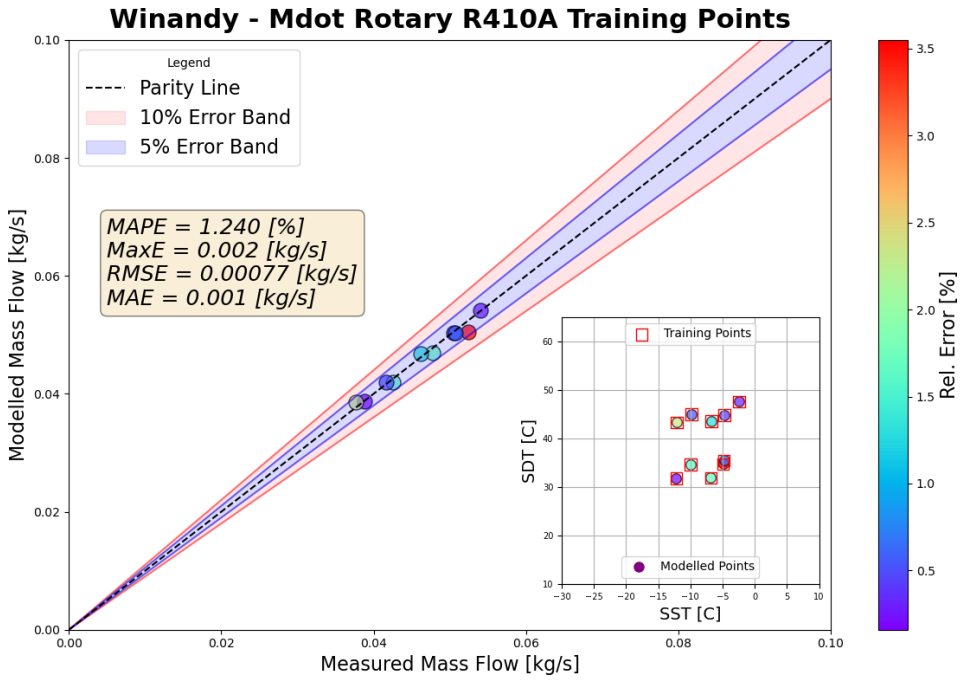

Figure A.55: Winandy model mass flow rate results for training data with rotary compressor utilizing R410A

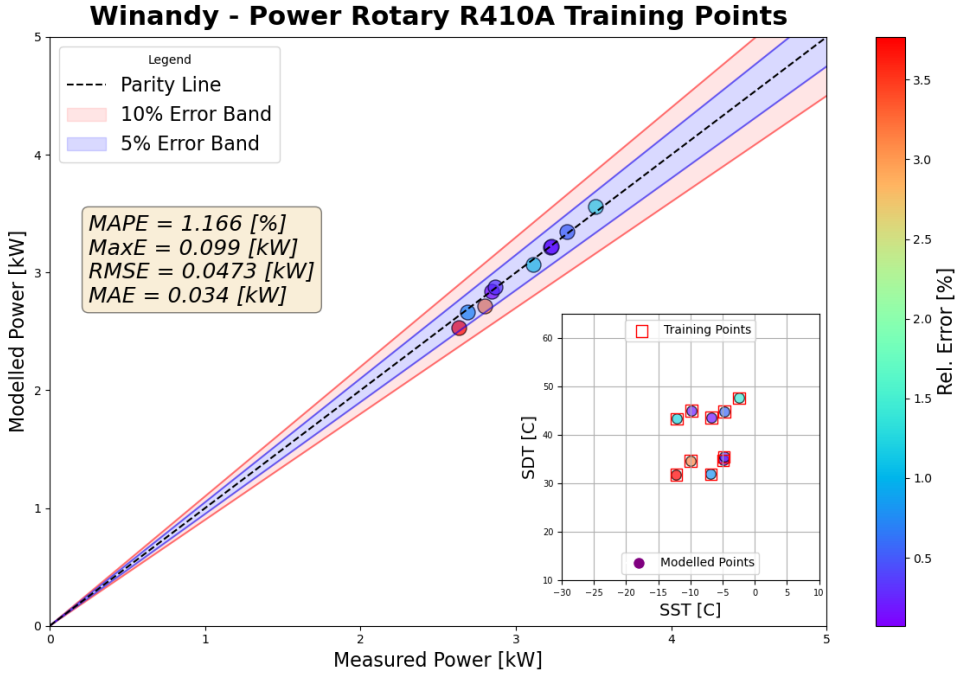

Figure A.56: Winandy model power results for training data with rotary compressor utilizing R410A

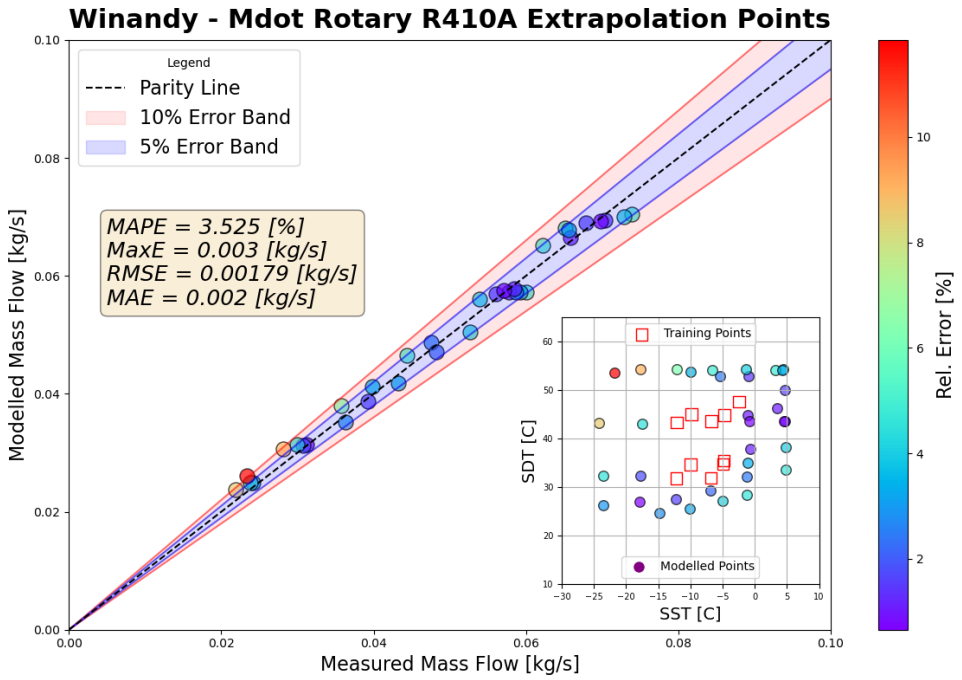

Figure A.57: Winandy model mass flow rate results for extrapolation data with rotary compressor utilizing R410A

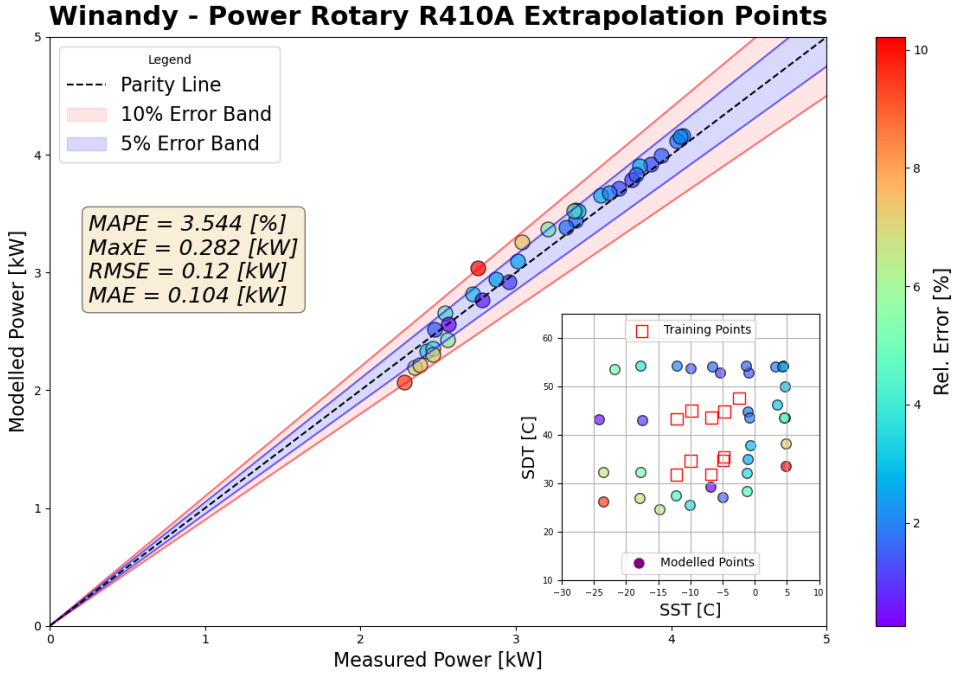

Figure A.58: Winandy model power results for extrapolation data with rotary compressor utilizing R410A

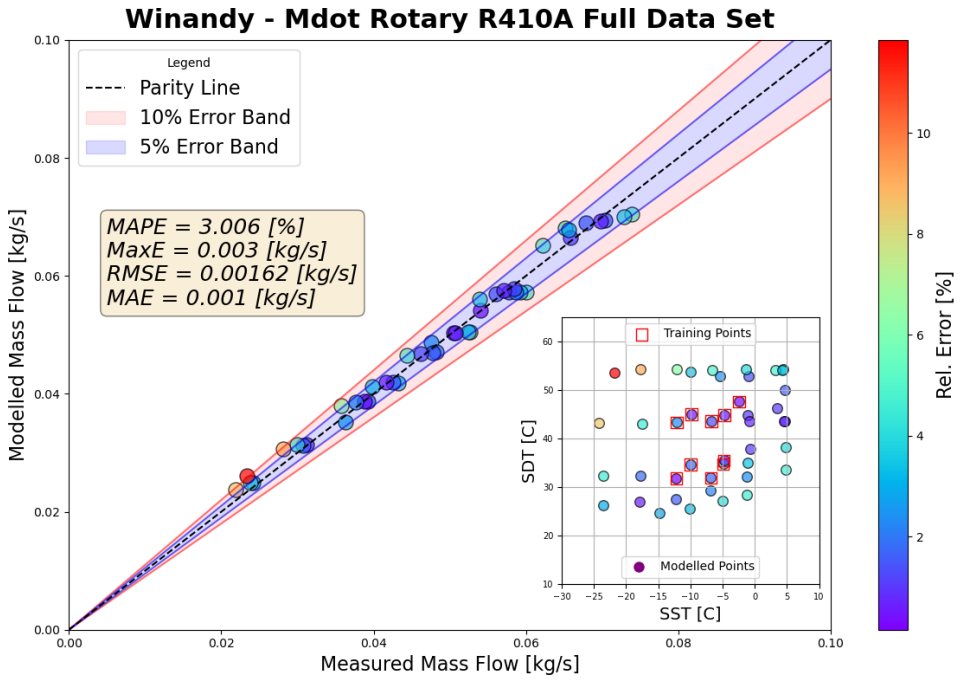

Figure A.59: Winandy model mass flow rate results for full data with rotary compressor utilizing R410A

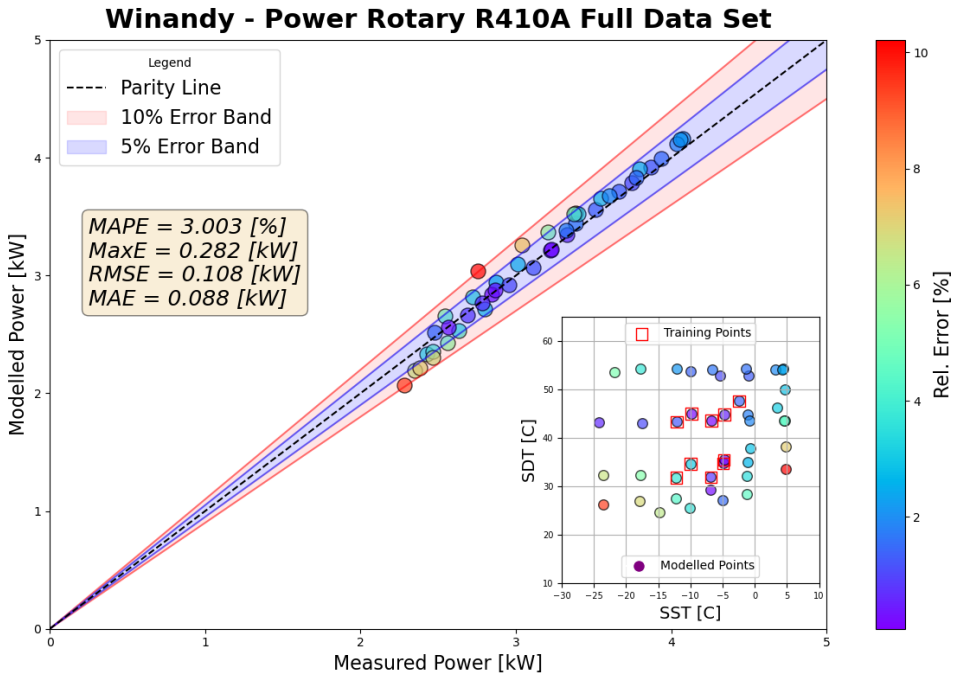

Figure A.60: Winandy model power results for full data with rotary compressor utilizing R410A

VITA

Kalen S. Gabel

Candidate for the Degree of

Master of Science

Thesis: QUANTITATIVE ANALYSIS OF POSITIVE-DISPLACEMENT COMPRESSOR MODELS TESTED IN EXTRAPOLATION SCENARIOS

Major Field: Mechanical and Aerospace Engineering

Biographical:

Education:

Completed the requirements for the Master of Science in Mechanical and Aerospace Engineering at Oklahoma State University, Stillwater, Oklahoma in December, 2022.

Completed the requirements for the Bachelor of Science in Mechanical Engineering at Oklahoma State University, Stillwater, Oklahoma in 2019.

Completed the requirements for the Bachelor of Science in Mathematics at Northwestern Oklahoma State University, Alva, Oklahoma in 2017.

Professional Memberships:

ASHRAE Student Member
ASME Member